Imperial College London

ICFO

The maximum refractive index of a 3D atomic array:

Multiple scattering meets quantum chemistry

Author:

Bennet Windt

Supervisor:

Prof. Darrick Chang

Submitted in partial fulfilment of the requirements for the degree of Master of Science of Imperial College London.

Research carried out at the Institute of Photonic Sciences (ICFO) under an ICFO Student Research Fellowship.

Abstract

All known optical materials have a refractive index of order unity. While this is well-established experimentally, there is as of yet no comprehensive theory to explain this observation, and in fact the saturation of the refractive index seems to contradict traditional theoretical models. We formulate here a theory of the optical properties of ordered atomic media at the interface of quantum optics, quantum chemistry, and multiple scattering of light, which is needed to resolve this issue. Specifically, using a minimal theoretical model, we are able to capture the effect of quantum chemistry interactions on the collective optical response of a 3D atomic array in the regime of linear optics. Contrary to traditional arguments, we propose that the onset of quantum chemistry at sufficiently high atomic densities leads to the emergence of fundamental inelastic scattering processes in the array, which attenuate the refractive index. In particular, we reproduce recent analytical results on the antiferromagnetically ordered Fermi-Hubbard model to argue that the ground-state charge fluctuations of our model represent the most significant source of these processes. By systematically dissecting the interactions encoded in the full problem, we are able to characterise the dominant effects associated with quantum chemistry and thus to support this argument, while also recovering the standard quantum optics limit in a physically rigorous fashion. Our work establishes a bridge between the generically incompatible paradigms of multiple scattering and quantum chemistry, to address a problem whose eventual solution promises to have wide-reaching implications – both in terms of the basic theory of electrodynamics and in terms of photonic technologies, since it suggests the possibility of realising optical materials with ultrahigh refractive indices.

Contents

Chapter 1

Introduction

1 Background & motivation

A key quantity which characterises the propagation of electromagnetic waves in a medium is the *refractive index* n, which relates the wavevector $\mathbf{k}$ of a plane wave in the medium to its wavevector $\mathbf{k}_0$ in the vacuum according to $\mathbf{k} = n\mathbf{k}_0$ [1]. In a non-absorbing medium, n is real and typically positive, although negative indices have also been engineered in artificial metamaterials [2, 3]. A real refractive index corresponds with the ratio of the speeds of light inside and outside and the medium and equivalently relates the wavelengths $\lambda = 2\pi/|\mathbf{k}|$ and $\lambda_0 = 2\pi/|\mathbf{k}_0|$ as $n = \lambda_0/\lambda$. From the perspective of photonics, the maximum refractive index of a material therefore places a lower bound on attainable length scales of optical elements fabricated from it. Rather curiously, the maximum refractive index of all optical materials with positive indices at visible wavelengths – for instance silica glass [4] and quartz glass [5] as well as common semiconductors [6–10] and other solids [11] – is on the order of unity. This observation is robust even close to the optical resonances of the materials, suggesting that there indeed exists some fundamental limitation on the value of n. Understanding the physical processes which lead to this saturation of the refractive index (and potential methods to circumvent them) could bear wide-reaching implications for photonic technologies, since being able to engineer ultra-high index materials could pave the way to developing optical circuitry at the nano-scale.

On a more fundamental level, developing a consistent theory of the refractive index would necessitate a re-examination of long-standing theoretical models. In particular, the low value of the maximum refractive index disagrees with current theories of optical response at the level of the most basic systems; for instance, a single atom by itself has a characteristically large optical response: the resonant scattering cross-section of an atom has a maximum value of $\sigma_{\mathrm{sc}} = 3\lambda_0^2/(2\pi)$, where λ_0 denotes the resonant wavelength associated with the targeted atomic transition [12]. In the visible range, $\lambda_0 \sim 10^{-7}m$ while the characteristic length scale of the atom is given by the *Bohr radius* $a_0 \approx 10^{-10}m$, therefore an atom typically has an effective optical target area much larger than its physical size.

Both intuition and generic *macroscopic* models of refractive index suggest that the index should grow with atomic density. However, the index problematically grows to unreasonable values, if one starts from the large single-atom response described above. In particular, perhaps the most familiar classical model for the refractive index is the *Drude-Lorentz model* [13]. Within this model, the refractive index

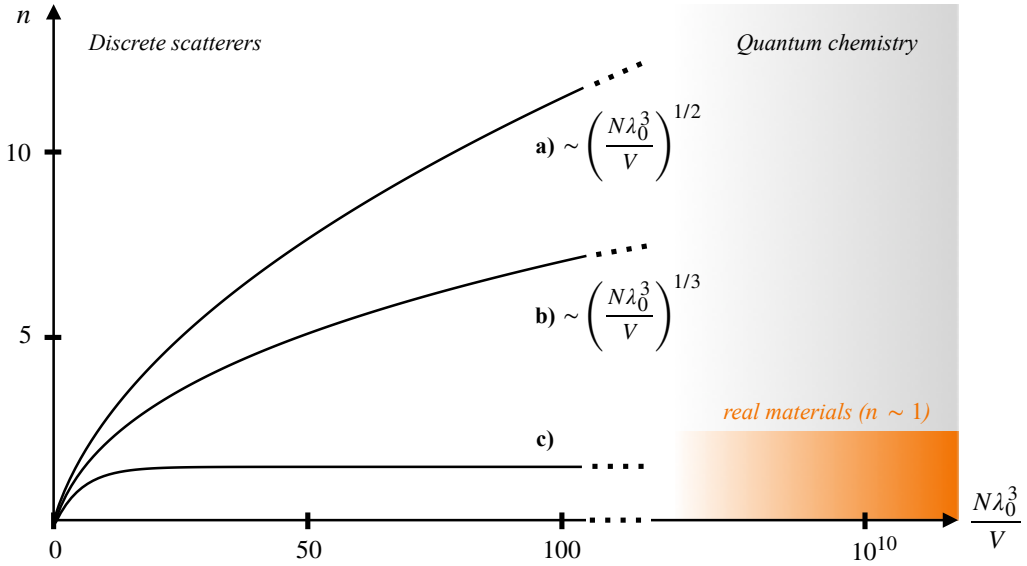

Figure 1.1 – **Maximum refractive index.** Scaling of the maximum real part of the refractive index n with the (re-scaled) atomic density $N\lambda_0^3/V$ for **a)** the Drude-Lorentz model, as well as **b)** a 3D atomic crystal and **c)** a disordered atomic ensemble, taking into consideration multiple scattering. The regime of dense atomic media, where quantum chemistry effects become non-negligible, is indicated as the grey shaded region, while the range of values of n for real materials is indicated in orange. The regime of non-interacting point scatterers, under which the predictions **a)**–**c)** are valid, is also indicated.

is computed from the product of the single-atom polarisability $\alpha(\omega)$ and atomic density N/V as

$$n(\omega) = \left(1 + \alpha(\omega)\frac{N}{V}\right)^{1/2}. \tag{1.1}$$

At suitable detuning, this model predicts a scaling of the maximum real part of the refractive index with the atomic density as $n \sim \left(N\lambda_0^3/V\right)^{1/2}$, which is of course unbounded as $N/V \to \infty$ (see Fig. 1.1a). The semi-classical *Maxwell-Bloch equations*, which treat the atoms as quantum mechanical two-level systems [14], lead to the same qualitative result.

As is intuitively evident from eq. (1.1), these models rely on the assumption that the optical response is characterised by the polarisation induced in each atom by the external electric field only. In fact, it is the *total* local electric field which polarises each atom, and this includes not only the external field but also the field re-scattered from all other atoms in the medium. The polarisation of each atom is therefore sensitive to the microscopic configuration of the entire system (i.e. the instantaneous positions and polarisations of all atoms), a fact which is entirely absent from the Drude-Lorentz model. Traditionally, the field experienced by an atom due to other atoms in a medium is accounted for in the spirit of the *Lorentz-Lorenz model*, which treats the collection of atoms as a smooth medium of uniform charge density N/V generating a uniform electric field. The local field at a given atomic position is then calculated by assuming that the atom sits in a small spherical vacuum exclusion, which leads to the well-known *Clausius-Mossotti relations* [13]. However, the maximum real refractive index predicted by the Lorentz-Lorenz model is still unbounded in the same way as for the Drude-Lorentz model. This is because the

assumption of a smooth medium with uniform density N/V does not account for the granularity of the atomic system, which crucially affects the local fields experienced by individual atoms.

In particular, the coherent scattering of light between atoms at discrete positions can lead to interference effects which drastically alter the optical properties of the atomic medium: this so-called *multiple scattering* enables a host of collective phenomena, including superradiance and subradiance [15–17], or resonance shifts and changes in lineshape [18–20]. These cooperative effects can be enhanced even further when the atomic scatterers are placed in ordered geometries [21], for instance enabling a strongly enhanced optical cross-section with respect to the single-atom limit [22, 23]. Multiple scattering calculations for light in atomic media are well-motivated by potential applications: for instance, they have led to the realisation of atomic mirrors [21, 24, 25] and there have been suggestions of their application to novel methods of laser amplification [26]. Given the proven relevance of multiple scattering effects in other contexts, it seems unavoidable that they should also play an important role in the problem of the maximum refractive index.

Indeed, in Ref. [27], a full numerical treatment of the multiple scattering of light in a dilute atomic gas was already shown to lead to results for the maximum refractive index consistent with the experimental paradigm. In the sub-wavelength regime, the scattering cross-section of each atom exceeds the typical inter-atomic spacing, and Ref. [27] shows that in this regime, multiple scattering becomes a non-perturbative problem. This particular problem can be solved using the *strong disorder renormalisation group*, a standard method for dealing with many-body systems with strongly varying interactions strengths [28, 29]. Specifically, the authors of Ref. [27] show that, due to the randomised atomic positions, the many-atom interactions can be treated as a hierarchy of pair-wise strong, coherent nearest-neighbour interactions. This leads to an effective inhomogeneous broadening across the ensemble, allowing for a mapping of the collection of identical atoms onto an ensemble of atoms with significantly varying resonances and lineshapes. Hence, light of a given frequency will only encounter roughly a single near-resonant atom per volume element λ_0^3, independent of the atomic density. This leads to a maximum real part of the refractive index of around $n \approx 1.7$ (see Fig. 1.1c).

The fact that the optical response of an atomic medium seems to be dominated by strong short-range interactions underlines the shortcomings of the smooth medium models. However, interestingly, while this explanation based purely on (classical) electrodynamics seems to be sufficient to explain the maximum attainable value of the refractive index in disordered atomic ensembles, the same cannot be said for the ordered case. An application of a non-perturbative multiple scattering formalism to an ordered array of well-separated atoms, which will be reviewed in Chapter 2 of this dissertation, predicts a scaling of the maximum refractive index with atomic density as $n \sim \left(N\lambda_0^3/V\right)^{1/3}$ (see Fig. 1.1b). While this result is certainly different from the textbook models, it still predicts no saturation of the index.

The missing puzzle piece are non-radiative interactions between the atomic scatterers, which are incompatible with the assumptions underlying the multiple scattering argument and are instead the subject of quantum chemistry. Specifically, when the atomic lattice spacing a becomes comparable to

the Bohr radius a_0, the outer atomic orbitals overlap, leading to interactions between the atoms as well as deformations of the orbitals [30–32]. In the case of ordered atomic media, these interactions cause the narrow atomic energy levels to broaden out and form continuous bands of states. The study of absorption and emission of light in such systems is well-studied and much more complex than in the case of a single atom [33]: in addition to photon-mediated transitions of electrons between bands, there are intra-band electronic transitions, phonon-assisted absorption, exciton-assisted absorption, or absorption via defects to account for. In principle, all of these effects contribute to the optical properties of solid-state matter in general, and to the refractive index in particular. Ignoring all of these subtleties and assuming an optical response purely characterised by the direct inter-band electronic transitions, a standard approach in quantum chemistry is to calculate the dielectric function $\varepsilon(\omega)$ using *Fermi's Golden Rule* according to the prescription (see e.g. Ref. [34])

$$\text{Im } \varepsilon(\omega) = \left(\frac{Vq^2}{2\pi\hbar m^2\omega^2}\right) \int d^3\mathbf{k} \sum_{m,m'} |\langle\phi_{\mathbf{k}m}|\hat{\mathbf{p}}|\mathbf{k}m'\rangle|^2 f(\mathbf{k}m)(1 - f(\mathbf{k}m'))\delta(E_{\mathbf{k}m} - E_{\mathbf{k}m'} - \hbar\omega)\,, \qquad (1.2)$$

where Re $\varepsilon(\omega)$ can be calculated from the well-known *Kramers-Kronig relations*. Here, $E_{\mathbf{k}m}$ denotes the m-th energy band, the state $|\phi_{\mathbf{k}m}\rangle$ denotes a crystal wave state, and $f(\mathbf{k}m)$ is the Fermi distribution. The problem of calculating optical properties then reduces to the problem of calculating electronic structure to obtain the form of the $|\phi_{\mathbf{k}m}\rangle$.

The starting point for this is the *Born-Oppenheimer approximation*, which assumes that the slow-moving nuclei can be treated as stationary relative to the electrons [35]. The main focus of quantum chemistry is then to find accurate and computationally feasible solutions to electronic Schrödinger equations. A number of standard techniques have been devised and fine-tuned to overcome the computational complexity of this challenge [36–38]. The most popular are methods which approximate the many-body problem self-consistently as a single-body problem for each electron, such as *Hartree-Fock Theory (HFT)* [39] or *Density Functional Theory (DFT)* [40]. In particular, DFT offers formidable (polynomial) scaling of computational effort while providing accurate results. Greater computational efficiency can be achieved by introducing external parameters, as done in a large number of so-called *semi-empirical* techniques [41–43]. The speedups of such approaches relative to conventional HFT or DFT come at the cost of numerical accuracy. On the other side of this tradeoff, the assumptions of HFT and DFT can be improved upon by accounting for instantaneous electron-electron Coulomb repulsion. This is the domain of *ab initio* (i.e. first-principles) calculations, based on many-body wavefunctions [44–46].

Importantly, state-of-the-art computational quantum chemistry simulations along the lines of eq. (1.2) produce similar orders of magnitude for the maximum refractive index as observed in experiments (see for example Refs. [47–49]). This suggests that the onset of quantum chemistry is responsible for the deviation of the scaling in Fig. 1.1b towards the order of unity. However, even if it were possible to calculate the electronic structure of the medium to arbitrary accuracy (i.e. to perform 'exact quantum chemistry'), Fermi's Golden Rule itself is an approximation and, in particular, corresponds to the lowest order expansion of a multiple scattering problem. Therefore, even the most advanced quantum chemistry

methods do not incorporate a full non-perturbative multiple scattering treatment, and so while they may reproduce accurate values of the refractive index, they are not able to resolve the related *conceptual* issues.

In summary, up to now, there is no theory that correctly describes the maximum value of the refractive index of optical media. It is clear that such a theory must not only unify quantum optics and quantum chemistry, in order to capture the transition from dilute atomic media to solid-state materials, but also incorporate multiple scattering of light in a non-perturbative fashion. The goal of this thesis is to develop such a theory for a simple 3D atomic crystal, which is valid around the transition from discrete atoms to quantum chemistry (i.e. as the line in Fig. 1.1b crosses the boundary of the grey shaded region). This theory will both elucidate the dominant physical mechanisms by which the predicted scaling of n saturates and eventually decreases, and predict that an ultrahigh refractive index (i.e. values of $n \sim 50 - 100$*) is in principle achievable.*

2 Minimal theoretical model

In the face of the individual complexity of both the multiple scattering and the quantum chemistry aspects of the problem outlined above, the challenge of accurately calculating the scaling of the maximum refractive index with density seems daunting. We briefly outline here the minimal model which we propose in order to reduce the complexity of the problem and tackle the interplay of quantum chemistry and multiple scattering in a systematic way.

The key conceptual step in our minimal model is an effective reduction of the dimensionality of the problem, both in terms of the quantum chemistry and multiple scattering aspects. To accomplish this, we view a generic 3D crystal as a layering of parallel square arrays with lattice constant a in the xy plane, spaced at intervals a_z in the z-direction. The advantage of this (initially purely formal) change of perspective is two-fold. Firstly, we can consider this model in the quantum optics limit i.e. at densities below the threshold for quantum chemistry interactions. While in this regime the optical properties of 3D atomic crystals are not well-understood, there has been key theoretical work on non-perturbative multiple scattering in 2D arrays [21, 24]. In particular, it has been established that square arrays display a remarkable cooperative response, whereby near-resonant normally incident plane waves with zero in-plane wavevector can only be re-radiated with the same wavevector, accompanied by a short-range evanescent field. For $a_z \gg a$, the effect of the evanescent field from each plane on atoms in other planes can be disregarded and the multiple scattering in the full 3D crystal simplifies to a repeated single-mode scattering at each plane. In this way, the multiple scattering aspect of the index problem is effectively reduced from 3D to 1D.

The second advantage of our model is that we may choose $a_z \gg a$ in such a way that quantum chemistry interactions persist within each 2D array but that the different planes will be sufficiently far separated for quantum chemistry interactions between them to be negligible. In this way, the quantum chemistry aspect of the index problem is effectively reduced from 3D to 2D. An obvious advantage of this assumption will be that it trivially reduces the complexity of the formal quantum chemistry

calculations – as we will see, the ground state manifold of our planar array is well-captured by the half-filled *Fermi-Hubbard model*, for which there exist a number of state-of-the-art quantum chemistry studies in 2D (for a review see e.g. Ref. [50]). However this assumption will also prove crucial to formulating our hypothesis of the effect of quantum chemistry on the refractive index: in the quantum optics limit, near-resonant light will experience a (large) phase shift at each 2D plane [24]. The summative phase shift of light propagating through the full 3D structure allows us to infer the (large) refractive index of the crystal, leading to the scaling in Fig. 1.1b. A controlled expansion around of the quantum chemistry interactions in $a_0/a \gg 1$ (i.e. around the onset of quantum chemistry interactions) then allows key processes associated with quantum chemistry within each 2D array to be included into its optical response in a perturbative way, and we simply have to look for those processes which reduce the phase shift at the plane, leading to an attenuation of the overall phase shift and therefore a saturation of the refractive index. This is the aim of this dissertation.

3 Structure of the thesis

The dissertation is structured as follows: In Chapter 2 we first formalise the description of the model introduced in the last section in the dilute limit where the atoms can be treated as discrete scatterers. In particular, we reproduce the multiple scattering analysis of the collective optical response of the individual 2D layers and derive an explicit expression for the scaling of the refractive index of the full 3D crystal. Chapter 2 serves as a point of reference for a treatment of non-perturbative multiple scattering during the next three chapters, where we focus instead on the effect of quantum chemistry on the optical properties of the 2D arrays.

In Chapter 3, we begin this discussion by setting up a formal (minimal) model for quantum chemistry on a 2D lattice. This model serves as the workhorse for the two following chapters. In particular, in Chapter 4 we analyse in some detail the ground state of this model. Using methods from many-body quantum field theory, we investigate the ground state charge dynamics and reproduce key results related to the formation of *holon-doublon pairs*, i.e. the double occupancy of a single site by two electrons, leaving behind an empty site. We introduce the main hypothesis of the thesis, namely that the associated buildup of density-density correlations in the ground state represents a source of inelastic scattering processes leading to the saturation of the index.

Chapter 5 is then dedicated to dissecting in detail the interactions of our model and demonstrating that the model is amenable to a multiple scattering analysis (akin to the one in Chapter 2) with some corrections exponentially small in a_0/a. In this way, we are able to show that the holon-doublon pairs characterised in Chapter 4 in fact represent the dominant correction to the quantum optics limit at the interface to the quantum chemistry regime. To make the relevance of this effect even more explicit, we return in Chapter 6 to the multiple scattering picture to make a convincing argument that the holon-doublon pairs may, with the exception of one other effect, be practically exclusively responsible for the saturation of the refractive index. We conclude by underlining the potential implications of this result.

Chapter 2

Quantum optics limit

In this chapter, we begin by examining the minimal model introduced in the previous chapter in the quantum optics limit, i.e. in the limit where the atoms are sufficiently far separated for quantum chemistry effects to be negligible. We submit the individual planar arrays to a non-perturbative multiple scattering treatment, firstly to derive the cooperative response advertised in the previous chapter (Section 2), and secondly, based on this, to obtain the scaling of the refractive index for the 3D crystal shown in Fig. 1.1b (Section 3). To preface the calculations presented in this chapter, we begin by introducing briefly the toolkit of the formal theory of multiple scattering (Section 1).

1 Multiple scattering theory

1.1 Quantisation in dispersive media

In our review of multiple scattering theory, we will focus in particular on a quantum spin model which has in the past been successfully used to study collective excitations and exotic optical properties in ordered atomic arrays [17, 51–53]. Underlying the spin model is a formalism for the quantisation of the scattered electric field based on the microscopic *Huttner-Barnett model* [54] and first introduced in Refs. [55, 56]. It has been devised primarily to describe macroscopic quantum electrodynamics within dispersive dielectric materials, where standard canonical quantisation becomes unfeasible since the irreversible dynamics of the polarisation noise do not preserve the field commutators. The procedure relies on the introduction of additional bosonic quantised 'loss' degrees of freedom to which the electric field can couple. Specifically, the electric field operator can then be defined as $\hat{\mathbf{E}}(\mathbf{r}) = \int d\omega\ \hat{\mathbf{E}}(\mathbf{r},\omega)$, with

$$\hat{\mathbf{E}}(\mathbf{r},\omega) = \underbrace{\mathrm{i}\sqrt{\frac{\hbar}{\pi\varepsilon_0}}\frac{\omega^2}{c^2}\int d^3\mathbf{r}'\sqrt{\mathrm{Im}\ \varepsilon(\mathbf{r}',\omega)}\mathbf{G}(\mathbf{r}-\mathbf{r}',\omega)\cdot\hat{\mathbf{f}}(\mathbf{r}',\omega)}_{\hat{\mathbf{E}}^{(+)}(\mathbf{r},\omega)} + \text{h.c.}\,, \tag{1.1}$$

where $\varepsilon(\mathbf{r}',\omega)$ is the permittivity. Here, $\hat{\mathbf{f}}(\mathbf{r}',\omega)$ denotes a bosonic operator associated with the medium-assisted field, which obeys standard bosonic canonical commutators, and we have indicated how to decompose the field into positive- and negative-frequency components as $\hat{\mathbf{E}}(\mathbf{r},\omega) = \hat{\mathbf{E}}^{(+)}(\mathbf{r},\omega) + \hat{\mathbf{E}}^{(-)}(\mathbf{r},\omega)$. The primary advantage of this formalism for our case of atoms in free space is that it allows us to circumvent the tedious technicalities of the textbook method of quantisation by mode decomposition.

1.2 Spin model formalism

We now consider a collection of N two-level atoms at positions $\mathbf{R}_i$ $(i = 1, \ldots, N)$, with an optically allowed transition between the ground ($|g\rangle$) and excited ($|e\rangle$) states, associated with resonance frequency ω_0 and dipole matrix element $\mathbf{d}_0$. For each atom, we define the atomic coherence operators $\hat{\sigma}^+ = |e\rangle\langle g|$ and $\hat{\sigma}^- = |g\rangle\langle e|$. Under a *dipole approximation* (i.e. assuming negligible variation in the field on the atomic length scale), the formal Hamiltonian for a coupling of the atoms to the field (1.1) is [57]

$$H = \underbrace{\sum_i \hbar\hat{\sigma}_i^+\hat{\sigma}_i^-}_{H_A} + \underbrace{\int d^3\mathbf{r} \int d\omega\ \hbar\omega\ \hat{\mathbf{f}}^\dagger(\mathbf{r},\omega)\hat{\mathbf{f}}(\mathbf{r},\omega)}_{H_F} \underbrace{- \int d\omega \sum_i \hat{\mathbf{d}}_i \cdot \hat{\mathbf{E}}(\mathbf{R}_i,\omega)}_{H_{AF}}, \tag{1.2}$$

where $\hat{\mathbf{d}}_i = \mathbf{d}_0^*\hat{\sigma}_i^+ + \mathbf{d}_0\hat{\sigma}_i^-$ is the atomic dipole moment operator. Here, H_A and H_F are the bare many-atom and field Hamiltonians and H_{AF} realises the light-matter interaction.

1.2.1 *Effective atomic master equation*

Tracing out the radiative degrees of freedom, the atomic dynamics governed by the Hamiltonian (1.2) are captured by a master equation for the atomic density matrix $\hat{\rho}_A$, which reads $\dot{\hat{\rho}}_A = -\mathrm{i}/\hbar[H_{\text{eff}}, \hat{\rho}_A] + \mathcal{L}[\hat{\rho}_A]$ with an effective Hamiltonian H_{eff} and Linblad operator $\mathcal{L}$ given by [52, 58]

$$\begin{aligned} H_{\text{eff}} &= \hbar\omega_0 \sum_i \hat{\sigma}_i^+\hat{\sigma}_i^- + \hbar\sum_{i,j} J^{ij}\hat{\sigma}_i^+\hat{\sigma}_j^- \\ \mathcal{L}[\hat{\rho}_A] &= \sum_{i,j} \frac{\Gamma^{ij}}{2}\left(\hat{\sigma}_i^+\hat{\sigma}_j^-\hat{\rho}_A + \hat{\rho}_A\hat{\sigma}_i^+\hat{\sigma}_j^- - 2\hat{\sigma}_i^-\rho\hat{\sigma}_j^+\right). \end{aligned} \tag{1.3}$$

Here, J^{ij} and Γ^{ij} are the rates for coherent and dissipative interactions, respectively, defined as [17]

$$\begin{aligned} J^{ij} &= -\frac{\mu_0\omega_0^2}{\hbar}\ \mathbf{d}_0^* \cdot \mathrm{Re}\ \mathbf{G}(\mathbf{R}_{ij},\omega_0)\cdot\mathbf{d}_0 \\ \Gamma^{ij} &= -\frac{2\mu_0\omega_0^2}{\hbar}\ \mathbf{d}_0^* \cdot \mathrm{Im}\ \mathbf{G}(\mathbf{R}_{ij},\omega_0)\cdot\mathbf{d}_0\,, \end{aligned} \tag{1.4}$$

where $\mathbf{R}_{ij} \equiv \mathbf{R}_j - \mathbf{R}_i$ and $\mathbf{G}(\mathbf{r},\omega_0)$ denotes the *dyadic Green's tensor* [59], i.e. the photonic propagator, whose properties we outline in the next section. Importantly, the derivation of the atomic master equation involves the *Born-Markov approximation* [60], which we encounter again in Chapter 5 and which is valid when the correlations in the radiation field decay much faster than the atomic correlations [57, 58, 61]. Additionally, the evaluation of the Green's tensor on-resonance in eq. (1.4) is only valid when retardation of the light propagating between atoms can be neglected [62]. This assumption is validated by the fact that when interacting with an atom, a photon incurs a delay on the timescale $\sim 1/\Gamma_0$. Since Γ_0 is small for real atoms, these delays dominate the retardation of photons in the atomic system, while the delay arising simply from the finite velocity of light is negligible. As a final approximation, in H_{eff} we have ignored the off-resonant van der Waals interactions between ground state atoms, which we also revisit in Chapter 5.

We note that, within the formalism of quantum jump operators [63], the atomic dynamics are alternatively captured by an effective non-Hermitian Hamiltonian [17]

$$\mathcal{H}_{\text{eff}} = \hbar\left(\omega_0 - \mathrm{i}\frac{\Gamma_0}{2}\right)\sum_i \hat{\sigma}_i^+\hat{\sigma}_i^- - \mu_0\omega_0^2\sum_{i,j\neq i}\mathbf{d}_0^*\cdot\mathbf{G}(\mathbf{R}_{ij},\omega_0)\cdot\mathbf{d}_0\;\hat{\sigma}_i^+\hat{\sigma}_j^-\,, \tag{1.5}$$

where $\Gamma_0 = \omega_0^3|\mathbf{d}_0|^2/(3\pi\varepsilon_0\hbar c^3)$ is the single-atom spontaneous decay rate. This is the version of the spin model that we will refer back to in later chapters.

1.2.2 Input-output relations

Given a solution to the atomic dynamics, the multiple-scattered field can be reconstructed. The starting point are the Heisenberg equations $\mathrm{i}\hbar\dot{\hat{\mathbf{f}}}(\mathbf{r},\omega) = [\hat{\mathbf{f}}(\mathbf{r},\omega), H]$ for the medium-assisted field operators [52],

$$\dot{\hat{\mathbf{f}}}(\mathbf{r},\omega) = -\mathrm{i}\omega\hat{\mathbf{f}}(\mathbf{r},\omega) + \frac{\omega^2}{c^2}\sqrt{\frac{1}{\pi\hbar\varepsilon_0}\mathrm{Im}\;\varepsilon(\mathbf{r}',\omega)}\sum_i\mathbf{G}(\mathbf{r}-\mathbf{R}_i,\omega)\cdot\mathbf{d}_0\;\hat{\sigma}_i^-\,. \tag{1.6}$$

This expression can be formally integrated, performing another Markov approximation and neglecting retardation for consistency with eqns. (1.4) and (1.5), to obtain the positive-frequency field component

$$\hat{\mathbf{E}}^{(+)}(\mathbf{r}) = \hat{\mathbf{E}}_0^{(+)}(\mathbf{r}) + \mu_0\omega_0^2\sum_i\mathbf{G}(\mathbf{r}-\mathbf{R}_i,\omega_0)\cdot\mathbf{d}_0\;\hat{\sigma}_i^-\,. \tag{1.7}$$

Here, $\hat{\mathbf{E}}_0^{(+)}(\mathbf{r})$ denotes the incident field, whereas the second term accounts for the scattering of the field by the atoms. This quantum *input-output formalism* for the electric field has been successfully used in the past to study light propagation in waveguides and nanostructures [58, 64, 65].

1.3 Dyadic Green's tensor

1.3.1 Basic definitions and properties

Before reviewing the application of the spin model formalism to the exactly solvable case of a square array in the next section, we pause for a moment to examine in more detail the structure and properties of $\mathbf{G}(\mathbf{r},\omega)$. First, we note that it is related to the conventional scalar *Green's function* $G_0(\mathbf{r},\omega) = \mathrm{e}^{\mathrm{i}kr}/(4\pi|\mathbf{r}|)$ [1, 12], familiar from the Lorenz gauge, according to

$$\mathbf{G}(\mathbf{r},\omega) = \left(\mathbb{1} + \frac{1}{k^2}\boldsymbol{\nabla}\otimes\boldsymbol{\nabla}\right)G_0(\omega,\mathbf{r})\,. \tag{1.8}$$

The position-space expression for the Green's tensor can be computed explicitly by eq. (1.8) as

$$\mathbf{G}(\mathbf{r},\omega) = \frac{\mathrm{e}^{\mathrm{i}kr}}{4\pi k^2}\left[\left(\frac{k^2}{r}+\frac{\mathrm{i}k}{r^2}-\frac{1}{r^3}\right)\mathbb{1} + \left(-\frac{k^2}{r}-\frac{3\mathrm{i}k}{r^2}+\frac{3}{r^3}\right)\frac{\mathbf{r}\otimes\mathbf{r}}{r^2}\right] - \frac{\mathbb{1}}{3k^2}\delta^{(3)}(\mathbf{r})\,. \tag{1.9}$$

where $k = \omega/c = |\mathbf{k}|$ and $r = |\mathbf{r}|$. The structure of this expression already gives some insight into the physics captured by the Green's tensor: in the near- and far-field regimes, the Green's tensor has a radial dependence of $\sim 1/r^3$ and $\sim 1/r$, respectively. The former can be identified with non-radiative, strong, coherent dipole-dipole coupling [27, 66], while the latter has the characteristic form of long-range radiative interactions [59]. We return to this point in Chapter 5.

Formally, the Green's tensor solves the (dyadic) Helmholtz equation with a δ-source, hence a general solution to the Maxwell equations with current density source $\mathbf{J}(\mathbf{r},\omega)$ takes the form [59]

$$\mathbf{E}(\mathbf{r},\omega) = \mathrm{i}\mu_0\omega \int d^3\mathbf{r}'\mathbf{G}(\mathbf{r}-\mathbf{r}',\omega)\cdot\mathbf{J}(\mathbf{r}',\omega)\,. \tag{1.10}$$

By inserting the current density $\mathbf{J}(\mathbf{r},\omega) = -\mathrm{i}\omega\mathbf{d}(\omega)\delta^{(3)}(\mathbf{r})$ for an oscillating classical dipole $\mathbf{d}(t) = \mathbf{d}(0)\mathrm{e}^{-\mathrm{i}\omega t}$ at $\mathbf{r}$ in this expression, it is evident that the components $G_{\alpha\beta}(\mathbf{r}-\mathbf{r}',\omega)$ ($\alpha,\beta\in\{x,y,z\}$) define the α-component of the electric field at point $\mathbf{r}$ due to a dipole at point $\mathbf{r}'$ oriented along the β-axis.

1.3.2 Longitudinal and transverse components

The field (1.10) can be decomposed into its longitudinal ($\parallel$) and transverse ($\perp$) components obeying $\boldsymbol{\nabla}\times\mathbf{E}^{\parallel}(\mathbf{r},\omega)=0$ and $\boldsymbol{\nabla}\cdot\mathbf{E}^{\perp}(\mathbf{r},\omega)=0$, respectively. This is simple in momentum space: using the fact that a general momentum-space vector field $\mathbf{V}(\mathbf{q})$ decomposes as $\mathbf{V}(\mathbf{q}) = \mathbf{V}^{\parallel}(\mathbf{q}) + \mathbf{V}^{\perp}(\mathbf{q})$ with

$$\begin{aligned}\mathbf{V}^{\parallel}(\mathbf{q}) &= \mathbf{q}\frac{\mathbf{q}\cdot\mathbf{V}(\mathbf{q})}{q^2}\\ \mathbf{V}^{\perp}(\mathbf{q}) &= \mathbf{V}(\mathbf{q}) - \mathbf{q}\frac{\mathbf{q}\cdot\mathbf{V}(\mathbf{q})}{q^2}\,,\end{aligned} \tag{1.11}$$

where $q=|\mathbf{q}|$, we can separate the momentum-space Maxwell equations for the electric field into equations for the longitudinal and transverse components, which read

$$\begin{aligned}\mathrm{i}\mathbf{q}\cdot\mathbf{E}^{\parallel}(\mathbf{q},\omega) &= \frac{\rho(\mathbf{q},\omega)}{\varepsilon_0}\\ \left(q^2-k^2\right)\mathbf{E}^{\perp}(\mathbf{q},\omega) &= \mathrm{i}\omega\mu_0\mathbf{J}^{\perp}(\mathbf{q},\omega)\,.\end{aligned} \tag{1.12}$$

Combining this with the additional momentum-space relation $\mathrm{i}\mathbf{q}\cdot\mathbf{J}^{\parallel}(\mathbf{q},\omega) = \mathrm{i}\omega\rho(\mathbf{q},\omega)$ which follows from the Maxwell equations, the momentum-space version of eq. (1.10) is

$$\mathbf{E}(\mathbf{q},\omega) = \frac{\mathrm{i}\mu_0\omega}{q^2-k^2}\mathbf{J}^{\perp}(\mathbf{q},\omega) + \frac{1}{\mathrm{i}\omega\varepsilon_0}\mathbf{J}^{\parallel}(\mathbf{q},\omega)\,. \tag{1.13}$$

We note also, writing the field as $\mathbf{E}(\mathbf{r},\omega) = \mathrm{i}\omega\mathbf{A}(\mathbf{r},\omega) - \nabla\phi(\mathbf{r},\omega)$ with scalar potential $\phi(\mathbf{r},\omega)$ and vector potential $\mathbf{A}(\mathbf{r},\omega)$, that in the Coulomb gauge ($\boldsymbol{\nabla}\cdot\mathbf{A}(\mathbf{r},\omega)=0$)

$$\begin{aligned}\mathbf{E}^{\parallel}(\mathbf{r},\omega) &= -\nabla\phi(\mathbf{r},\omega)\\ \mathbf{E}^{\perp}(\mathbf{r},\omega) &= \mathrm{i}\omega\mathbf{A}(\mathbf{r},\omega)\,.\end{aligned} \tag{1.14}$$

For an arbitrary charge distribution, the Coulombic electrostatic interactions will be encoded by the scalar potential $\phi(\mathbf{r},\omega)$ while the radiative interactions will result from a coupling to $\mathbf{A}(\mathbf{r},\omega)$. Therefore eq. (1.13) implies a decomposition of the Green's tensor into longitudinal and transverse components

$$\begin{aligned}\mathbf{G}^{\parallel}(\mathbf{q},\omega) &= -\frac{1}{k^2}\frac{\mathbf{q}\otimes\mathbf{q}}{q^2}\\ \mathbf{G}^{\perp}(\mathbf{q},\omega) &= \frac{\mathbb{1}-\dfrac{\mathbf{q}\otimes\mathbf{q}}{q^2}}{q^2-k^2}\,,\end{aligned} \tag{1.15}$$

which, based on eq. (1.14) and assuming the Coulomb gauge, we identify as encoding the electrostatic and radiative interactions in our system, respectively [67]. The interactions in the spin model Hamiltonian (1.5) can then be decomposed naturally into direct Coulombic and photon-mediated interactions according to the decomposition of the Green's tensor. We will revisit this idea in Chapter 5. We can also obtain explicit expressions for the components (1.15) in position-space by performing the inverse Fourier transform of the above equations to obtain [12]

$$\begin{aligned}\mathbf{G}^{\parallel}(\mathbf{r},\omega) &= \frac{1}{4\pi k^2}\left[-\frac{\mathbb{1}}{r^3}+\frac{3}{r^3}\frac{\mathbf{r}\otimes\mathbf{r}}{r^2}\right]-\frac{\mathbb{1}}{3k^2}\delta^{(3)}(\mathbf{r})\\ \mathbf{G}^{\perp}(\mathbf{r},\omega) &= \frac{\mathrm{e}^{\mathrm{i}kr}}{4\pi k^2}\left[\left(\frac{k^2}{r}+\frac{\mathrm{i}k}{r^2}\right)\mathbb{1}+\left(-\frac{k^2}{r}-\frac{3\mathrm{i}k}{r^2}\right)\frac{\mathbf{r}\otimes\mathbf{r}}{r^2}\right]+\frac{\mathrm{e}^{\mathrm{i}kr}-1}{4\pi k^2}\left[-\frac{\mathbb{1}}{r^3}+\frac{3}{r^3}\frac{\mathbf{r}\otimes\mathbf{r}}{r^2}\right].\end{aligned} \tag{1.16}$$

2 Optical response in 2D

Having introduced a minimal toolkit for a non-perturbative treatment of multiple scattering in many-atom systems, we now apply it to the case of a square atomic array. Specifically, we consider N two-level atoms (ground state $|g\rangle$, excited state $|e\rangle$, resonance ω_0) arranged at fixed positions $\mathbf{R}_i$ $(i = 1,\dots,N)$ in a square array with lattice constant a. For concreteness, we choose the array to lie in the xy-plane, with primitive lattice vectors $\mathbf{a}_1 = a\hat{\mathbf{x}}$ and $\mathbf{a}_2 = a\hat{\mathbf{y}}$. We work in the sub-wavelength regime $a < \lambda_0$ ($\lambda_0 = 2\pi c/\omega_0$) and we also assume that the array side length $L = (\sqrt{N}-1)a \gg \lambda_0$, which allows us to approximate the lattice as infinitely extended and perfectly crystalline. The system is then translationally invariant and hence the atomic eigenmodes of the spin model Hamiltonian obey *Bloch's Theorem* [68]. We will also assume that the atoms are purely radiative, and that the excited state decays with spontaneous decay rate Γ_0. Our setup is shown in Fig. 2.1a,b.

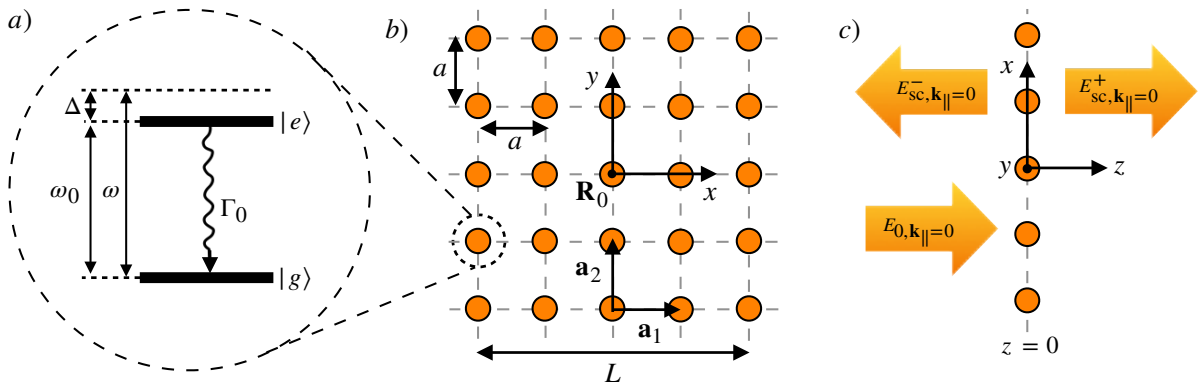

Figure 2.1 – 2D atomic array. a) Generic (purely radiative) two-level atom in the array, interacting with a field at frequency ω (detuning $\Delta = \omega - \omega_0$). **b)** Lattice structure of the 2D array in the xy-plane. **c)** Scattering of a normally incident field by the 2D array.

2.1 Weak-driving regime

In terms of the refractive index problem, we are interested only in the regime of *linear optics*, i.e. of a weak driving field. This essentially implies a single incident photon, so we can truncate the spin model Hilbert space to a single-excitation subspace. By Bloch's theorem, single excitations in the system will be delocalised across the lattice in the form of a *spin-wave* $|\psi_{\mathbf{k}}\rangle = \sum_i \mathrm{e}^{\mathrm{i}\mathbf{k}\cdot\mathbf{R}_i}\hat{\sigma}_i^+|g\rangle$ of fixed crystal momentum $\mathbf{k}$ [17, 51, 53]. Within the single-excitation subspace, the spin model Hamiltonian $\mathcal{H}_{\text{eff}}$ can then be diagonalised in a basis of these spin-wave states. Technically, the assumption of an excitation shared coherently between the atomic degrees of freedom in this way is an approximation: the excitation is actually stored in the lattice as a *polariton*, i.e a photon-atom composition. Discarding the radiative contribution is valid in our limit of negligible retardation between atoms.

In the single-excitation and low-saturation ($\langle\hat{\sigma}_i^+\hat{\sigma}_i^-\rangle \sim 0$) regime, the Heisenberg equations for the atomic coherence operators map onto coupled equations for N classical dipoles $\mathbf{d}_i$ $(i = 1, \ldots, N)$ [52],

$$\mathbf{d}_i(\omega) = \mathbf{d}_{i,0}(\omega) + \alpha(\omega)\mu_0\omega^2 \sum_{j\neq i} \mathbf{G}(\mathbf{R}_{ij}, \omega)\cdot\mathbf{d}_j(\omega)\,. \tag{2.1}$$

where $\mathbf{d}_{i,0}(\omega)$ is the value of $\mathbf{d}_i(\omega)$ in the presence of no other dipoles. This allows for a purely classical treatment of the problem, which has been successfully applied in a number many-atom systems [21, 24, 25]. The underlying physical assumption is that in response to a local (classical) field, an atom develops an induced dipole moment $\mathbf{d}_i(\omega) = \alpha(\omega)\mathbf{E}(\mathbf{R}_i, \omega)$, where $\alpha(\omega)$ is the *electric polarisability* [69]. For a two-level atom driven by light at detuning $\Delta = \omega - \omega_0$ ($|\Delta| \ll \omega_0$) [70, 71],

$$\alpha(\omega) \approx -\frac{3\varepsilon_0}{4\pi^2}\lambda_0^3 \frac{\Gamma_0/2}{\omega - \omega_0 + \mathrm{i}\Gamma_0/2} \equiv -\frac{\alpha_0}{\Delta + \mathrm{i}\Gamma_0/2}\,. \tag{2.2}$$

Note than in eq. (2.1) we have neglected the re-scattered field from the dipole itself, i.e. we have effectively ignored coupling to on-site fluctuations in the electric field. This is self-consistent if we assume that we have already incorporated into the atomic spectra the *Lamb shift*, i.e. the shift in the atomic energies due to local vacuum fluctuations [24, 72].

Under the above set of assumptions, we now treat our atomic lattice as a square array of classical dipoles governed by eq. (2.1). Following Ref. [24], we will show that such an array displays a remarkable cooperative response which allows for a simple effective description of the array, and which allows us to build up the formal theory of the minimal model outlined in Chapter 1. We will restrict ourselves to presenting the key arguments of the calculation, with the full technical detail in Appendix A.

2.2 Collective optical response

2.2.1 Cooperative radiative response

We note that a general wavevector $\mathbf{k} = (k_x, k_y, k_z)$ can be decomposed as $\mathbf{k} = \mathbf{k}_\parallel + k_z\hat{\mathbf{z}}$, where $\mathbf{k}_\parallel = (k_x, k_y, 0)$ is the component of $\mathbf{k}$ in the lattice plane. We will consider incident fields of the form

$$\mathbf{E}_0(\mathbf{r}) = \sum_{\mathbf{k}_\parallel} \mathbf{E}_{0,\mathbf{k}_\parallel}\mathrm{e}^{\mathrm{i}\mathbf{k}_\parallel\cdot\mathbf{r}}\mathrm{e}^{\mathrm{i}k_z z}\,, \tag{2.3}$$

where we assume that the plane wave amplitudes $\mathbf{E}_{0,\mathbf{k}_\parallel}$ lie entirely in the xy-plane. Fourier transforming the dipole equations (2.1), we are simply able to read off the self-consistent formal solution

$$\mathbf{d}(\mathbf{k}_\parallel) = \frac{4\pi^2\alpha}{Na^2}\left(\mathbb{1} - \frac{4\pi^2\alpha}{\lambda^2\varepsilon_0}\mathbf{g}(\mathbf{k}_\parallel)\right)^{-1} \cdot \sum_{\mathbf{q}_\parallel} \mathbf{E}_{0,\mathbf{q}_\parallel}\delta^{(2)}(\mathbf{q}_\parallel - \mathbf{k}_\parallel)\,, \tag{2.4}$$

where $\mathbf{g}(\mathbf{k}_\parallel) = \sum_{i\neq 0}\mathbf{G}(\omega,\mathbf{R}_i)\mathrm{e}^{-\mathrm{i}\mathbf{k}_\parallel\cdot\mathbf{R}_i}$ with $\mathbf{R}_0 = (0,0)$. This already encodes the first important qualitative point regarding the collective response of the array: an incident plane wave can only excited a collective mode at the same in-plane wavevector $\mathbf{k}_\parallel$ as its own.

This observation motivates us to write the Fourier decomposition of the dipoles $\mathbf{d}_i$ in a form more closely resembling the plane wave decomposition (2.3), as $\mathbf{d}_i = \sum_{\mathbf{k}_\parallel}\mathbf{d}_{0,\mathbf{k}_\parallel}\mathrm{e}^{\mathrm{i}\mathbf{k}_\parallel\cdot\mathbf{R}_i}$, where the sum is performed over the same wavevectors as for the incident field and where $\mathbf{d}_{0,\mathbf{k}_\parallel} = \boldsymbol{\alpha}_e(\mathbf{k}_\parallel)\cdot\mathbf{E}_{0,\mathbf{k}_\parallel}$ with

$$\boldsymbol{\alpha}_e(\mathbf{k}_\parallel) = -\frac{3\varepsilon_0}{4\pi^2}\lambda_0^3\frac{\Gamma_0/2}{\Delta + (\lambda_0/\lambda)^3\boldsymbol{\Delta}_e(\mathbf{k}_\parallel) + \mathrm{i}(\lambda_0/\lambda)^3\boldsymbol{\Gamma}_e(\mathbf{k}_\parallel)/2}\,. \tag{2.5}$$

By comparison with eq. (2.2), it is clear that $\boldsymbol{\alpha}_e(\mathbf{k}_\parallel)$ represents an effective polarisability, which is no longer isotropic, and that the interaction of the light with the array leads to a collective radiative response characterised by a cooperative frequency shift $\boldsymbol{\Delta}_e$ and a cooperative radiative decay rate $\boldsymbol{\Gamma}_e$,

$$\boldsymbol{\Delta}_e(\mathbf{k}_\parallel) = \frac{3\lambda\Gamma_0}{2}\,\mathrm{Re}\mathbf{g}(\mathbf{k}_\parallel) \tag{2.6}$$

$$\boldsymbol{\Gamma}_e(\mathbf{k}_\parallel) = 3\lambda\Gamma_0\,\mathrm{Im}\mathbf{g}(\mathbf{k}_\parallel) + \Gamma_0\,. \tag{2.7}$$

In fact, we are able to obtain a more convenient form of the cooperative linewidth (2.7). We make the simplifying assumption that $\mathbf{E}_0(\mathbf{r}) = E_0(\mathbf{r})\hat{\mathbf{x}}$ so that $\mathbf{d}_i = d_i\hat{\mathbf{x}}$. Then the cooperative linewidth becomes

$$\Gamma_{e,xx}(\mathbf{k}_\parallel) = \sum_{\mathbf{G}} \underbrace{\frac{3\pi\Gamma_0}{a^2k^3}\frac{k^2 - |\mathbf{k}_\parallel - \mathbf{G}|_x^2}{\sqrt{k^2 - |\mathbf{k}_\parallel - \mathbf{G}|^2}}}_{\Gamma_{xx}|_{\mathbf{k}_\parallel,\mathbf{G}}}\,. \tag{2.8}$$

where $\boldsymbol{\Gamma}|_{\mathbf{k}_\parallel,\mathbf{G}}$ denotes the 'partial decay rate' for the diffraction associated with the reciprocal vector $\mathbf{G}$. We can alternatively write $\Gamma_{e,xx}(\mathbf{k}_\parallel) = \sum_m \Gamma_{xx}|_{\mathbf{k}_\parallel,\mathbf{G}_m}$, where $\mathbf{G}_m\cdot\mathbf{R}_i = 2\pi M$ with $M\in\mathbb{Z}$ unique for each pair $m,i\in\mathbb{Z}$. We refer to m as the *diffraction order*, and on the square lattice we note that we can simply identify $m\sim(m_x,m_y)$ with $\mathbf{G}_m = (2\pi/a)(m_x\hat{\mathbf{x}} + m_y\hat{\mathbf{y}})$ (for $m_x,m_y\in\mathbb{Z}$) [24].

2.2.2 Scattered electric field

So far our discussion of the optical response has been focused entirely on the atoms, however a classical analogue of the input-output relation for the electric field introduced in the previous section are readily obtained by substituting $\mathbf{d}_i = \alpha_{e,xx}(\mathbf{k}_\parallel)E_{0,\mathbf{k}_\parallel}\mathrm{e}^{\mathrm{i}\mathbf{k}_\parallel\cdot\mathbf{R}_i}\hat{\mathbf{x}}$ into the dipole equations. Using the same arguments as above, the scattered field due to an incident plane-wave with in-plane momentum $\mathbf{k}_\parallel$ reads

$$E_{\mathrm{sc},\mathbf{k}_\parallel}(\mathbf{r}) = \alpha_{e,xx}(\mathbf{k}_\parallel)E_{0,\mathbf{k}_\parallel}\frac{k^3}{3\pi\varepsilon_0\Gamma_0}\sum_m \frac{\mathrm{i}\Gamma_{xx}|_{\mathbf{k}_\parallel,\mathbf{G}_m}}{2}\mathrm{e}^{\mathrm{i}k_z|z|}\mathrm{e}^{\mathrm{i}(\mathbf{k}_\parallel+\mathbf{G}_m)\cdot\mathbf{r}_\parallel}\,. \tag{2.9}$$

This expression emphasises the fact that the array scatters back into the mode of the incident wave, which is the second crucial qualitative observation.

With reference to eq. (2.8), we note that for a diffraction order m to contribute to the cooperative linewidth, the associated partial decay rate $\Gamma_{xx}|_{\mathbf{k}_\parallel,\mathbf{G}_m}$ must be imaginary according to eq. (2.7). By eq. (2.8), this imposes the condition $k > |\mathbf{k}_\parallel - \mathbf{G}_m|$, which limits the number of diffraction orders that participate in the radiative response. In fact, this condition amounts to the requirement that the field propagate out of the lattice plane [24]. Therefore in eq. (2.9), for diffraction orders m with $k < |\mathbf{k}_\parallel - \mathbf{G}_m|$ the scattered field becomes *evanescent*, i.e. short-range and non-propagating [59].

2.3 Response at normal incidence

We now want to consider the special case of a normally incident wave, i.e. the case where $\mathbf{k}_\parallel = 0$, leaving only a single incident plane wave mode with amplitude $\mathbf{E}_{0,\mathbf{k}_\parallel=0}$ which we choose as $\mathbf{E}_{0,\mathbf{k}_\parallel=0} = E_0\hat{\mathbf{x}}$ such that the incident field is simply a plane wave $\mathbf{E}_0(z) = E_0 \mathrm{e}^{\mathrm{i}k_z z}\hat{\mathbf{x}}$.

2.3.1 Effective description

At normal incidence, the cooperative response of the 2D array is actually captured by a simple effective model: The fact that an incident plane wave with $\mathbf{k}_\parallel = 0$ can only excite collective modes with $\mathbf{k}_\parallel = 0$ as well implies that, in the linear optics regime, the light only couples only to a single spin-wave state, $|\psi_{\mathbf{k}_\parallel=0}\rangle$. In the single-excitation subspace, the atomic spin model Hamiltonian which we can construct for the 2D array is therefore diagonal in the 2-dimensional basis of states $\{|G\rangle, |E\rangle\}$ with

$$\begin{aligned} |G\rangle &\equiv |g\rangle^{\otimes N} \\ |E\rangle &\equiv |\psi_{\mathbf{k}_\parallel=0}\rangle = \frac{1}{\sqrt{N}} \sum_i \hat{\sigma}_i^+ |g\rangle \,. \end{aligned} \tag{2.10}$$

This means we can think of the array at normal incidence as an effective single-mode system with ground state $|G\rangle$ and excited state $|E\rangle$, resonance frequency $\omega_{\mathrm{coop}} \equiv \omega_0 - \mathbf{\Delta}_{e,xx}(\mathbf{k}_\parallel = 0)$, and radiative linewidth $\Gamma_{\mathrm{coop}} \equiv \Gamma_{e,xx}(\mathbf{k}_\parallel = 0)$. This effective description is depicted in Fig. 2.2c.

2.3.2 Cooperative linewidth

In fact, at normal incidence we can obtain the cooperative linewidth Γ_{coop} analytically. Specifically, if we assume $a < \lambda/2$, only the zero diffraction order ($m = 0$ i.e. $\mathbf{G} = 0$) contributes to the radiative response. Substituting $\mathbf{k}_\parallel = \mathbf{G} = 0$ in eq. (2.8),

$$\Gamma_{\mathrm{coop}} = \frac{3\Gamma_0}{4\pi} \left(\frac{\lambda_0}{a}\right)^2 . \tag{2.11}$$

The cooperative frequency shift $\mathbf{\Delta}_{e,xx}(\mathbf{k}_\parallel = 0)$ can be computed numerically [24, 73–75], but its specific value (a small fraction of the bare atomic frequency ω_0) is not of importance here.

2.3.3 Scattered electric field

To characterise the optical properties of our effective single-mode system, we then apply the same considerations we used to arrive at eq. (2.11) to the expression for the scattered field (2.9), whereby

$$E_{\mathrm{sc},\mathbf{k}_\parallel=0}(z) \approx -\frac{\mathrm{i}\Gamma_{\mathrm{coop}}/2}{\Delta_{\mathrm{coop}} + \mathrm{i}(\Gamma_{\mathrm{coop}} + \Gamma_0)/2} E_0 \mathrm{e}^{\mathrm{i}k_z|z|}\,, \tag{2.12}$$

having assumed that $(\lambda_0/\lambda)^3 \approx 1$ for small detuning and defined $\Delta_{\mathrm{coop}} = \omega - \omega_{\mathrm{coop}}$. At a normal scattering interface, the total field then decomposes into the incident field $E_{0,\mathbf{k}=0}$ as well as the components $E^{\pm}_{\mathrm{sc},\mathbf{k}_\parallel=0}$ of the scattered field $E_{\mathrm{sc},\mathbf{k}_\parallel=0}$ propagating into the $\pm z$ direction (see Fig. 2.1c). We can calculate the associated amplitudes of transmission t and reflection r as

$$t = \lim_{z\to+\infty} \frac{E^{+}_{\mathrm{sc},\mathbf{k}_\parallel=0}(z)}{E_0(z)} \quad \text{and} \quad r = \lim_{z\to-\infty} \frac{E^{-}_{\mathrm{sc},\mathbf{k}_\parallel=0}(z)}{E^{*}_0(z)}\,, \tag{2.13}$$

which are related by $t = 1 + r$. By examination of eq. (2.12), it is simple to see that

$$t(\Delta_{\mathrm{coop}}) = \frac{2\mathrm{i}\Delta_{\mathrm{coop}}}{\Gamma_{\mathrm{coop}} - 2\mathrm{i}\Delta_{\mathrm{coop}}} \quad \text{and} \quad r(\Delta_{\mathrm{coop}}) = \frac{-\Gamma_{\mathrm{coop}}}{\Gamma_{\mathrm{coop}} - 2\mathrm{i}\Delta_{\mathrm{coop}}}\,. \tag{2.14}$$

In particular, we note that $r(\Delta_{\mathrm{coop}} = 0) = -1$ i.e. on-resonance the array becomes perfectly reflecting with a phase shift of π. We also note that close to resonance, the transmission coefficient, while small, still implies a large phase shift of $\sim \pi/2$ for transmitted light.

This cooperative resonance agrees with numerical studies predicting a drastically enhanced optical cross-section for fine-tuned ordering and lattice spacing in atomic arrays and relating this to a subradiant collective mode of the array [21]. The perfect reflectivity is a striking example of the impact of order on multiple scattering, since for disordered atomic systems, multiple scattering actually greatly impedes optical extinction [76–79]. Even more fundamentally, it underlines the importance of accounting for non-perturbative multiple scattering: disregarding multiple scattering effects, $r = -1$ could only be achieved in the limit of infinite atomic density [80].

3 Refractive index in 3D

Having discussed the simpler and better understood problem of multiple scattering in 2D, we now return to our initial problem of a 3D atomic array. We will single out the z-direction as the direction of propagation of the incident electric field and the x-direction as its direction of polarisation, so that we consider incident plane waves at wavevector $\mathbf{k} = k\hat{\mathbf{z}}$ of the form $\mathbf{E}_0(z) = E_0\mathrm{e}^{\mathrm{i}kz}\hat{\mathbf{x}}$, as in the case above. As for the 2D case, we will require that the crystal is perfectly translationally invariant and that the atoms are non-absorbing, in which case incident light will propagate losslessly in the atomic crystal, implying a purely real and isotropic refractive index n. Within the crystal, incident plane waves will scatter into collective spin-wave excitations propagating at a modified wavevector $\mathbf{k}' = n\mathbf{k}$. The refractive index can then be inferred from the total phase shift $\Delta\varphi = nkL_z$ incurred by a plane wave after it has propagated through the crystal, where L_z denotes the length of the crystal in the z-direction.

3.1 Effective 1D description

As described in Chapter 1, we adopt the perspective of the 3D crystal as a layering of m equidistant planar arrays (see Fig. 2.2a). If we choose these to be separated by $a_z \gg a$, for normally incident light this is equivalent to a line of m single-mode emitters, since the evanescent field from each emitter can be ignored and the emitters couple only via the scattered incident plane wave (see Fig. 2.2b). The scattering is characterised by the reflectivity and transmittivity derived above. This is the reduction of the multiple scattering aspect of the problem to 1D promised in Chapter 1. If we consider near-resonant incident light, then the propagation of light through the crystal simply amounts to a phase $\sim \pi$ picked up at each of the emitters, amounting to a total phase of $\Delta\varphi \sim m\pi$ picked up after propagation through the full crystal. This implies a refractive index $n \sim \lambda_0/a_z$, which leads to the scaling in Fig. 1.1b.

3.2 Quantum chemistry effects

We argued in Chapter 1 that our minimal model allows us to incorporate the effects of quantum chemistry in a simple way. We can now formalise this idea using the effective single-mode description of the 2D arrays: if we include an inelastic decay channel with linewidth Γ in our single-mode model,

$$r(\Delta_{\text{coop}}) = -\frac{\Gamma_{\text{coop}}}{\Gamma_{\text{coop}} + \Gamma - 2\mathrm{i}\Delta_{\text{coop}}}\,, \tag{3.1}$$

leading to imperfect reflectivity. According to the above reasoning, since $r \neq -1$ implies a lower phase shift at each 2D plane this will lead to a lower value of n. One possible source of such an additional linewidth Γ could be imperfections not captured by our idealised atomic array model (e.g. atomic motion), and indeed such effects are often heuristically cited as the reason for the saturation of n. *Instead, we will argue that the inelastic linewidth is associated with fundamental processes which emerge with the onset of quantum chemistry, leading to a saturation of the refractive index at densities where these processes become non-negligible.*

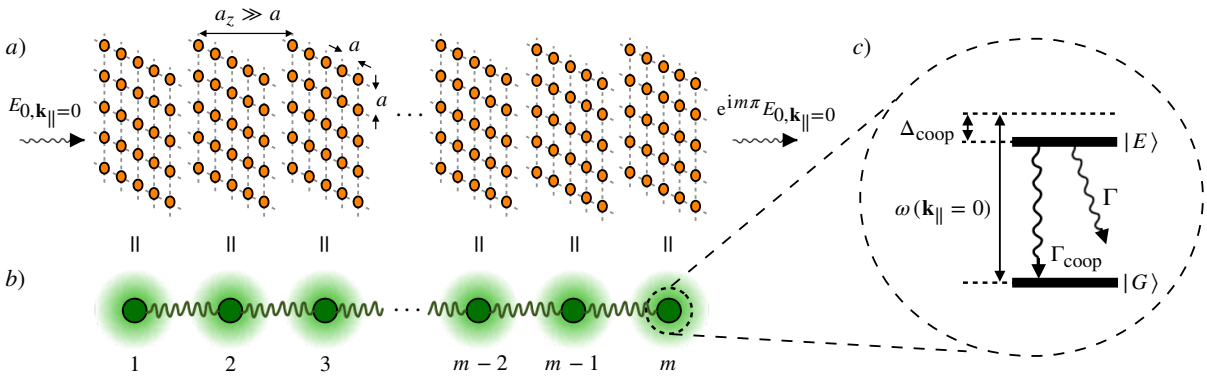

Figure 2.2 – 3D atomic array. **a)** Structure of a 3D atomic crystal in terms of square atomic arrays and phase shift of a normally incident plane wave propagating through the crystal. **b)** Equivalent description of the 3D crystal as a chain of effective single-mode emitters. The short-range evanescent and propagating fields are indicated as green shaded regions and plane waves. **c)** Structure of the effective single-mode emitters.

Chapter 3

Quantum chemistry I: *Minimal 2D model*

In order to identify quantum chemistry effects which introduce inelastic scattering processes in the manner outlined previously, we now move to the regime where the atomic density within our 2D arrays is sufficiently high for quantum chemistry effects to become non-negligible. To study the optical properties of the arrays in this new regime, where the discrete scatterer assumption of the previous chapter breaks down, our starting point must be the formal description of the array, including the electrostatic interactions between the atoms as well as the coupling of each atom to the electromagnetic field.

While the two-level atom model of the previous chapter is valid for any number of closed singlet-triplet atomic transitions [21] (e.g. in alkaline-earth-metal atoms [81, 82]), we restrict ourselves to the simple case of hydrogen atoms (see Appendix C). In particular, we will consider only a single atomic transition between $1s$ and $2p$ states, which we denote as $|s\rangle$ and $|p\rangle$. This is consistent with the assumption of the single-excitation regime we introduced above. For consistency with the preceding notation, we will denote the resonance frequency and wavelength of the transition by ω_0 and λ_0.

1 Electronic Hamiltonian

Based on the perspective of quantum chemistry, we set up the problem of a hydrogen atom lattice from the formal Hamiltonian for N interacting electrons (charge q) on a background of protons at fixed positions $\mathbf{R}_i$ $(i = 1, \ldots, N)$, coupled to an electromagnetic field with vector potential $\mathbf{A}(\mathbf{r})$. This formulation of the problem is exact up to the Born-Oppenheimer approximation. We assume that each electron is localised around a single atomic site, allowing us to label the electrons by the atomic indices. In the language of first quantisation, the i-th electron is characterised by position $\hat{\mathbf{r}}_i$ and momentum $\hat{\mathbf{p}}_i$, obeying the commutator $[\hat{\mathbf{r}}_i, \hat{\mathbf{p}}_j] = \mathrm{i}\hbar\delta_{ij}$. The full Hamiltonian describing the lattice can then be written in the *minimal coupling form* [67] as

$$H = \frac{1}{2m}\sum_i \left(\hat{\mathbf{p}}_i - q\hat{\mathbf{A}}(\hat{\mathbf{r}}_i)\right)^2 - \sum_{ij} V(|\hat{\mathbf{r}}_i - \mathbf{R}_j|) + \frac{1}{2}\sum_{ij\neq i} V(|\hat{\mathbf{r}}_i - \hat{\mathbf{r}}_j|)\,. \tag{1.1}$$

The first term of the Hamiltonian corresponds with a sum of gauge-invariant single-particle Hamiltonians for a free electron interacting with a quantised electromagnetic field, while the second and third terms encode the electron-proton and electron-electron interactions, respectively, with Coulomb potential

$$V(|\mathbf{r} - \mathbf{r}'|) = \frac{q^2}{4\pi\varepsilon_0}\frac{1}{|\mathbf{r} - \mathbf{r}'|}\,. \tag{1.2}$$

1.1 Gauge fixing

The quadratic atom-field coupling term in (1.1) can be expanded in any gauge but it is most convenient to choose the *Coulomb gauge* $\boldsymbol{\nabla}\cdot\hat{\mathbf{A}}(\mathbf{r})=0$. We note that the Coulomb gauge is essentially the statement that $\hat{\mathbf{p}}\cdot\hat{\mathbf{A}}(\mathbf{r})=0$ expressed in a position basis $|\mathbf{r}\rangle$ where $\langle\mathbf{r}|\hat{\mathbf{p}}|\psi\rangle=-\mathrm{i}\hbar\boldsymbol{\nabla}\langle\mathbf{r}|\psi\rangle$. Noting that

$$\boldsymbol{\nabla}\cdot\hat{\mathbf{A}}\psi+\hat{\mathbf{A}}\cdot(\boldsymbol{\nabla}\psi)=(\boldsymbol{\nabla}\cdot\hat{\mathbf{A}})\psi+2\hat{\mathbf{A}}\cdot(\boldsymbol{\nabla}\psi)\xrightarrow[\boldsymbol{\nabla}\cdot\hat{\mathbf{A}}=0]{}2\hat{\mathbf{A}}\cdot(\boldsymbol{\nabla}\psi)\,, \tag{1.3}$$

we see that the Coulomb gauge simplifies the cross-terms in the expansion of the coupling term. Then,

$$H\approx\underbrace{\sum_i\frac{\hat{\mathbf{p}}_i^2}{2m}}_{T}\underbrace{-\frac{q}{m}\sum_i\hat{\mathbf{p}}_i\cdot\hat{\mathbf{A}}(\hat{\mathbf{r}}_i)}_{V}\underbrace{-\sum_{ij}V(|\hat{\mathbf{r}}_i-\mathbf{R}_j|)}_{U_p}\underbrace{+\frac{1}{2}\sum_{ij\neq i}V(|\hat{\mathbf{r}}_i-\hat{\mathbf{r}}_j|)}_{U_e}\,. \tag{1.4}$$

Here we have also made the approximation that the term quadratic in $\hat{\mathbf{A}}(\mathbf{r})$ is negligible. This is reasonable if we recall that we are working in the sub-wavelength regime $a<\lambda_0$. Since $a\gg a_0$, this automatically places us in the *long-wavelength limit* $\lambda_0\gg a_0$, under which we are able to approximate that $\hat{\mathbf{A}}(\hat{\mathbf{r}}_i)\approx\hat{\mathbf{A}}(\mathbf{R}_i)$ [67]. This assumption only becomes invalid for particularly high-energy photons (e.g. x-rays) or fields that are strong enough to force the electron far from the nucleus (e.g. ionizing fields). Since the quadratic term then no longer couples to the atomic states, we can safely ignore it. The new form (1.4) of the Hamiltonian neatly discerns the different contributions to the Hamiltonian, separating not only the electron-proton (U_p) and electron-electron (U_e) electrostatic interactions, but also a purely kinetic term (T) and the term capturing the atom-field interaction (V).

1.2 Electromagnetic field

As a final formal point, we note that we will treat the electromagnetic field from the very beginning using second quantisation, i.e. we will assume that the vector potential admits the mode decomposition [83]

$$\hat{\mathbf{A}}(\mathbf{r})=\sum_{\mathbf{k}}\mathbf{f}_{\mathbf{k}}\left(\hat{a}_{\mathbf{k}}\mathrm{e}^{\mathrm{i}\mathbf{k}\cdot\mathbf{r}}+\mathrm{h.c.}\right)\quad\text{with}\quad\mathbf{f}_{\mathbf{k}}=\left(\frac{\hbar}{2\omega_{\mathbf{k}}\varepsilon_0 V}\right)^{1/2}\hat{\mathbf{e}}_{\mathbf{k}}\,, \tag{1.5}$$

where $\omega_{\mathbf{k}}=c|\mathbf{k}|$ is the photonic dispersion relation and $\hat{\mathbf{e}}_{\mathbf{k}}$ is the unit polarisation vector for the transverse field, defined such that $\hat{\mathbf{e}}_{\mathbf{k}}\cdot\mathbf{k}=0$. The operators $\hat{a}^\dagger_{\mathbf{k}},\hat{a}_{\mathbf{k}}$ are the bosonic creation and annihilation operators for photons at wavevector $\mathbf{k}$, obeying the canonical commutation relations

$$\begin{aligned}[\hat{a}_{\mathbf{k}},\hat{a}_{\mathbf{k}'}]&=[\hat{a}^\dagger_{\mathbf{k}},\hat{a}^\dagger_{\mathbf{k}'}]=0\\ [\hat{a}_{\mathbf{k}},\hat{a}^\dagger_{\mathbf{k}'}]&=\delta_{\mathbf{k}\mathbf{k}'}\,.\end{aligned} \tag{1.6}$$

A multi-photon state containing $n_{\mathbf{k}}$ photons at wavevector $\mathbf{k}$ is constructed using these operators with respect to the bosonic vacuum $|0_a\rangle$ (defined by $\hat{a}_{\mathbf{k}}|0_a\rangle=0$) as [83]

$$|n_{\mathbf{k}_1},n_{\mathbf{k}_2},\ldots\rangle=\frac{\left(\hat{a}^\dagger_{\mathbf{k}_1}\right)^{n_{\mathbf{k}_1}}}{\sqrt{n_{\mathbf{k}_1}}}\frac{\left(\hat{a}^\dagger_{\mathbf{k}_2}\right)^{n_{\mathbf{k}_2}}}{\sqrt{n_{\mathbf{k}_2}}}\ldots|0_a\rangle\,. \tag{1.7}$$

2 Bloch & Wannier electrons

2.1 Bloch electrons

We now turn to the problem of diagonalising the Hamiltonian (1.4). Neglecting for a moment the electron-electron interaction, the Hamiltonian (1.1) decomposes as $H = \sum_i h_i$ into a sum of single-particle Hamiltonians defined for each atomic electron according to

$$h = \frac{\hat{\mathbf{p}}^2}{2m} - V_{\text{nuc}}(\hat{\mathbf{r}})\,, \tag{2.1}$$

which describe the motion of an electron in the potential $V_{\text{nuc}}(\mathbf{r}) = \sum_i V(|\mathbf{r}-\mathbf{R}_i|)$ formed by the protons on the lattice. Notably, the potential $V_{\text{nuc}}(\mathbf{r})$ inherits the periodicity of the lattice: for a general lattice vector $\mathbf{R} = m_x\mathbf{a}_1 + m_y\mathbf{a}_2$ ($m_x, m_y \in \mathbb{Z}$), it satisfies $V_{\text{nuc}}(\mathbf{r}+\mathbf{R}) = V_{\text{nuc}}(\mathbf{r})$.

The form of the eigenfunctions $\phi_{\mathbf{k}\alpha}(\mathbf{r}) = \langle\mathbf{r}|\phi_{\mathbf{k}\alpha}\rangle$ (eigenvalue $E_{\mathbf{k}\alpha}$) of a generic many-body Hamiltonian which decomposes in this way into single-particle Hamiltonians with a periodic potential is dictated by Bloch's Theorem, which states that $\phi_{\mathbf{k}\alpha}(\mathbf{r}) = u_{\mathbf{k}\alpha}(\mathbf{r})\mathrm{e}^{\mathrm{i}\mathbf{k}\cdot\mathbf{r}}$ with crystal momentum $\mathbf{k}$ lying in the *First Brillouin Zone* (1BZ) and $u_{\mathbf{k}\alpha}(\mathbf{r}) = u_{\mathbf{k}\alpha}(\mathbf{r}+\mathbf{R})$. Such eigenstates describe electrons completely delocalised across the crystal, where α labels distinct bands of electrons [68, 84]. In our particular case, α subsumes both an index μ, which labels the state of an electron with respect to the atomic energy levels, and the spin index $\sigma \in \{\uparrow,\downarrow\}$: when the inter-atomic spacing a is decreased, the atomic μ-orbitals between sites hybridise to form two degenerate delocalised orbitals (i.e. bands) each, with the degeneracy associated with different spin values. The Hamiltonian therefore has Bloch eigenstates $|\phi_{\mathbf{k}\mu\sigma}\rangle$, associated with spin-$\sigma$ electrons in the μ-orbital band, at crystal momentum $\mathbf{k}$.

2.2 Wannier electrons

The plane wave structure of the Bloch eigenfunctions $|\phi_{\mathbf{k}\mu\sigma}\rangle$ motivates the construction of a localised electron wavepacket by a suitable superposition of Bloch modes with a sufficiently broad range of crystal momenta. Explicitly, we define a transformation between delocalised Bloch states $|\phi_{\mathbf{k}\mu\sigma}\rangle$ and localised *Wannier states* $|\phi_{i\mu\sigma}\rangle$ [85] according to

$$\begin{aligned} |\phi_{i\mu\sigma}\rangle &= \frac{1}{\sqrt{N}}\sum_{\mathbf{k}\in 1\text{BZ}} \mathrm{e}^{-\mathrm{i}\mathbf{k}\cdot\mathbf{R}_i}|\phi_{\mathbf{k}\mu\sigma}\rangle \\ |\phi_{\mathbf{k}\mu\sigma}\rangle &= \frac{1}{\sqrt{N}}\sum_{i} \mathrm{e}^{\mathrm{i}\mathbf{k}\cdot\mathbf{R}_i}|\phi_{i\mu\sigma}\rangle \end{aligned} \tag{2.2}$$

To be precise, the Wannier states have the form $|\phi_{i\mu\sigma}\rangle = |\phi_{i\mu}\rangle|\sigma\rangle$. In a position basis $|\mathbf{r}\rangle$, the Wannier wavefunctions $\phi_{i\mu}(\mathbf{r}) = \langle\mathbf{r}|\phi_{i\mu}\rangle$ are identical in the sense that $\phi_{i\mu}(\mathbf{r}) = \phi_\mu(\mathbf{r}-\mathbf{R}_i)$, where we assume that $\phi_\mu(\mathbf{r})$ is strongly localised in $\mathbf{r}$. Since the choice of Wannier functions is actually non-unique [86, 87], we will assume for the sake of concreteness so-called *maximally localised Wannier functions* [88], which are known to be exponentially localised [89]. At very short distances from the atomic site, the Wannier orbitals are practically indistinguishable from the underlying hydrogenic orbitals, which is a property that we will make use of repeatedly in Chapter 5.

Term	Element	Integral expression
T	$T\|_{ij\mu\mu'}$	$-\frac{\hbar^2}{2m}\int d^3\mathbf{r}\ \phi^*_\mu(\mathbf{r}-\mathbf{R}_i)\nabla^2_r\phi_{\mu'}(\mathbf{r}-\mathbf{R}_j)$
U_p	$U_p\|_{ijk\mu\mu'}$	$-\frac{q^2}{4\pi\varepsilon_0}\int d^3\mathbf{r}\ \phi^*_\mu(\mathbf{r}-\mathbf{R}_i)\frac{1}{\|\mathbf{r}-\mathbf{R}_k\|}\phi_{\mu'}(\mathbf{r}-\mathbf{R}_j)$
U_e	$U_e\|_{ijkl\mu\mu'\nu\nu'}$	$+\frac{q^2}{8\pi\varepsilon_0}\int d^3\mathbf{r}\ \phi^*_\mu(\mathbf{r}-\mathbf{R}_i)\left(\int d^3\mathbf{r}'\phi^*_\nu(\mathbf{r}'-\mathbf{R}_j)\frac{1}{\|\mathbf{r}-\mathbf{r}'\|}\phi_{\nu'}(\mathbf{r}'-\mathbf{R}_l)\right)\phi_{\mu'}(\mathbf{r}-\mathbf{R}_k)$
V	$V\|_{ij\mu\mu';\mathbf{k}}$	$+\frac{i\hbar q}{m}\mathbf{f}_\mathbf{k}\cdot\int d^3\mathbf{r}\ \mathrm{e}^{i\mathbf{k}\cdot\mathbf{R}_i}\phi^*_\mu(\mathbf{r}-\mathbf{R}_i)\boldsymbol{\nabla}\phi_{\mu'}(\mathbf{r}-\mathbf{R}_j)$

Table 1 – Second quantisation matrix elements. The table shows a summary of the matrix elements associated with the kinetic (T), electrostatic (U_p+U_e) and atom-field coupling (V) terms in the Hamiltonian, as well as their explicit expressions in terms of the Wannier functions $\phi_{i\mu}(\mathbf{r})=\phi_\mu(\mathbf{r}-\mathbf{R}_i)$. Note than in the matrix element for V we have made the long-wavelength approximation

3 Second quantisation

In the framework of solid state physics or quantum chemistry, the suitable language in which to tackle a many-body Hamiltonian such as (1.4) is the formalism of second quantisation. We therefore define a set of fermionic creation operators $\hat{c}^\dagger_{i\mu\sigma}$, which act on a fermionic vacuum state $|0_c\rangle$ (defined by $\hat{c}_{i\mu\sigma}|0_c\rangle=0$) to create a Wannier electron with spin σ in the μ-orbital localised around the i-th site as $|\phi_{i\mu\sigma}\rangle=\hat{c}^\dagger_{i\mu\sigma}|0_c\rangle$, and which obey canonical anticommutation relations

$$\begin{aligned}\{\hat{c}_{i\mu\sigma},\hat{c}_{j\mu'\sigma'}\}&=\{\hat{c}^\dagger_{i\mu\sigma},\hat{c}^\dagger_{j\mu'\sigma'}\}=0\\ \{\hat{c}_{i\mu\sigma},\hat{c}^\dagger_{j\mu'\sigma'}\}&=\delta_{ij}\delta_{\mu\mu'}\delta_{\sigma\sigma'}\,.\end{aligned}\tag{3.1}$$

Within the formalism of second quantisation, an n-body operator $\hat{O}$ can be written in terms of the fermionic operators $\hat{c}_{i\mu\sigma},\hat{c}^\dagger_{i\mu\sigma}$ according to the prescription [90]

$$\hat{O}=\sum_{\substack{i_1\ldots i_n\\ i'_1\ldots i'_n}}\sum_{\substack{\mu_1\ldots\mu_n\\ \mu'_1\ldots\mu'_n}}\sum_{\substack{\sigma_1\ldots\sigma_n\\ \sigma'_1\ldots\sigma'_n}}\langle\phi_{i_1\mu_1\sigma_1}\ldots|\hat{O}|\phi_{i'_1\mu'_1\sigma'_1}\ldots\rangle\ \hat{c}^\dagger_{i_1\mu_1\sigma_1}\ldots\hat{c}^\dagger_{i_n\mu_n\sigma_n}\hat{c}_{i'_n\mu'_n\sigma'_n}\ldots\hat{c}_{i'_1\mu'_1\sigma'_1}\,.\tag{3.2}$$

In particular, applying this to the electronic Hamiltonian, we arrive at the second quantised Hamiltonian which provides the starting point for an analysis of the 2D lattice using standard methods from quantum chemistry and condensed matter theory:

$$\begin{aligned}H=&\underbrace{\sum_{ij}\sum_{\mu\nu}\sum_{\sigma}T|_{ij\mu\nu}\hat{c}^\dagger_{i\mu\sigma}\hat{c}_{j\nu\sigma}}_{T}\\ &+\underbrace{\sum_{ijk}\sum_{\mu\nu}\sum_{\sigma}U_p|_{ijk\mu\nu}\hat{c}^\dagger_{i\mu\sigma}\hat{c}_{j\nu\sigma}}_{U_p}+\underbrace{\sum_{ijkl}\sum_{\mu\mu'\nu\nu'}\sum_{\sigma\sigma'}U_e|_{ijkl\mu\mu'\nu\nu'}\hat{c}^\dagger_{i\mu\sigma}\hat{c}^\dagger_{j\nu\sigma'}\hat{c}_{l\nu'\sigma'}\hat{c}_{k\mu'\sigma}}_{U_e}\\ &+\underbrace{\sum_{ij}\sum_{\mu\nu}\sum_{\sigma}\sum_{\mathbf{k}}\left(V|_{ij\mu\nu;\mathbf{k}}\hat{a}_\mathbf{k}\hat{c}^\dagger_{i\mu\sigma}\hat{c}_{j\nu\sigma}+\text{h.c.}\right)}_{V}\end{aligned}\tag{3.3}$$

The matrix elements associated with each of the interaction terms can be written explicitly in terms of real space overlap integrals involving the Wannier functions $\phi_{i\mu\sigma}$ as shown in Table 1.

Chapter 4

Quantum chemistry II: *Ground state*

In this chapter, we begin our analysis of the model introduced in the preceding chapter by studying its ground state. We first derive an effective Hamiltonian for the ground state manifold of the model (Section 1.1) and analyse its structure, identifying in particular a tension between the spin and charge sectors (Section 1.2).

We highlight one specific characteristic effect associated with the interplay between the spin and charge sectors, namely the buildup of density-density correlations in the ground state. The resulting imbalance of electrons on individual sites has a direct effect on the optical response of the lattice: atoms with an excess or deficit of electrons will not respond to light in the same way as an isolated hydrogen atom. To an incoming photon, the true ground state then resembles a lattice with random pairs of neighbouring atoms 'punched out' on those sites where there are holon-doublon pairs which do not participate in the collective optical response. The effective holes in the lattice scatter incident incoherently into all directions. *This suggests that the ground state charge fluctuations give rise to such fundamental inelastic scattering processes as contribute to the saturation of the refractive index.*

Denoting the fraction of sites with holes punched out as $2D/N$, where D is the *doublon occupancy* i.e. the average number of doubly occupied sites in the ground state, a reasonable estimate of the change in radiative response is that it introduces a new inelastic linewidth $\Gamma = (\sigma_{\text{eff}}/\sigma_{\text{sc}})(2D/N)\Gamma_{\text{coop}}$. Here, σ_{eff} and σ_{sc} denote the effective cross-sections of a punched out hole and an atom. In Chapter 6, we will show that σ_{eff} is actually significantly larger than σ_{sc}. *This implies that the holes punched out by the density-density correlations span a large number of lattice sites, i.e. a single punched out hole can break the collective optical response of a large number of surrounding atoms.*

In order to understand how this effect is 'activated' with the transition from the quantum optics limit to the quantum chemistry regime, we therefore round off this chapter by developing a formal quantum field theoretic description for the ground state manifold (Sections 2 and 3), which in particular allows us to derive an asymptotic value for D around the onset of quantum chemistry.

1 Ground state model

1.1 Effective Hamiltonian

In the absence of photon-mediated excitations to the p-orbital, the atomic electrons in the lattice will be confined to the lower-energy s-orbital. Starting from the full quantum chemistry Hamiltonian, the effective Hamiltonian on the ground state manifold then becomes

$$H = \sum_{ij}\sum_{\sigma} T|_{ijss}\hat{c}^{\dagger}_{i\sigma}\hat{c}_{j\sigma} + \sum_{ijk}\sum_{\sigma} U_p|_{ijkss}\hat{c}^{\dagger}_{i\sigma}\hat{c}_{j\sigma} + \sum_{ijkl}\sum_{\sigma\sigma'} U_e|_{ijklssss}\hat{c}^{\dagger}_{i\sigma}\hat{c}^{\dagger}_{j\sigma'}\hat{c}_{l\sigma'}\hat{c}_{k\sigma}\,, \tag{1.1}$$

where the orbital index $\mu = s$ is suppressed. For exponentially localised Wannier orbitals, we assume that only nearest-neighbour terms contribute significantly to the Hamiltonian. Under this assumption,

$$H \approx \mu\sum_i (\hat{n}_{i\uparrow}+\hat{n}_{i\downarrow}) \underbrace{-t\sum_{\langle i,j\rangle}\sum_{\sigma}\hat{c}^{\dagger}_{i\sigma}\hat{c}_{j\sigma}}_{H_K} + \underbrace{U\sum_i \hat{n}_{i\uparrow}\hat{n}_{i\downarrow}}_{H_U}\,. \tag{1.2}$$

We can identify the role of each of the three terms in this Hamiltonian: The first term controls the occupation number in the model via a chemical potential $\mu = T_{iiss} + U_p|_{iiss}$. Since we consider a fixed electron number N, we may ignore this term. The second term (H_K) induces a short-range tunnelling of electrons between neighbouring sites, well-known from solid state tight-binding models as *nearest-neighbour hopping* [68], with amplitude $t \equiv U_p|_{ijiss}$. If we assume periodic boundary conditions, it can be written as $H_K = -t\sum_{\langle i,j\rangle}\sum_{\sigma}\hat{c}^{\dagger}_{i\sigma}\hat{c}_{j\sigma} = -t\sum_{i,\boldsymbol{\delta},\sigma}\left(\hat{c}^{\dagger}_{i\sigma}\hat{c}_{i+\boldsymbol{\delta}\sigma} + \text{h.c.}\right)$, where we only sum over half of the connecting vectors, i.e. $\boldsymbol{\delta} \in \{\mathbf{a}_1, \mathbf{a}_2\}$. Finally, the third term (H_U) represents an energy penalty $U \equiv U_e|_{iiiissss}$ associated with the double occupancy of a site by two electrons. We note that this is only the on-site contribution of the third term in (1.1), while we have ignored the nearest-neighbour terms associated with matrix elements like $U_e|_{i+\boldsymbol{\delta}iiissss}$. We will see in the next chapter that these terms act to renormalise the value of t in the ground state manifold. Since we are assuming $a_0/a \ll 1$, we are working in the *strong coupling regime* $U \gg t$, i.e. the on-site interaction is large compared to the tunnelling.

1.1.1 Particle-hole symmetry

We make one more formal change in the Hamiltonian (1.2) to highlight the *particle-hole symmetry* [91] of the hopping term. Under the operator transformation $\hat{b}_{i\sigma} = (-1)^i\hat{c}^{\dagger}_{i\sigma}$, we can see that $\hat{b}^{\dagger}_{i\sigma}\hat{b}_{i\sigma} = (-1)^{2i}\hat{c}_{i\sigma}\hat{c}^{\dagger}_{i\sigma} = \hat{c}_{i\sigma}\hat{c}^{\dagger}_{i\sigma} = 1 - \hat{c}^{\dagger}_{i\sigma}\hat{c}_{i\sigma}$. The transformation therefore interchanges the number of particles (i.e. electrons) and holes (i.e. empty sites). Notably, on the square lattice H_K is invariant under such a transformation, however H_U is not. Since particle-hole symmetry is an important feature, for instance allowing for numerical approaches using Quantum Monte Carlo algorithms [92, 93], we write

$$H = -t\sum_{i,\boldsymbol{\delta},\sigma}\left(\hat{c}^{\dagger}_{i\sigma}\hat{c}_{i+\boldsymbol{\delta}\sigma} + \text{h.c.}\right) + U\sum_i\left(\hat{n}_{i\uparrow} - \frac{1}{2}\right)\left(\hat{n}_{i\downarrow} - \frac{1}{2}\right)\,. \tag{1.3}$$

This differs from our Hamiltonian only by a constant energy shift and a shift in the chemical potential, both of which are irrelevant for us, and is clearly now invariant under the particle-hole transformation.

1.1.2 Fermi-Hubbard model

We recognise (1.3) as the single-band *Fermi-Hubbard model* [94, 95] at half-filling (i.e. N electrons in a system of N sites). This equivalence between the effective low-energy Hamiltonian of an array of hydrogen atoms and the Fermi-Hubbard model has been confirmed by full quantum chemistry calculations in one dimension [96, 97], and we will assume that this holds also in the 2D case. The Hubbard model is the minimal model describing strongly-interacting electronic systems. It was first introduced to study the magnetic properties of transition metals [98, 99] but has more recently been a major workhorse for the study of transitions of conductors to a *Mott insulator phase* [100]. There has been extensive research on this topic, sparked by the experimental observation that some transition-metal show unexpected insulating behaviour [101] as a consequence of strong Coulombic repulsion of the electrons [102–104].

1.2 Spin and charge dynamics

Despite its simple structure, the Hubbard model is not exactly solvable in arbitrary dimensions. Analytical approaches exist in 1D [105] and infinite dimensions [106], and in two dimensions asymptotically exact solutions models have been constructed (which we will draw on here) [107–109]. Away from these limiting cases, one needs to resort to numerical methods (for a review, see e.g. Ref. [50]). The subtleties of strongly correlated electronic systems such as the Hubbard model reside for the most part in the interplay between the charge and spin degrees of freedoms associated with the electrons. In fact, a prime example of the effect of spin on charge dynamics is the ground state $|G\rangle$ of the Hubbard model in our strong-coupling regime of $U \gg t$, which is defined both by a charge and a spin configuration.

1.2.1 Ground state fluctuations

At zero order in t/U, the ground state charge distribution at half-filling is trivially the one which minimises H_U, i.e. the occupation of each site by exactly one electron, implying $|G\rangle \approx \hat{c}^\dagger_{1\sigma_1}\hat{c}^\dagger_{2\sigma_2}\dots\hat{c}^\dagger_{N\sigma_N}|\Omega\rangle$. At this order, the spin configuration $(\sigma_1, \sigma_2, \dots, \sigma_N)$ is irrelevant. However, at leading order in t/U, the ground state spin configuration becomes crucial: with every site occupied by one electron, an electron hopping to a neighbouring site incurs an energy penalty U, making such a process distinctly off-resonant (see Fig. 4.1). Therefore we consider the *virtual process* of an electron hopping to a neighbouring sites and back (intermittently violating energy conservation, see Fig. 4.1). Such virtual processes arise at second order in a perturbative treatment of the problem. It can be shown that the second-order perturbative energy correction due to a single virtual hopping event is $\propto -t^2/U$, thus reducing the ground state energy and making it energetically favourable for the ground state to host virtual hopping. By the Pauli exclusion principle, an electron can only hop to an occupied site if it has the opposite spin value to the electron already present on the site. Therefore, the most energetically favourable spin configuration is the antiferromagnetically (AF) ordered one. In this manner, the ground state charge fluctuations induce an effective spin interaction.

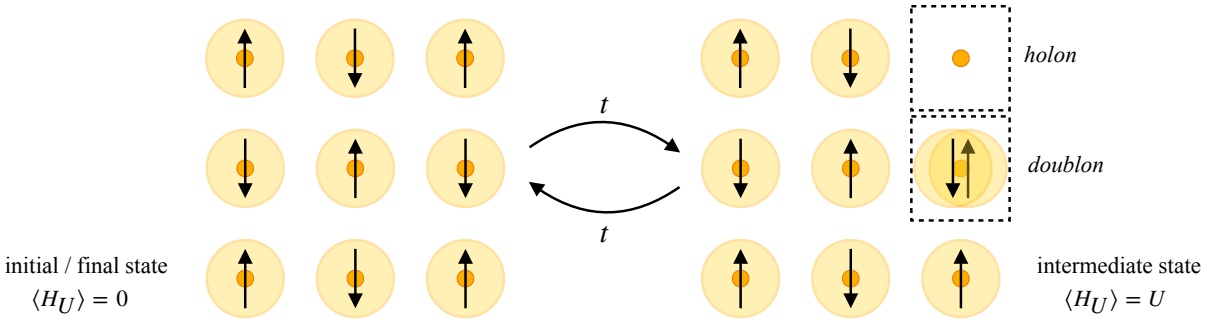

Figure 4.1 – Virtual hopping in the ground state. Diagrammatic representation of the off-resonant formation of a holon-doublon pair from an antiferromagnetically ordered initial state. The initial and final states belong to the low-energy sector (LES) of the model, while the intermediate state is marked by an energy difference U.

1.2.2 Heisenberg spin interaction

The above qualitative reasoning can be formalised in the spirit of Ref. [110], by projecting the eigenvalue equation of the full Hamiltonian onto the low-energy sector (LES) of the Hubbard model Hilbert space containing only the 2^N degenerate states where each site is singly occupied. To lowest order in t/U, the effective Hamiltonian in the LES becomes

$$H_{\text{eff}} = \frac{J}{2} \sum_{i,j} \left(\mathbf{S}_i \cdot \mathbf{S}_j - \frac{1}{4} \right) , \tag{1.4}$$

where $J = 4t^2/U > 0$ and $\mathbf{S}_i$ is the vector of spin operators $\mathbf{S}_i = (S_i^x, S_i^y, S_i^z)^T$ on the i-th site, defined in terms of the vector of Pauli matrices $\boldsymbol{\sigma} = (\sigma^x, \sigma^y, \sigma^z)^T$ as [111]

$$\mathbf{S}_i = \frac{1}{2} \sum_{\sigma,\sigma'} \hat{c}_{i\sigma}^\dagger \boldsymbol{\sigma}_{\sigma\sigma'} \hat{c}_{i\sigma'} . \tag{1.5}$$

The Hamiltonian (1.4), which was first derived in Ref. [112], is called the *Heisenberg model*, and it provides a fundamental description of quantum magnetism [113]. We consider in particular the AF spin-1/2 (i.e. for electrons) and *isotropic* (i.e. invariant under rotations in spin space) Heisenberg model [114].

1.2.3 Slave-fermion formalism

From the preceding discussion, it is already clear that charge and spin are treated essentially independently from each other in the strong-coupling limit $U/t \gg 1$: rather than considering the spin and number density of the electrons as inextricably linked, we treat electrons as consisting of two separate quasiparticle excitations, the *spinon* (associated with the electron spin) and *chargon* (associated with the electron number). Our conventional picture of the electron then arises as a bound state of the two. To be specific, on a lattice we may distinguish in the charge sector between two local quasiparticle excitations, the *holon* (an absence of electrons at a site) and the *doublon* (two electrons occupying a site). As shown in Fig. 4.1, the charge fluctuations in the ground state generate holons and doublons, which appear pairwise on neighbouring sites and are otherwise largely uncorrelated [115].

A suitable formalism in which to treat these spin-charge separated dynamics is the so-called *slave-fermion formalism*, which decomposes the fermionic operators $\hat{c}^\dagger_{i\sigma}$ explicitly into bosonic operators $\hat{s}^\dagger_{i\sigma}$, which create a single spin at the i-th site, and fermionic operators $\hat{d}^\dagger_i$ or $\hat{e}^\dagger_i$, which create a doublon or holon at the i-th site from the vacuum $|0_c\rangle$ ($\hat{s}_{i\sigma}|0_c\rangle = \hat{d}_i|0_c\rangle = \hat{e}_i|0_c\rangle = 0$). Explicitly,

$$\hat{c}_{i\sigma} = \hat{s}^\dagger_{i\overline{\sigma}}\hat{d}_i + \mathrm{sign}(\sigma)\hat{e}^\dagger_i\hat{s}_{i\sigma} \tag{1.6}$$

where $\overline{\sigma}$ denotes the opposite spin to σ and where $\mathrm{sign}(\sigma)$ takes the values $+1$ for $\sigma =\uparrow$ and -1 for $\sigma =\downarrow$ [108]. The local conservation of electron number imposes the constraint

$$\mathbb{1} = \hat{d}^\dagger_i\hat{d}_i + \hat{e}^\dagger_i\hat{e}_i + \hat{s}^\dagger_{i\uparrow}\hat{s}_{i\uparrow} + \hat{s}^\dagger_{i\downarrow}\hat{s}_{i\downarrow}\,. \tag{1.7}$$

Rather than accounting for this constraint via a Lagrange multiplier in the Hamiltonian, we will implement it self-consistently in our calculations, following the approach in Ref. [108].

2 Spin sector dynamics

Before we are able to quantify the ground state fluctuations in the charge sector, we have to develop a formal way to treat the spin sector Heisenberg dynamics. A key property of the spin-1/2 Heisenberg model is that its ground state supports long-range AF order [116]. Although this has only been rigorously proven in 1D [117] and 3D [118], as well as for non-square 2D lattices [119, 120], it is generally accepted that this is also true on square lattices [116, 121] at zero temperature [122].

2.1 Néel mean-field theory

Perfect AF order corresponds with the *Néel state* $|\Psi_{\mathrm{AF}}\rangle = |\uparrow\rangle^{\otimes\mathcal{A}}|\downarrow\rangle^{\otimes\mathcal{B}}$, where $\mathcal{A}$ and $\mathcal{B}$ denote the sub-lattices of the square lattice under a bipartition. Formally, Néel order in the spin sector can be realised by a mean-field assumption [108]

$$\begin{aligned} \hat{s}^\dagger_{i\uparrow} \to \langle\hat{s}^\dagger_{i\uparrow}\rangle = b_0 \quad \text{and} \quad \hat{s}_{i\uparrow} \to \langle\hat{s}_{i\uparrow}\rangle = b_0 \qquad \text{for } i \in \mathcal{A} \\ \hat{s}^\dagger_{i\downarrow} \to \langle\hat{s}^\dagger_{i\downarrow}\rangle = b_0 \quad \text{and} \quad \hat{s}_{i\downarrow} \to \langle\hat{s}_{i\downarrow}\rangle = b_0 \qquad \text{for } i \in \mathcal{B} \end{aligned} \tag{2.1}$$

where $b_0 \in \mathbb{R}$. The way in which we implement this assumption is by simply replacing suitable combinations of spin operators with these mean-field expectation values. Applied to (1.7), this implies that

$$b_0^2 = \begin{cases} 1 - \langle\hat{d}^\dagger_i\hat{d}_i\rangle - \langle\hat{e}^\dagger_i\hat{e}_i\rangle - \langle\hat{s}^\dagger_{i\downarrow}\hat{s}_{i\downarrow}\rangle & \text{for } i \in A \\ 1 - \langle\hat{d}^\dagger_i\hat{d}_i\rangle - \langle\hat{e}^\dagger_i\hat{e}_i\rangle - \langle\hat{s}^\dagger_{i\uparrow}\hat{s}_{i\uparrow}\rangle & \text{for } i \in B \end{cases} \tag{2.2}$$

which gives us the condition for self-consistency of our slave-fermion approach. Intuitively, the assumption of static spins on each sub-lattice amounts to a renormalisation of the exchange interaction as $J \to Jb_0^2$ when dealing with spin dynamics on the other sub-lattice, which we implement below.

2.2 Linear spin-wave theory

In fact, the Néel state is the ground state of the *classical* Heisenberg model, however in the quantum case we must account for zero-point quantum fluctuations around $|\Psi_{\mathrm{AF}}\rangle$. These low-lying collective excitations are traditionally treated using *linear spin-wave theory* [123, 124]. This approach can be thought of, essentially, as a leading-order semiclassical expansion around the Néel state [123, 124].

The semiclassical expansion is equivalent to an expansion in the inverse of the spin value S, where the classical limit corresponds with $S \to \infty$. We realise this via the Holstein-Primakoff transformation [125]

$$S_i^+ = \hat{b}_i \sqrt{2S - \hat{b}_i^\dagger \hat{b}_i} \quad \text{and} \quad S_i^z = S - \hat{b}_i^\dagger \hat{b}_i \,, \tag{2.3}$$

where $\hat{b}_i^\dagger$ is shorthand for $\hat{s}_{i\sigma}^\dagger$ with the spin σ suppressed since on $\mathcal{A}, \mathcal{B}$ the value of σ is fixed. It is advantageous to define transformed spin operators $\tilde{S}_i^x = S_i^x$, $\tilde{S}_i^y = -S_i^y$ and $\tilde{S}_i^z = -S_i^z$ for $i \in \mathcal{B}$, corresponding with a rotation of the spins on sublattice B by π [116]. Noting that $\tilde{S}_i^\pm = \tilde{S}_i^\mp$,

$$H_{\mathrm{eff}} = J b_0^2 \sum_{i,\boldsymbol{\delta}} \left(-S_i^z \tilde{S}_{i+\boldsymbol{\delta}}^z + \frac{1}{2} \left(S_i^+ \tilde{S}_{i+\boldsymbol{\delta}}^+ + S_i^- \tilde{S}_{i+\boldsymbol{\delta}}^- \right) \right) . \tag{2.4}$$

Under the Holstein-Primakoff transformation, to leading order in $1/S$, we can then approximate

$$H_{\mathrm{eff}} = -\frac{J b_0^2 N S^2 z}{2} + J b_0^2 S \sum_i \sum_{\boldsymbol{\delta}} \left(\hat{b}_i^\dagger \hat{b}_i + \hat{b}_{i+\boldsymbol{\delta}}^\dagger \hat{b}_{i+\boldsymbol{\delta}} + \hat{b}_i \hat{b}_{i+\boldsymbol{\delta}} + \hat{b}_i^\dagger \hat{b}_{i+\boldsymbol{\delta}}^\dagger \right) + \dots \,,$$

where $z = 4$ is the coordination number of our square lattice and where $\dots$ indicates terms $\mathrm{O}(S^0)$. As we show in Appendix B, in reciprocal space H_{eff} takes the form

$$H_{\mathrm{eff}} = -\frac{J b_0^2 N S(S+1) z}{2} + \frac{J b_0^2 S z}{2} \sum_{\mathbf{k} \in 1\mathrm{BZ}} \begin{pmatrix} \hat{b}_{\mathbf{k}}^\dagger & \hat{b}_{-\mathbf{k}} \end{pmatrix} \begin{pmatrix} 1 & \gamma_{\mathbf{k}} \\ \gamma_{\mathbf{k}} & 1 \end{pmatrix} \begin{pmatrix} \hat{b}_{\mathbf{k}} \\ \hat{b}_{-\mathbf{k}}^\dagger \end{pmatrix} , \tag{2.5}$$

where we have defined the *tight-binding parameter* $\gamma_{\mathbf{k}} = 2z^{-1} \sum_{\boldsymbol{\delta}} \mathrm{e}^{\mathrm{i}\mathbf{k}\cdot\boldsymbol{\delta}}$. This Hamiltonian can be diagonalised by a *bosonic Bogoliubov transformation*, i.e. an isomorphism between sets of creation / annihilation operators obeying the same commutators [126]. Specifically, we consider a transformation

$$\begin{pmatrix} \hat{b}_{\mathbf{k}} \\ \hat{b}_{-\mathbf{k}}^\dagger \end{pmatrix} = \begin{pmatrix} u_{\mathbf{k}} & v_{\mathbf{k}} \\ v_{\mathbf{k}} & u_{\mathbf{k}} \end{pmatrix} \begin{pmatrix} \hat{\beta}_{\mathbf{k}} \\ \hat{\beta}_{-\mathbf{k}}^\dagger \end{pmatrix} , \tag{2.6}$$

and choose $u_{\mathbf{k}}, v_{\mathbf{k}}$ to be real and spherically symmetric in $\mathbf{k}$. We require $u_{\mathbf{k}}^2 - v_{\mathbf{k}}^2 = 1$ to preserve the operator algebra. For appropriately chosen $u_{\mathbf{k}}, v_{\mathbf{k}}$ (see Appendix B),

$$H_{\mathrm{eff}} = \underbrace{-\frac{J b_0^2 N S(S+1) z}{2} + \frac{J b_0^2 S z}{2} \sum_{\mathbf{k} \in 1\mathrm{BZ}} \omega_{\mathbf{k}}}_{\text{zero-point energy}} + \sum_{\mathbf{k} \in 1\mathrm{BZ}} \Omega_{\mathbf{k}} \hat{\beta}_{\mathbf{k}}^\dagger \hat{\beta}_{\mathbf{k}} \,, \tag{2.7}$$

where $\Omega_{\mathbf{k}} = J b_0^2 S z \sqrt{1 - \gamma_{\mathbf{k}}^2}$. Under the linear spin-wave approximation, the Hamiltonian therefore supports a single band of free magnonic quasiparticle excitations with energy dispersion $\Omega_{\mathbf{k}}$.

3 Field theoretic description

We now turn to the full problem of the charge dynamics on the AF spin background. We formulate in this section the quantum field theory (QTF) treatment of this problem, as introduced in Refs. [108, 121], which allows us to calculate D in the strong coupling regime $t/U \ll 1$. A brief review of the many-body QFT formalism is given in Appendix B.

Conceptually, to treat the full Hubbard dynamics we assume that the spin sector is described by the Heisenberg model under linear spin-wave theory, an assumption that is known to reproduce quantitatively well key observables like the sub-lattice magnetisation [116]. Then, the effect on the charge dynamics due to the coupling of the charge sector to the spin background can be calculated, assuming that the charge dynamics do not exhibit back-action on the spin properties.

3.1 Slave-fermion Hamiltonian

3.1.1 Mean-field assumption

For consistency with our treatment of the AF background, we first re-write the full Hubbard Hamiltonian in terms slave-fermion formalism operators as $H = H^{(0)} + H^{(1)}$ with [108]

$$\begin{aligned} H^{(0)} &= \frac{U}{2}\sum_{i}\left(\hat{d}_i^\dagger\hat{d}_i + \hat{e}_i^\dagger\hat{e}_i - \frac{1}{2}\right) - t\sum_{i,\boldsymbol{\delta},\sigma}\mathrm{sign}(\sigma)\left(\left(\hat{d}_i^\dagger\hat{e}_{i+\boldsymbol{\delta}}^\dagger + \hat{e}_i^\dagger\hat{d}_{i+\boldsymbol{\delta}}^\dagger\right)\hat{s}_{i\sigma}\hat{s}_{i+\boldsymbol{\delta}\bar{\sigma}} + \mathrm{h.c.}\right) \\ H^{(1)} &= -t\sum_{i,\boldsymbol{\delta},\sigma}\left(\left(\hat{d}_{i+\boldsymbol{\delta}}^\dagger\hat{d}_i - \hat{e}_{i+\boldsymbol{\delta}}^\dagger\hat{e}_i\right)\hat{s}_{i\sigma}^\dagger\hat{s}_{i+\boldsymbol{\delta}\sigma} + \mathrm{h.c.}\right). \end{aligned} \tag{3.1}$$

We note that $H^{(0)}$ contains only pairs of spin operators consistent with the mean-field assumption, in the sense that the spins on the different sub-lattices have opposite orientations. On the other hand, $H^{(1)}$ contains pairs of spin operators which go beyond the Néel state approximation. Therefore, while $H^{(0)}$ captures the motion of free chargons on a perfectly AF ordered spin background, $H^{(1)}$ describes a coupling of the chargon degrees of freedom to the low-lying excitations in the spin background. Enforcing the mean-field assumption (2.1) and defining $\mathbf{Q} = (\pi/a, \pi/a)$, a derivation like in Section 2 leads to [108]

$$\begin{aligned} H^{(0)} &= -\frac{NU}{4} + \sum_{\mathbf{k},\mathbf{q}\in 1\mathrm{BZ}}\left(\begin{array}{cc}\hat{d}_{\mathbf{Q}-\mathbf{k}}^\dagger & \hat{e}_{\mathbf{k}}\end{array}\right)\left(\begin{array}{cc} U/2 & tb_0^2 z \\ tb_0^2 z & U/2\end{array}\right)\left(\begin{array}{c}\hat{d}_{\mathbf{Q}-\mathbf{k}} \\ \hat{e}_{\mathbf{k}}^\dagger\end{array}\right) \\ H^{(1)} &= \frac{tb_0 z}{\sqrt{N}}\sum_{\mathbf{k},\mathbf{q}\in 1\mathrm{BZ}}\left(\begin{array}{cc}\hat{d}_{\mathbf{Q}-\mathbf{k}}^\dagger & \hat{e}_{\mathbf{k}}\end{array}\right)\left(\begin{array}{cc}\gamma_{\mathbf{k}-\mathbf{q}}\hat{b}_{-\mathbf{q}} + \gamma_{\mathbf{k}}\hat{b}_{\mathbf{q}}^\dagger & 0 \\ 0 & \gamma_{\mathbf{k}-\mathbf{q}}\hat{b}_{\mathbf{q}} + \gamma_{\mathbf{k}}\hat{b}_{-\mathbf{q}}^\dagger\end{array}\right)\left(\begin{array}{c}\hat{d}_{\mathbf{Q}-\mathbf{k}+\mathbf{q}} \\ \hat{e}_{\mathbf{k}-\mathbf{q}}^\dagger\end{array}\right). \end{aligned} \tag{3.2}$$

3.1.2 Bogoliubov transformations

To express the spin-charge interaction in a physically sensible way, we re-write $H^{(1)}$ by direct substitution of the Bogoliubov transformation (2.6) in terms of a coupling to the collective spin modes as

$$H^{(1)} = \sum_{\mathbf{k},\mathbf{q}\in 1\mathrm{BZ}} m(\mathbf{k},\mathbf{q})\left(\hat{d}_{\mathbf{k}}^\dagger\hat{d}_{\mathbf{k}+\mathbf{q}}\hat{\beta}_{\mathbf{q}}^\dagger + \hat{e}_{\mathbf{k}+\mathbf{q}}\hat{e}_{\mathbf{k}}^\dagger\hat{\beta}_{\mathbf{q}}^\dagger + \mathrm{h.c.}\right), \tag{3.3}$$

where we have defined the coefficient $m(\mathbf{k},\mathbf{q}) = -tb_0 z(\gamma_{\mathbf{k}+\mathbf{q}}u_{\mathbf{q}} + \gamma_{\mathbf{k}}v_{\mathbf{q}})/\sqrt{N}$ to lighten the notation (see Appendix B). To develop this expression further, we note that $H^{(0)}$ can be diagonalised similar to the spin-wave Hamiltonian using a *fermionic Bogoliubov transformation* [126],

$$\begin{pmatrix} \hat{d}_{\mathbf{Q}-\mathbf{k}} \\ \hat{e}^{\dagger}_{\mathbf{k}} \end{pmatrix} = \begin{pmatrix} \mu_{\mathbf{k}} & \nu_{\mathbf{k}} \\ -\nu_{\mathbf{k}} & \mu_{\mathbf{k}} \end{pmatrix} \begin{pmatrix} \hat{f}_{-\mathbf{k}} \\ \hat{g}^{\dagger}_{\mathbf{k}} \end{pmatrix}, \tag{3.4}$$

where now $\mu^2_{\mathbf{k}} + \nu_{\mathbf{k}} = 1$ to preserve the anticommutators. Under this transformation and including the magnonic self-energy term, the (diagonal) Hamiltonian $H^{(0)}$ then becomes

$$H^{(0)} = E + \sum_{\mathbf{k}\in 1\mathrm{BZ}} \Omega_{\mathbf{k}} \hat{\beta}^{\dagger}_{\mathbf{k}} \hat{\beta}_{\mathbf{k}} + \sum_{\mathbf{k}\in 1\mathrm{BZ}} E_{\mathbf{k}} \left(\hat{f}^{\dagger}_{\mathbf{k}} \hat{f}_{\mathbf{k}} + \hat{g}^{\dagger}_{\mathbf{k}} \hat{g}_{\mathbf{k}} \right), \tag{3.5}$$

where E denotes the sum of the magnonic and fermionic zero-point energies and where $E_{\mathbf{k}} = \sqrt{U^2/4 + (tb_0^2 z\gamma_{\mathbf{k}})^2}$ (see Appendix B). In terms of the transformed operators, $H^{(1)}$ becomes

$$\begin{aligned} H^{(1)} = &\sum_{\mathbf{k},\mathbf{q}\in 1\mathrm{BZ}} M_1(\mathbf{k},\mathbf{q}) \left(\hat{f}^{\dagger}_{\mathbf{k}+\mathbf{q}} \hat{f}_{\mathbf{k}} \hat{\beta}_{\mathbf{q}} + \mathrm{h.c.} \right) + \sum_{\mathbf{k},\mathbf{q}\in 1\mathrm{BZ}} M_2(\mathbf{k},\mathbf{q}) \left(\hat{g}_{\mathbf{k}} \hat{g}^{\dagger}_{\mathbf{k}+\mathbf{q}} \hat{\beta}_{\mathbf{q}} + \mathrm{h.c.} \right) \\ &+ \sum_{\mathbf{k},\mathbf{q}\in 1\mathrm{BZ}} M_3(\mathbf{k},\mathbf{q}) \left(\hat{f}^{\dagger}_{-\mathbf{k}} \hat{g}^{\dagger}_{\mathbf{k}+\mathbf{q}} \hat{\beta}_{\mathbf{q}} + \mathrm{h.c.} \right) + \sum_{\mathbf{k},\mathbf{q}\in 1\mathrm{BZ}} M_4(\mathbf{k},\mathbf{q}) \left(\hat{f}^{\dagger}_{-\mathbf{k}} \hat{g}^{\dagger}_{\mathbf{k}+\mathbf{q}} \hat{\beta}^{\dagger}_{-\mathbf{q}} + \mathrm{h.c.} \right). \end{aligned} \tag{3.6}$$

where the coefficients $M_i(\mathbf{k},\mathbf{q})$ are derived explicitly in Appendix B.

3.2 Diagrammatic analysis

3.2.1 Interaction vertices

We have now arrived at a full description of the Hubbard charge dynamics coupled to the low-lying excitations in the AF spin background. The interacting quantum field theory we obtain after our Bogoliubov transformations comprises two fermionic fields (associated with the f-type and g-type chargons) and one collective bosonic field (associated with the magnons). A prime advantage of working with these auxiliary fields (associated with operators $\hat{f}_{\mathbf{k}}$, $\hat{g}_{\mathbf{k}}$, and $\hat{\beta}_{\mathbf{k}}$) rather than the physical fields (associated with operators $\hat{d}_{\mathbf{k}}$, $\hat{e}_{\mathbf{k}}$, and $\hat{b}_{\mathbf{k}}$) is that the many-body ground state $|G\rangle$, while non-trivial to define in terms of the latter, is simply the free theory vacuum for the former, i.e.

$$\hat{f}_{\mathbf{k}}|G\rangle = \hat{g}_{\mathbf{k}}|G\rangle = \hat{\beta}_{\mathbf{k}}|G\rangle = 0\,. \tag{3.7}$$

From the form of the interation Hamiltonian (3.6), there follows naturally a diagrammatic description of the full Hubbard dynamics, in terms of the trivalent spin-charge coupling vertices shown in Fig. 4.2. The fact that $|G\rangle$ is annihilated by $\hat{f}_{\mathbf{k}}$, $\hat{g}_{\mathbf{k}}$, and $\hat{\beta}_{\mathbf{k}}$ then in particular allows us to apply the machinery of Feynman diagrams to the auxiliary fields without reservation (calculating scattering matrix elements using a perturbative expansion in terms of free theory vacuum expectation values – i.e. many-body ground state correlators – , Wick contracting the correlators, deriving Feynman rules, etc.).

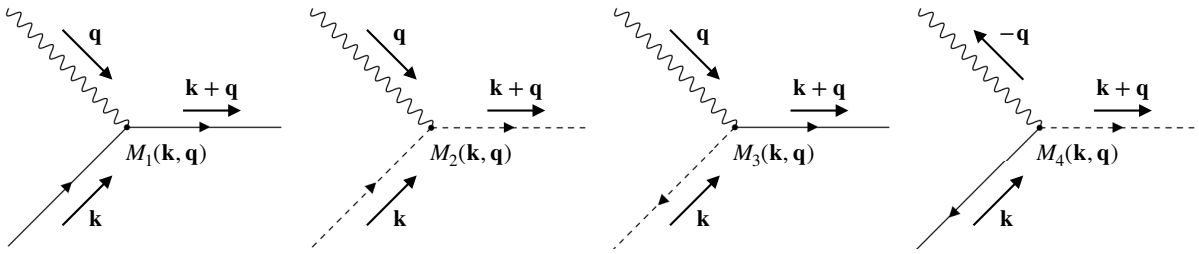

Figure 4.2 – Hubbard interaction vertices. Representative interaction vertices, with f-type (solid) and g-type (dashed) fermionic, as well as magnonic (wavy) propagators indicated.

3.2.2 Physical & auxiliary propagators

In particular, in order to calculate the doublon occupancy D we will be interested in the spectral function for the doublons, and accordingly in the doublon Green's function $\mathcal{G}(\mathbf{k},t) = \langle\Omega|T\hat{d}_{\mathbf{k}}(t)\hat{d}^{\dagger}_{\mathbf{k}}(0)|\Omega\rangle$, where $|\Omega\rangle$ denotes the interacting theory vacuum. Under the fermionic Bogoliubov transformation,

$$\hat{d}^{\dagger}_{\mathbf{Q}-\mathbf{k}}\hat{d}_{\mathbf{Q}-\mathbf{k}} = \frac{2E_{\mathbf{k}}+U}{4E_{\mathbf{k}}}\hat{f}^{\dagger}_{\mathbf{k}}\hat{f}_{\mathbf{k}} - \frac{tb_0^2 z\gamma_{\mathbf{k}}}{4E_{\mathbf{k}}}\hat{f}^{\dagger}_{\mathbf{k}}\hat{g}^{\dagger}_{\mathbf{k}} + \frac{2E_{\mathbf{k}}-U}{4E_{\mathbf{k}}}\hat{g}_{\mathbf{k}}\hat{g}^{\dagger}_{\mathbf{k}} - \frac{tb_0^2 z\gamma_{\mathbf{k}}}{4E_{\mathbf{k}}}\hat{g}_{\mathbf{k}}\hat{f}_{\mathbf{k}} \tag{3.8}$$

which allows us to relate $\mathcal{G}(\mathbf{Q}-\mathbf{k},t)$ directly to the 2-point correlators for the auxiliary fields. As already expressed above, these can then be calculated perturbatively in a diagrammatic fashion, using the free fermionic Green's functions (see Appendix B)

$$\begin{aligned}\langle G|T\hat{f}_{\mathbf{k}}(t)\hat{f}^{\dagger}_{\mathbf{k}}(0)|G\rangle &= \langle G|T\hat{g}_{\mathbf{k}}(t)\hat{g}^{\dagger}_{\mathbf{k}}(0)|G\rangle = \int d\omega\ \mathrm{e}^{-\mathrm{i}\omega t}\frac{\mathrm{i}}{\omega - E_{\mathbf{k}} + \mathrm{i}0^{+}}\\ \langle G|T\hat{f}^{\dagger}_{\mathbf{k}}(t)\hat{g}^{\dagger}_{\mathbf{k}}(0)|G\rangle &= \langle G|T\hat{g}_{\mathbf{k}}(t)\hat{f}_{\mathbf{k}}(0)|G\rangle = 0\end{aligned} \tag{3.9}$$

3.2.3 Non-crossing approximation

A traditional approach to evaluate the perturbative expansion is to employ the *self-consistent Born approximation (SCBA)*, and this has yielded successful results in qualiatively similar problems involving the coupling of a chargon to the low-lying excitations of a spin background [121, 127–131]. In fact, the SCBA is much more broadly applicable and is a well-known tool in many areas of condensed matter physics, including electron-phonon coupling [132, 133] or impurity scattering [134, 135]. The SCBA is best explained by considering a simpler version of our interacting field theory, comprised from only a single fermionic field $\hat{f}_{\mathbf{k}}$ and a collective bosonic field $\hat{\beta}_{\mathbf{k}}$. Under the SCBA, the self-energy associated with the fermionic propagator $G(\mathbf{k},t)$ is approximated by neglecting those diagrams in an infinite-order perturbative expansion which contain crossing interaction lines [135]. In particular, for a trivalent vertex of the form $\sum_{\mathbf{k},\mathbf{q}} M(\mathbf{k},\mathbf{q})\left(\hat{f}^{\dagger}_{\mathbf{k}+\mathbf{q}}\hat{f}_{\mathbf{k}}\hat{\beta}_{\mathbf{q}} + \text{h.c.}\right)$, this means that the correction to the free propagator is simply the 'Fock'-type diagram in Fig. 4.3a with the virtual fermionic propagator dressed by all loop corrections to the self-energy. The explicit expression of this diagram in terms of the re-summed 1-particle irreducible diagrams without crossing interaction lines is shown in Fig. 4.3b. In our case, the SCBA only neglects the vertex renormalisation, which does not qualitatively change the results of interest [108, 121].

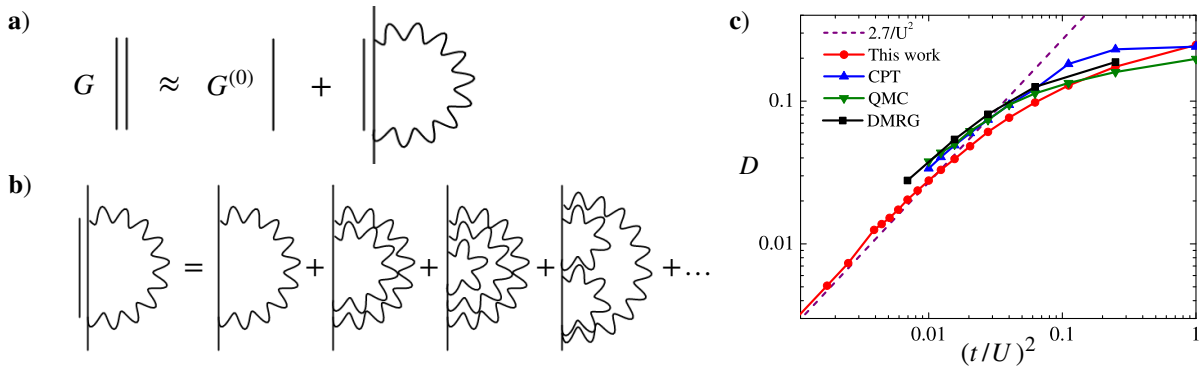

Figure 4.3 – Doublon occupancy in the SCBA. a) Diagrammatic self-consistent Born approximation (SCBA) and **b)** explicit expression of the SCBA diagram in terms of re-summed non-crossing 1-particle irreducible diagrams. Double [single] solid lines represent the dressed [bare] fermionic propagators G [$G^{(0)}$], and wavey lines represent bosonic propagators. **c)** Scaling of the doublon occupancy D with $(t/U)^2$, reproduced from Ref. [108]. The graphs show the calculation based on the SCBA compared with state-of-the-art numerics for $t/U > 0$ as well as the asymptotic value in the limit of $t/U \to 0$.

The SCBA inherits its name from the well-known *Born approximation*, which is well-suited for weak coupling constants and involves taking into consideration only the 1-loop correction to the self-energy (i.e. the contribution of the first loop diagram in Fig. 4.3b) [135]. In fact, a particular advantage of the SCBA is that the diagrammatic statement of Fig. 4.3a can be translated into a closed-form expression for the propagator once we have calculated the self-energy under the Born approximation. In Appendix B, we show that for a generic field theory like the one considered above, this has the form

$$\Sigma_{\text{1-loop}}(\mathbf{k},\omega) = \sum_{\mathbf{q}} M^2(\mathbf{k}-\mathbf{q},\mathbf{q}) \times G^{(0)}(\mathbf{k}-\mathbf{q},\omega-\Omega_{\mathbf{q}})\,. \tag{3.10}$$

Enforcing the SCBA then amounts to replacing the bare fermionic propagator with the dressed one in this expression, to obtain the self-consistent prescription for the propagator as

$$G(\mathbf{k},\omega) = \frac{1}{\omega - E_{\mathbf{k}} - \sum_{\mathbf{q}} M^2(\mathbf{k}-\mathbf{q},\mathbf{q}) \times G(\mathbf{k}-\mathbf{q},\omega-\Omega_{\mathbf{q}})}\,. \tag{3.11}$$

Crucially, the right hand side of this self-consistent equation is evaluated only at lower frequencies than the left hand side, which implies that in practice the full interacting propagator $G(\mathbf{k},\omega)$ can be calculated by sweeping from very small to very large frequency values. We will not implement these numerics here but refer the reader to the numerics in Ref. [108].

3.3 Doublon occupancy

Having developed the formal field theoretic tools to describe the charge dynamics on the AF background, we are now in a position to calculate the ground state doublon occupancy D, which we can formally define in real and reciprocal space as

$$D = \frac{1}{N}\sum_i \langle\Omega|\hat{d}_i^\dagger \hat{d}_i|\Omega\rangle = \frac{1}{N}\sum_{\mathbf{k}\in 1\text{BZ}} \langle\Omega|\hat{d}_{\mathbf{k}}^\dagger \hat{d}_{\mathbf{k}}|\Omega\rangle\,. \tag{3.12}$$

3.3.1 Numerical evaluation for $t/U > 0$

Within the QFT framework of the previous section, the doublon occupancy can be expressed as [108]

$$D = -\frac{1}{N\pi} \sum_{\mathbf{k}\in 1\mathrm{BZ}} \int d\omega \; f(\omega) \; \mathrm{Im} \; \mathcal{G}(\mathbf{k}, \omega - \mathrm{i}\delta) \, . \tag{3.13}$$

where $f(\omega)$ is the Fermi distribution. The propagators for the auxiliary fields can be calculated numerically for various values of t/U by the self-consistent method of the previous section, and the retarded doublon propagator $\mathcal{G}(\mathbf{k}, \omega - \mathrm{i}\delta)$ can be inferred from this. This allows us to calculate D numerically using eq. (3.13). This was done in Ref. [108], leading to the scaling in Fig. 4.3c. Evidently, the scaling compares favourably with state-of-the-art Quantum Monte Carlo (QMC) [136, 137], Cluster Perturbation Theory (CPT) [138], and Density Matrix Renormalisation Group (DMRG) [50] numerics.

3.3.2 Asymptotic value for $t/U \to 0$

In fact, the studies in Fig. 4.3c, while they provide us with a precise characterisation of the ground state manifold, are not strictly speaking necessary for our problem of the saturation of the refractive index. As alluded to previously, the limit of $t = 0$ corresponds with an absence of quantum chemistry (i.e. at sufficiently large atomic separations there is no tunnelling between sites), and so if we want to estimate the effect of the ground state charge fluctuations at the onset of quantum chemistry, the more relevant result is the asymptotic scaling of D with t/U as $t/U \to 0$.

This is obtained from the free chargon Green's function in Ref. [108], however in our notation we are able to obtain it in a more direct manner: for $t/U \to 0$, the spin background is frozen in AF order so that $H \to H^{(0)}$ and hence $|\Omega\rangle \to |G\rangle$. Using $\sum_{\mathbf{k}\in 1\mathrm{BZ}} \hat{d}^\dagger_{\mathbf{k}} \hat{d}_{\mathbf{k}} = \sum_{\mathbf{k}\in 1\mathrm{BZ}} \hat{d}^\dagger_{\mathbf{Q}-\mathbf{k}} \hat{d}_{\mathbf{Q}-\mathbf{k}}$ and performing the inverse Bogoliubov transformation as in eq. (3.8), we obtain

$$D = \frac{1}{N} \sum_{\mathbf{k}\in 1\mathrm{BZ}} \frac{E_{\mathbf{k}} - U/2}{2E_{\mathbf{k}}} \underbrace{\langle G | \hat{g}_{\mathbf{k}} \hat{g}^\dagger_{\mathbf{k}} | G \rangle}_{=1} + \text{vanishing expectation values} \tag{3.14}$$

To compute the asymptotic scaling of D, we perform a Taylor expansion in t/U, whereby

$$D \approx \frac{1}{N} \sum_{\mathbf{k}\in 1\mathrm{BZ}} \frac{1}{U} \left(\frac{U}{2} \left(1 + 2 \left(\frac{t}{U} \right)^2 (b_0^2 z \gamma_{\mathbf{k}})^2 \right) - \frac{U}{2} + \ldots \right) \approx \left(\frac{t}{U} \right)^2 \frac{(b_0^2 z)^2}{N} \sum_{\mathbf{k}\in 1\mathrm{BZ}} \gamma_{\mathbf{k}}^2 \, , \tag{3.15}$$

which leads to the final result that $D \approx 2.7(t/U)^2$ in the asymptotic strong coupling limit. Fig. 4.3c confirms this by comparison with the numerical results.

In summary, we have shown that at the onset of quantum chemistry, virtual tunnelling in the ground state leads to a buildup of density-density correlations on a fraction of $\sim 2.7(t/U)^2$ sites. In principle, these correlations have the potential to affect the collective response of each planar array in our minimal model. To be precise, we formulate the hypothesis that: 1. the ground state charge fluctuations are the dominant correction to the quantum optics limit and 2. their effect on the optical response is sufficiently large to affect the refractive index in a significant way. We provide arguments to confirm these two aspects of our hypothesis in the next two chapters.

Chapter 5

Quantum chemistry III: *Excited states*

To understand how the occurrence of holon-doublon pairs compares to other effects that emerge with the onset of quantum chemistry, we now move on to dissect the dynamics encoded by the full 2D Hamiltonian. We consider first the kinetic and electrostatic contributions (Section 1), and then the photon-mediated contributions (Section 2).

We will assume a hierarchy of processes associated with, in order of decreasing contribution, three types of the matrix elements: (i) between the same Wannier orbital on the same site, (ii) between different Wannier orbitals on the same site, and (iii) between Wannier orbitals on different sites. This allows us to tackle the effect of quantum chemistry in a controlled way: the hierarchisation amounts to an effective expansion of the interactions in $a_0/a \ll 1$. The leading-order terms encode the first effects to become prominent as the atomic density is increased. Using a variety of arguments, we will estimate the role of these effects on the optical response of the array. We will show in particular that, except for the interaction which leads to the formation of holon-doublon pairs, the corrections to the quantum optics limit due to quantum chemistry effects are exponentially small in a_0/a. To underline this point, we will show that we are able to recover the spin model description of the array as a limiting case (Section 3).

1 Electrostatic interactions

1.1 On-site electron energies

The most dominant contributions to $T+U$ will be type (i) on-site processes. In particular, the kinetic and electron-proton on-site matrix elements contribute a term of the form

$$E_1 = \sum_i \varepsilon_s \left(\hat{n}_{is\uparrow} + \hat{n}_{is\downarrow}\right) + \sum_i \varepsilon_p \left(\hat{n}_{ip\uparrow} + \hat{n}_{ip\downarrow}\right) , \tag{1.1}$$

with $\varepsilon_\mu = T|_{ii\mu\mu} + U_p|_{iii\mu\mu}$. We recognise this to be the energy contribution ε_μ associated with an electron in the μ-orbital, comprised from its kinetic energy and atomic binding energy. This becomes more intuitive when we estimate the value of ε_μ (or rather of $T|_{ii\mu\mu}$ and $U_p|_{iii\mu\mu}$) by approximating the Wannier functions by the hydrogen wavefunctions. Doing this (see Appendix C), we find that

$$T|_{ii\mu\mu} = \frac{1}{n_\mu^2}\frac{mq^4}{2(4\pi\varepsilon_0\hbar)^2} \quad \text{and} \quad U_p|_{iii\mu\mu} = -\frac{1}{n_\mu^2}\frac{mq^4}{(4\pi\varepsilon_0\hbar)^2} , \tag{1.2}$$

where n_μ denotes the principal quantum number ($n_s = 1, n_p = 2$). We recognise (1.2) to be the average gross structure kinetic and potential energy for atomic electrons in a hydrogen atom, respectively [72].

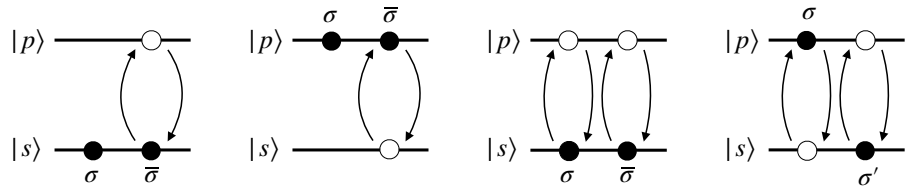

Figure 5.1 – Doublon quantum chemistry. Diagrammatic representation of type (ii) processes on doubly occupied sites captured only by full quantum chemistry. Black [white] circles denote electrons [the absence of electrons] and $\sigma \in \{\uparrow, \downarrow\}$ denotes the associated spin value, with $\overline{\sigma}$ indicating the opposite spin value of σ.

Intuitively, while the on-site electron-proton interaction leads to a binding energy of the form (1.1), the electron-electron on-site repulsion will lead to an energy penalty for the simultaneous occupation of a site by two electrons. The type (i) matrix element $U_e|_{iiii\mu\mu'\nu\nu'}$ is associated with terms

$$E_2 = \sum_i u_s \hat{n}_{is\uparrow}\hat{n}_{is\downarrow} + \sum_i u_p \hat{n}_{ip\uparrow}\hat{n}_{ip\downarrow} \tag{1.3}$$

$$E_3 = \sum_i \sum_{\sigma,\sigma'} u_{sp}^{\sigma\sigma'} \hat{n}_{is\sigma}\hat{n}_{ip\sigma'} \tag{1.4}$$

with coefficients $u_\mu = U_e|_{iiii\mu\mu\mu\mu}$ + c.c., $u_{sp}^{\uparrow\uparrow} = u_{sp}^{\downarrow\downarrow} = U_e|_{iiiisspp} + U_e|_{iiiispps}$ + c.c., and $u_{sp}^{\uparrow\downarrow} = u_{sp}^{\downarrow\uparrow} = U_e|_{iiiisspp}$ + c.c.. Indeed, E_2 encodes the on-site repulsion of two electrons in the same orbital (with opposite spins to obey Pauli exclusion), while E_3 encodes the on-site repulsion of two electrons in different orbitals. We also note that in fact $u_{sp}^{\sigma\sigma}$ contains both the dominant type (i) contribution $U_e|_{iiiisspp}$ and a smaller type (ii) contribution $U_e|_{iiiispps}$. In the notation of the previous chapter, $u_s = U$ and we can now estimate this on-site electron-electron repulsion using the hydrogen wavefunctions as (see Appendix C)

$$U = \frac{5\varepsilon_s}{4}\,. \tag{1.5}$$

1.2 Doublon quantum chemistry

In addition to the type (i) matrix elements associated with (1.3) and (1.4), the on-site electron-electron interaction also encodes type (ii) processes involving transitions of a single electron which creates or breaks up doublons (e.g. $U_e|_{iiiisssp}$), as well as less strong contributions (e.g. $U_e|_{iiiispps}$) involving two simultaneous electron transitions on-site, as shown in Fig. 5.1.

These terms constitute a subset of full quantum chemistry: two electrons on the same atomic site have (correlated) orbitals that do not in general resemble the single-electron orbitals. Therefore these processes, which will be inherently non-perturbative, are not amenable to any simple solution. This also means that we are in general unable to quantify these terms, however this is not of immediate interest to our problem; In the previous chapter, we have already introduced the effect of density-density correlations in the form of holon-doublon pairs within the Hubbard model. The processes in Fig. 5.1 will change the results we obtained in this context quantitatively, but not qualitatively, since they are in some sense 'internal' to the density-density correlation buildup on individual sites. This statement has been verified in state-of-the-art quantum chemistry calculations on the 1D hydrogen chain.

1.3 Dipole interactions

In the discussion above, we have not yet considered another class of 'on-site' terms arising from the electron-proton interaction, with matrix elements $U_p|_{iij\mu\mu'}$ $(j \neq i)$. Since the matrix element $U_{ijkl\mu\mu'\nu\nu'}$ for electron-electron interaction is composed of two individual overlaps of Wannier functions, there exist similar terms for $i = k, j = l, i \neq j$. Although such terms involve two distinct sites, dominant type (i) and (ii) processes can still arise. The relevant matrix elements are

$$U_p|_{iij\mu\mu'} = -\frac{q^2}{4\pi\varepsilon_0}\int d^3\mathbf{x}\ \phi^*_\mu(\mathbf{x})\phi_{\mu'}(\mathbf{x})\frac{1}{|\mathbf{x}+\mathbf{R}_{ij}|} \tag{1.6}$$

$$U_e|_{ijij\mu\mu'\nu\nu'} = \frac{q^2}{8\pi\varepsilon_0}\int d^3\mathbf{x}\ \phi^*_\mu(\mathbf{x})\phi_{\mu'}(\mathbf{x})\int d^3\mathbf{y}\phi^*_\nu(\mathbf{y})\phi_{\nu'}(\mathbf{y})\frac{1}{|\mathbf{x}-\mathbf{y}+\mathbf{R}_{ij}|}\,, \tag{1.7}$$

where we have performed the changes of variable $\mathbf{x} = \mathbf{r} - \mathbf{R}_i$ and $\mathbf{y} = \mathbf{r} - \mathbf{R}_j$, and defined $\mathbf{R}_{ij} = \mathbf{R}_i - \mathbf{R}_j$. We can see that these terms should be slightly less dominant than the type (i) terms we considered above, since the integrand is of order $\mathrm{O}(a^{-1})$ rather than order $\mathrm{O}(a_0^{-1})$.

The localisation of the Wannier functions will mean that the integrand in the matrix elements in eq. (1.6) (or eq. (1.7)) will be negligible for all $\mathbf{x}$ (or $\mathbf{x}-\mathbf{y}$) except in some vicinity of the atomic site on the order of a_0. Therefore $\mathbf{x}$ (or $\mathbf{x}-\mathbf{y}$) can be viewed as a small correction to $\mathbf{R}_{ij}$ in the limit $a_0/a \ll 1$, and we can Taylor expand the integrand around $\mathbf{x} = 0$ (or $\mathbf{x}-\mathbf{y} = 0$) to approximate these processes.

1.3.1 Electron-proton potential expansion

In the case of the electron-proton matrix element (1.6), the single-variable Taylor expansion in $\mathbf{x}$ reads

$$\frac{1}{|\mathbf{x}+\mathbf{R}_{ij}|} = \underbrace{\frac{1}{R_{ij}}}_{\mathrm{O}(|\mathbf{x}|^0)} \underbrace{-\mathbf{x}\cdot\frac{\mathbf{R}_{ij}}{R^3_{ij}}}_{\mathrm{O}(|\mathbf{x}|^1)} \underbrace{-\frac{1}{2}\frac{|\mathbf{x}|^2}{R^3_{ij}} + \frac{3}{2}\frac{|\mathbf{x}\cdot\mathbf{R}_{ij}|^2}{R^5_{ij}}}_{\mathrm{O}(|\mathbf{x}|^2)} + \dots\,, \tag{1.8}$$

where we have defined $R_{ij} = |\mathbf{R}_{ij}|$. We note that this is in fact nothing other than the standard multipole expansion of the Coulomb potential in Cartesian coordinates [1]. The interaction terms which arise from this are, to quadratic order in $|\mathbf{x}|$,

$$\begin{aligned}
\text{at order } \mathrm{O}(|\mathbf{x}^0|): &\quad -\frac{q^2}{4\pi\varepsilon_0}\sum_{i,j\neq i}\sum_{\mu}\sum_{\sigma}\frac{1}{R_{ij}}\hat{n}_{i\mu\sigma} \\
\text{at order } \mathrm{O}(|\mathbf{x}^1|): &\quad +\frac{q}{4\pi\varepsilon_0}\sum_{i,j\neq i}\sum_{\mu,\mu'\neq\mu}\sum_{\sigma}\frac{\mathbf{d}_{\mu\mu'}\cdot\mathbf{R}_{ij}}{R^3_{ij}}\hat{c}^\dagger_{i\mu\sigma}\hat{c}_{i\mu'\sigma} \\
\text{at order } \mathrm{O}(|\mathbf{x}^2|): &\quad -\frac{q}{8\pi\varepsilon_0}\sum_{i,j\neq i}\sum_{\mu}\sum_{\sigma}\frac{\mathbf{R}_{ij}\cdot\mathbf{q}_{\mu\mu}\cdot\mathbf{R}_{ij}}{R^5_{ij}}\hat{n}_{i\mu\sigma}\,,
\end{aligned} \tag{1.9}$$

where we have defined the dipole and quadrupole matrix elements

$$\begin{aligned}
\mathbf{d}_{\mu\mu'} &= q\int d^3\mathbf{x}\ \mathbf{x}\ \phi^*_\mu(\mathbf{x})\phi_{\mu'}(\mathbf{x}) \\
\mathbf{q}_{\mu\mu'} &= q\int d^3\mathbf{x}\ (3\mathbf{x}\otimes\mathbf{x} - |\mathbf{x}|^2)\ \phi^*_\mu(\mathbf{x})\phi_{\mu'}(\mathbf{x})
\end{aligned}$$

and where we also noted that, by the parity of the Wannier functions, $\mathbf{d}_{\mu\mu} = 0$ and $\mathbf{q}_{\mu\mu'\neq\mu} = 0$.

Once again approximating the Wannier functions by the hydrogen wavefunctions, and assuming that only the p_x-orbital participates optically, we find that the dipole matrix element is aligned with the x-axis, i.e. $\mathbf{d}_{sp} = d_{sp}\hat{\mathbf{x}}$, and has a magnitude $d_{sp} = d_{ps} = 256a_0q/(243\sqrt{2})$. With reference to classical electrostatics, the physical interpretation of the terms in (1.9) becomes clear: The first term corresponds with a sum of charge-charge interactions between electrons on the i-th site and the protons on all other sites. The second term corresponds with a sum of charge-dipole interactions between the polarisation associated with the electron at the i-th site and the protons, which drives transitions between the s- and p-orbitals on the i-th site. The third term is a higher-order quadrupole interaction process.

1.3.2 Electron-electron potential expansion

The case of the electron-electron matrix element (1.7) requires a Taylor expansion in two variables, which contains a number of terms identical to those in (1.8) as well as a cross term at quadratic order in $|\mathbf{x}|$,

$$\begin{aligned}\frac{1}{|\mathbf{x}-\mathbf{y}+\mathbf{R}_{ij}|} = &\underbrace{\frac{1}{R_{ij}}}_{\mathrm{O}(|\mathbf{x}|^0)} \underbrace{-(\mathbf{x}-\mathbf{y})\cdot\frac{\mathbf{R}_{ij}}{R_{ij}^3}}_{\mathrm{O}(|\mathbf{x}|^1)} \\ &\underbrace{-\frac{1}{2}\frac{|\mathbf{x}|^2+|\mathbf{y}|^2}{R_{ij}^3}+\frac{3}{2}\frac{|\mathbf{x}\cdot\mathbf{R}_{ij}|^2+|\mathbf{y}\cdot\mathbf{R}_{ij}|^2}{R_{ij}^5}+\frac{\mathbf{x}\cdot\mathbf{y}}{R_{ij}^3}-\frac{3(\mathbf{x}\cdot\mathbf{R}_{ij})(\mathbf{y}\cdot\mathbf{R}_{ij})}{R_{ij}^5}}_{\mathrm{O}(|\mathbf{x}|^2)}+\dots .\end{aligned} \tag{1.10}$$

Most of the terms in this expansion lead to interactions of the same form as those in (1.9), namely

$$\begin{aligned}\text{at order O}(|\mathbf{x}^1|): \quad &+\frac{q^2}{8\pi\varepsilon_0}\sum_{i,j\neq i}\sum_{\mu,\nu}\sum_{\sigma,\sigma'}\frac{1}{R_{ij}}\hat{n}_{i\mu\sigma}\hat{n}_{j\nu\sigma'} \\ \text{at order O}(|\mathbf{x}^2|): \quad &-\frac{q}{4\pi\varepsilon_0}\sum_{i,j\neq i}\sum_{\nu}\sum_{\mu,\mu'\neq\mu}\sum_{\sigma,\sigma'}\frac{\mathbf{d}_{\mu\mu'}\cdot\mathbf{R}_{ij}}{R_{ij}^3}\hat{n}_{j\nu\sigma'}\hat{c}^\dagger_{i\mu\sigma}\hat{c}_{i\mu'\sigma} - {}^{i\leftrightarrow j}_{\mu\leftrightarrow\nu} \\ \text{at order O}(|\mathbf{x}^2|): \quad &+\frac{q}{8\pi\varepsilon_0}\sum_{i,j\neq i}\sum_{\mu,\nu}\sum_{\sigma,\sigma'}\frac{\mathbf{R}_{ij}\cdot\mathbf{q}_{\mu\mu}\cdot\mathbf{R}_{ij}}{R_{ij}^5}\hat{n}_{i\mu\sigma}\hat{n}_{j\nu\sigma'} + {}^{i\leftrightarrow j}_{\mu\leftrightarrow\nu},\end{aligned} \tag{1.11}$$

which represent repulsive charge-charge and charge-dipole interactions of (possibly multiple) electrons on different sites. However, the cross-term leads to an additional new term

$$\text{at order O}(|\mathbf{x}^2|): \quad \sum_{i,j\neq i}\sum_{\substack{\mu,\mu'\neq\mu\\ \nu,\nu'\neq\nu}}\sum_{\sigma,\sigma'}\frac{\mathbf{d}_{\mu\mu'}\cdot(\mathbb{1}-3\hat{\mathbf{R}}_{ij}\otimes\hat{\mathbf{R}}_{ij})\cdot\mathbf{d}_{\nu\nu'}}{8\pi\varepsilon_0 R_{ij}^3}\hat{c}^\dagger_{i\mu\sigma}\hat{c}_{i\mu'\sigma}\hat{c}^\dagger_{j\nu\sigma'}\hat{c}_{j\nu'\sigma'}, \tag{1.12}$$

where $\hat{\mathbf{R}}_{ij} = \mathbf{R}_{ij}/R_{ij}$. This amounts to a sum of pairwise interactions of the electronic dipoles at each site, which drives transitions of the electrons between the s- and p-like orbitals on either site.

In terms of the optical response, since we are working in the single-photon regime, we will be interested only in individual excitation from the ground state $|G\rangle$. As we outlined in the previous chapter, to lowest order $|G\rangle \approx |g\rangle^{\otimes N}|\Psi_{AF}\rangle$ i.e. each atomic site is occupied by a single electron with a spin value dictated by the antiferromagnetic spin order. To this order, it is easy to see that all terms in (1.9) exactly cancel the terms in (1.11), leaving only the dipole-dipole interaction term (1.12).

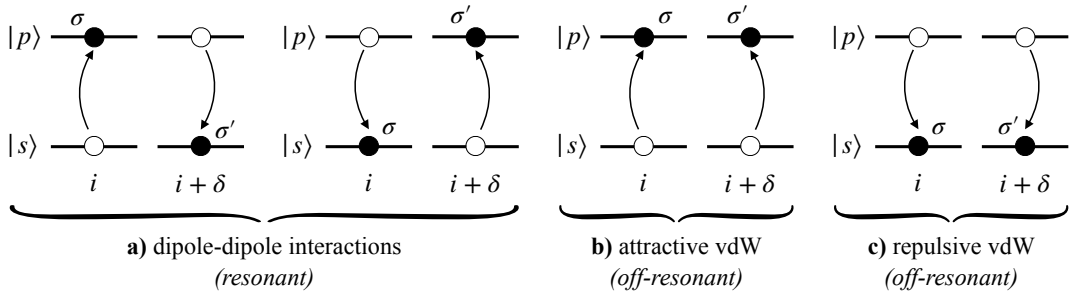

Figure 5.2 – **Dipole interactions.** Diagrammatic representation of the type (i) and (ii) processes associated with the residual electrostatic interaction (1.12). Black [white] circles denote electrons [the absence of electrons] and $\sigma, \sigma' \in \{\uparrow, \downarrow\}$ denote the associated spin value.

1.3.3 Dipole-dipole and dispersion forces

In fact, the dipole-dipole term gives rise to two distinct types of processes, depicted in Fig. 5.2. The processes in Fig. 5.2a are resonant, since the energy of both the initial and final states is $\varepsilon_s + \varepsilon_p$. They reflect the dipole-dipole resonance forces [139], which scale with atomic separation R_{ij}. as $\sim 1/R_{ij}^3$ and are captured by the multiple scattering formalism [12, 66]. On the other hand, in Fig. 5.2b,c the initial and final states are marked by an energy difference of $\pm(2\varepsilon_p - 2\varepsilon_s) = \pm 2\hbar\omega_0$, making them off-resonant. We deal with these processes using second order perturbation theory.

The result of the perturbative calculation is an effective inter-atomic potential which scales with the atomic separation R_{ij} as $\sim 1/R_{ij}^6$, and which is attractive for ground-state atoms and repulsive for excited-state atoms, as indicated in Fig. 5.2d,c. An alternative derivation based on the medium-assisted field quantisation introduced in Chapter 1 leads to the same result [140]. We identify this effective interaction as the well-known van der Waals (vdW) interaction [141–145]. It is fundamentally different in nature to the Coulomb interactions, which rely on a permanent dipole moment: the vdW attraction arises because one atom induces a polarisation in another, thereby correlating the electron states of both atoms. This may occur for initially neutral charge configurations ($E^{(1)} = 0$) and also results in similar interactions between single atoms and macroscopic conducting bodies [146]. Because it depends fundamentally on the frequency-dependent polarisability of the atoms, the vdW interaction is called a *dispersion force* [147], while the dipolar Coulomb interaction is called an *orientation force* [148]. We will encounter another key example of a dispersion force in Section 2.

1.3.4 Local Stark shift

Moving beyond the lowest order approximation to $|G\rangle$, we will have to account for the effects of holon-doublon pairs. Within a minimal semiclassical toy model of a single atom interacting with the classical electric field due to a holon-doublon pair modelled as a static dipole, the effect of a static electric field on an atom is a shift in the atomic energy levels. This is known as the *Stark effect* [72]. However, it can be shown that the effect of this local Stark shift is negligible for $a \gg a_0$.

1.4 Nearest-neighbour hopping

So far we have only considered the type (i) and (ii) matrix elements corresponding with on-site terms. If we consider now type (iii) matrix elements between different sites, the exponential localisation of the Wannier orbital will ensure that we can safely neglect interactions beyond nearest-neighbour terms. The type (iii) matrix elements of interest are therefore $T|_{i+\boldsymbol{\delta} i\mu\nu}, U_p|_{i+\boldsymbol{\delta} ii\mu\nu}$, and $U_p|_{i+\boldsymbol{\delta} iii\mu\mu'\nu\nu'}$ (up to permutations of the atomic site index). Note that here we have also disregarded those matrix elements with integrands on the order $\mathrm{O}(a^{-1})$ discussed above, since these will be sub-dominant.

1.4.1 Hopping Hamiltonian

Starting with only the contributions from the kinetic and electron-proton terms, we note that those matrix elements are associated with the hopping of a single electron between nearest-neighbour sites (see Fig. 5.3a,b). The most efficient way to describe this effect is in terms of the single-particle electronic hamiltonian h, defined in eq. (2.1). Using the fact that h is band diagonal, the full Hamiltonian including the nearest-neighbour hopping terms from both the kinetic and electron-proton terms can be written as

$$H_{\text{hopping}} = \sum_i \sum_{\boldsymbol{\delta}} \sum_{\mu} \sum_{\sigma} t_{\mu\boldsymbol{\delta}} \left(\hat{c}^\dagger_{i\mu\sigma} \hat{c}_{i+\boldsymbol{\delta}\mu\sigma} + \text{h.c.} \right) , \tag{1.13}$$

where we have defined the hopping parameters $t_{\mu\boldsymbol{\delta}} = \langle \phi_{i+\boldsymbol{\delta}\mu\sigma} | h | \phi_{i\mu\sigma} \rangle = U_p|_{i+\boldsymbol{\delta} ii\mu\mu} + T_{i+\boldsymbol{\delta} i\mu\mu}$. We note that while the kinetic and electron-proton terms may individually induce inter-band hopping (e.g. through $U_p|_{i+\boldsymbol{\delta} iips} \neq 0$, see Fig. 5.3b), their matrix elements for such processes cancel in the final Hamiltonian. In fact, the electron-electron interaction also induces a nearest-neighbour intra-band hopping, however in this case, an electron will only hop to a site that is already occupied by another electron, either in the same orbital (see Fig. 5.3c) or in a different orbital (see Fig. 5.3d).

1.4.2 Renormalised hopping parameter

We consider first the former case, shown in Fig. 5.3c. This interaction-induced short-range tunneling can still be captured by the Hamiltonian (1.13) with a different hopping parameter. In general, the renormalisation of the hopping parameter will be local and dynamical, since it depends on the occupation and spin configuration of neighbouring sites. However in the ground state manifold, where we consider only single-band hopping with $t_{s\boldsymbol{\delta}} = t$, the antiferromagnetic spin ordering will result in a global renormalisation $t \to t'$ of the hopping parameter and consequently of the Heisenberg coupling $J \to (t'/t)^2 J$. Again, since we consider only single-photon excitations out of this manifold, this will be the more relevant case.

While the hopping parameters could certainly be evaluated using the hydrogen wavefunctions, this will not yield good results due to small oscillations in the tail of the Wannier orbitals which persist qualitatively even for the maximally localised choice of Wannier functions and which are not reproduced by the hydrogen wavefunctions. This leads to a sign error which results in an inversion of the bands associated with (1.13). Instead, the (renormalised) hopping parameters can be inferred from the energy splitting in hydrogen H_2 molecules [149].

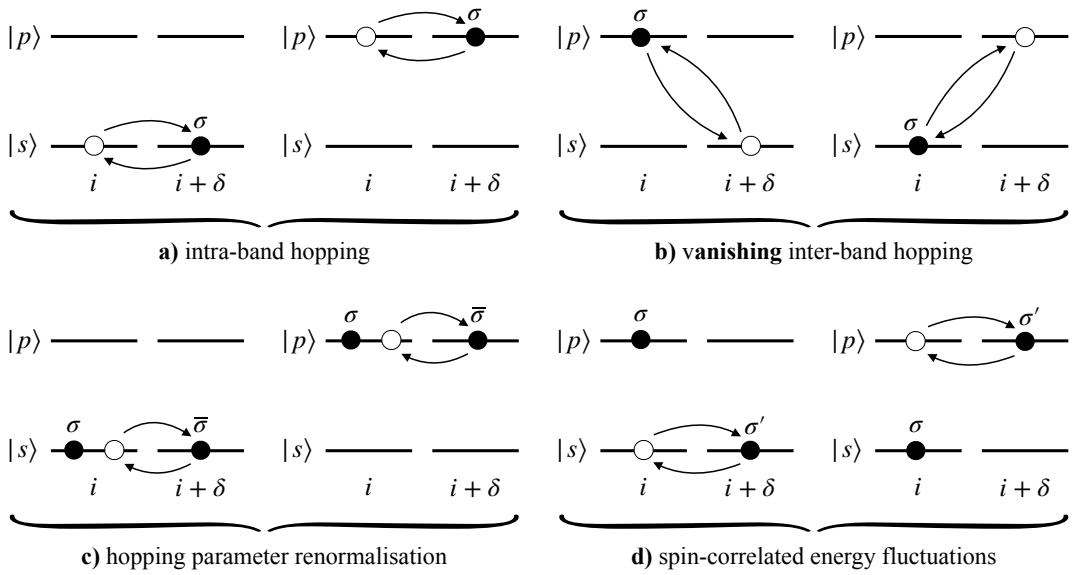

Figure 5.3 – **Nearest-neighbour hopping.** Diagrammatic representation of the different kinds of type (iii) nearest-neighbour hopping processes and their effect. Black [white] circles denote electrons [the absence of electrons] and $\sigma, \sigma' \in \{\uparrow, \downarrow\}$ denote the associated spin value, with $\overline{\sigma}$ indicating the opposite spin value of σ.

1.4.3 Spin-correlated energy fluctuations

Turning to the latter case, shown in Fig. 5.3d, we have to consider the intra-band hopping of an s-orbital electron to a site already occupied by a p-orbital electron and vice versa. The associated Hamiltonian is

$$H'_{\text{hopping}} = \sum_i \sum_{\boldsymbol{\delta}} \sum_{\mu} \sum_{\sigma,\sigma'} \left(t^{\sigma\sigma'}_{\mu\boldsymbol{\delta}} \hat{n}_{i\overline{\mu}\sigma} \hat{c}^{\dagger}_{i+\boldsymbol{\delta}\mu\sigma'} \hat{c}_{i\mu\sigma'} + \text{h.c.} \right) , \tag{1.14}$$

where we have defined hopping amplitudes $t^{\sigma\sigma'}_{\mu\boldsymbol{\delta}}$ which crucially depend on the spin-spin correlations with the electrons on its neighbouring sites. We also note that the final states associated with these hopping processes incur an energy penalty of $u^{\sigma\sigma'}_{sp}$, therefore the processes are distinctly off-resonant and can once again be treated using perturbation theory, with leading order correction $\Delta\omega_0 \propto (t^{\sigma\sigma'}_{\mu\boldsymbol{\delta}})^2 / u^{\sigma\sigma'}_{sp}$.

The effect of these hopping processes then amounts to an inhomogeneous shift in the atomic resonances across the array, depending on the spin-spin correlations of each atom with its nearest neighbours. However, it is reasonable to assume that $\Delta\omega_0 \ll \Gamma_0$ and that therefore this effect will not be appreciable in terms of the collective optical response. This could be confirmed using coupled-dipole simulations for an array of non-identical atoms similar to those in Ref. [27].

1.4.4 Travelling excitation 'impurity'

In fact, there is a higher-order process associated with this hopping to an already occupied site which we need to consider. It is shown in Fig. 5.4a and involves an excited electron tunneling to a neighbouring site (incurring an energy penalty $u^{\uparrow\downarrow}_{sp}$) and the ground-state electron on this site tunnelling to the now unoccupied site, therefore effectively 'switching places' with the excited electron.

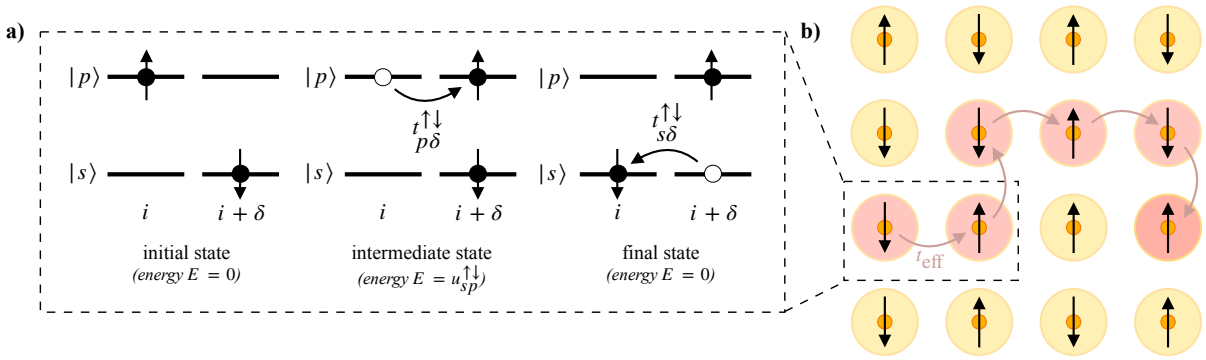

Figure 5.4 – **Second order photon-mediated interactions. a)** Diagrammatic representation of the higher-order process initiating the formation of a propagating magnetic polaron. **b)** Propagation of the impurity through the AF ordered lattice leaving behind a trail of flipped spins.

Intuitively, this process can influence the optical properties of the array: after an incident photon has excited a single electron from the AF ground state $|G\rangle$, through repeated switching of sites with neighbouring ground-state atoms, the 'impurity' of the excitation among the ground-state atoms can propagate through the lattice, leaving behind a trail of flipped spins (see Fig. 5.4b). Eventually, the electron will then decay radiatively to a state with a different spin configuration than $|G\rangle$, therefore this higher-order process opens up a new inelastic decay channel.

The process in Fig. 5.4a can be viewed as a hopping of the impurity with effective hopping amplitude $t_{\text{eff}} \sim (t^{\uparrow\downarrow}_{p\boldsymbol{\delta}})^2/u^{\uparrow\downarrow}_{sp}$. In terms of the Hubbard model parameters $t = t_{s\boldsymbol{\delta}}$ and $U = u_s$, we know that $t^{\uparrow\downarrow}_{p\boldsymbol{\delta}} \gg t$ due to the longer tails of the real-space excited-state wavefunctions. In the strong-coupling regime $t/U \ll 1$, assuming $u^{\uparrow\downarrow}_{sp} \sim U$ this implies that $t_{\text{eff}} \gg t$ as well. The short characteristic timescales of the photon are then comparable only with the timescale $\hbar/t_{\text{eff}}$ and not $\hbar/t$. Hence, the excited electron de-excites under re-emission of a photon before the AF spin order is significantly disturbed. If we assume that on the photonic timescales the hopping process only takes place a single time, then after the 'swap' in Fig. 5.4, a first estimate of the linewidth Γ associated with this new inelastic decay channel is simply $\Gamma \sim t_{\text{eff}} \sim (t^{\uparrow\downarrow}_{p\boldsymbol{\delta}}/U)^2 U$. Clearly, since $t^{\uparrow\downarrow}_{p\boldsymbol{\delta}} \gg t$ this actually implies that this mechanism sets in earlier than the holon-doublon mechanism which scales as $(t/U)^2$, therefore at the onset of quantum chemistry, this new process seems to be the dominant one.

We defer a rigorous study of this process and its effect on the refractive index to later work and note here only that the problem of a propagating impurity in in a Heisenberg antiferromagnet is actually well-established in condensed matter theory [150–152]. Formally, the local distortion of the spin background due to the coupling of the impurity to the low-lying magnonic excitations has been interpreted as the creation and subsequent diffusion of a magnetic polaron [153]. Both the transient dynamics [154] and the long-time dynamics [155] of such polarons have been resolved experimentally. As a matter of fact, the field theoretic approach of Chapter 4 has been instrumental in developing the quasiparticle description of the polaron dynamics, along with formulations in terms of *quantum walks* on Cayley trees [151, 156].

1.5 Other processes

There are, of course, a number of other type (iii) processes which arise due to the electron-electron interaction. Specifically, these are processes involving an inter-band transition of a single electron between nearest-neighbour sites, an inter-band transition of an electron on a single site accompanied by an intra-band nearest-neighbour hopping, or the least dominant processes involving two inter-band transitions, some of which create or break up a doublon. These processes are schematically collected in Fig. 5.5. We will not investigate these effects in any detail since they are sub-dominant.

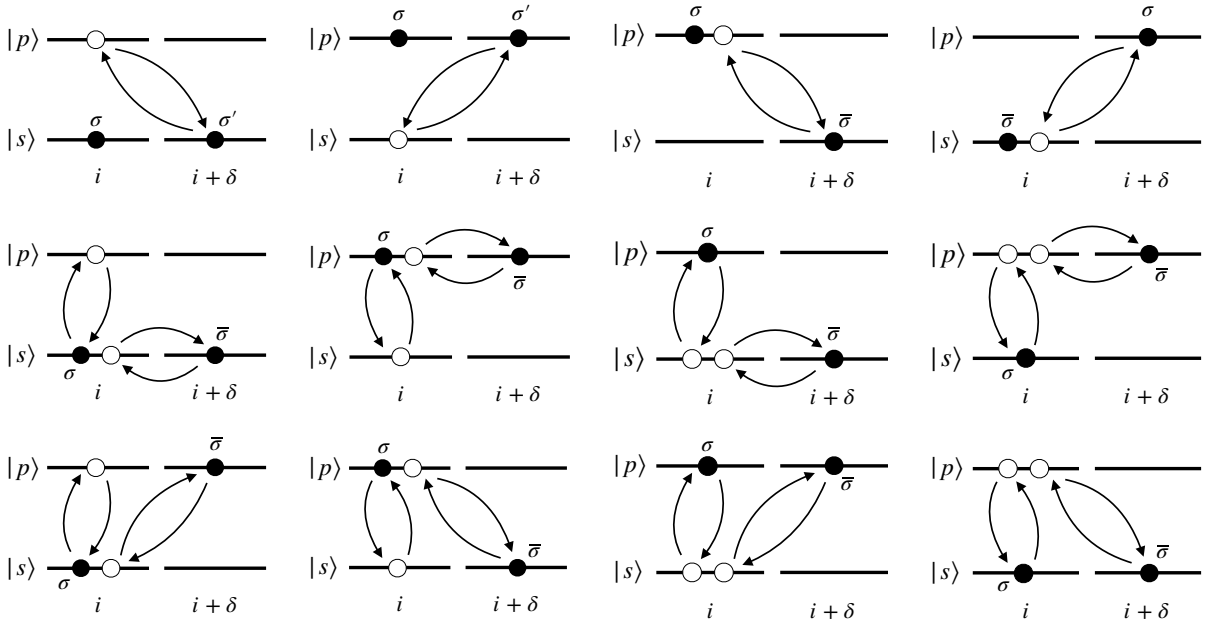

Figure 5.5 – **Other nearest-neighbour processes.** Diagrammatic representation of the least dominant type (iii) processes arising from the electron-electron interaction. Black [white] circles denote electrons [the absence of electrons] and $\sigma, \sigma' \in \{\uparrow, \downarrow\}$ denote the associated spin value, with $\overline{\sigma}$ indicating the opposite spin value of σ.

2 Photon-mediated interactions

2.1 On-site atom-light interactions

We now move on to the photon-mediated interactions, starting with the dominant type (i) and (ii) on-site processes. These processes are simply the well-known resonant and off-resonant excitation and de-excitation of a single atom by a single photon [14], associated with the interaction Hamiltonian

$$H_{AF} = \frac{\mathrm{i}\hbar q}{m} \sum_i \sum_{\mathbf{k}} \mathbf{f}_{\mathbf{k}} \cdot \left(\mathbf{p}_{sp} \mathrm{e}^{\mathrm{i}\mathbf{k}\cdot\mathbf{R}_i}\ \hat{a}^\dagger_{\mathbf{k}} \hat{c}^\dagger_{i\sigma s} \hat{c}_{i\sigma p} + \mathbf{p}_{sp} \mathrm{e}^{-\mathrm{i}\mathbf{k}\cdot\mathbf{R}_i} \hat{a}_{\mathbf{k}} \hat{c}^\dagger_{i\sigma s} \hat{c}_{i\sigma p} - \text{h.c.} \right) , \tag{2.1}$$

where we have re-substituted the expression for the on-site matrix elements $V|_{ii\mu\nu;\mathbf{k}}$ and defined

$$\mathbf{p}_{sp} = \int d^3\mathbf{r}\ \phi^*_s(\mathbf{r}) \boldsymbol{\nabla} \phi_p(\mathbf{r}) = \frac{\mathrm{i}}{\hbar} \langle s | \hat{\mathbf{p}} | p \rangle \, . \tag{2.2}$$

By standard arguments, $\mathbf{p}_{sp}$ is related to the dipole matrix element according to $\mathbf{p}_{sp} = -m\omega_0 \mathbf{d}_{sp}/(q\hbar)$ [67].

2.2 Long-range interactions

These processes involve only a single atom, however they combine to form higher-order processes involving the exchange of a photon between two different atoms (see Fig. 5.6). They are the photon-mediated counterparts to the processes in Fig. 5.2; while the latter arise from the direct atom-atom coupling via the Coulomb potential, in this case the interactions are mediated by the field, leading to retardation. As in the electrostatic case, we again discern resonant (Fig. 5.6a) and off-resonant (Fig. 5.6b) terms. The resonant terms represent the retarded dipole-dipole interactions which combine with the instantaneous electrostatic dipole-dipole interactions (Fig. 5.2a) in the multiple scattering picture. They show a dependence $\sim 1/R_{ij}$ as well as spatial oscillations of the potential, characteristic of radiative long-range interactions [157–159].

Similarly, the off-resonant interactions provide the retarded counterparts to the vdW interactions (Fig. 5.2b,c), which are commonly referred to as *Casimir-Polder (CP) forces* and represent the second well-known class of dispersion forces [147]. the vdW and CP interactions represent the opposing limiting cases of $R_{ij} \ll \lambda_0$ and $R_{ij} \gg \lambda_0$, respectively. Unlike the their vdW couterpart, the CP interactions cannot be captured by the standard perturbative approach of Ref. [144], but using normal mode quantum electrodynamics can be shown to scale as $\sim R_{ij}^7$ for ground-state atoms [160], and $\sim R_{ij}^2$ for excited-state atoms [161], although there remains uncertainty about associated spatial modulations [147]. Since the off-resonant processes fall off more strongly with atomic separation than the resonant interactions, they are sub-dominant.

2.3 Photon-assisted hopping

The most dominant of the type (iii) processes, involving hopping of electrons between nearest-neighbour sites accompanied by an emission or absorption of a photon, are shown in Fig. 5.7. Again, these can be separated into processes which are resonant and off-resonant. In terms of the optical properties of the array, the 'worst-case scenario' associated with a photon assisted excitation of an s-orbital electron to the p-orbital of a neighbouring atom would be a radiative decay of the electron to the s-orbital of the new atom, since this would be inelastic. The radiative decay of a p-orbital electron to the s-orbital of a neighbouring sites represents a similar inelastic process. We can therefore account for the processes in Fig. 5.7a simply by modifying $\Gamma_{\text{coop}} \to \Gamma_{\text{coop}} + \Gamma_{\text{inel}}$, where Γ_{inel} denotes the (radiative) decay rate associated with the inelastic processes.

2.4 Other processes

As in the electrostatic case, there are of course many other type (iii) processes included in the term V, most importantly the sub-dominant hopping processes shown in Fig. 5.8. However, by the same argument as before, we argue that the modifications to the optical response due to more dominant processes is already exponentially small in a_0/a.

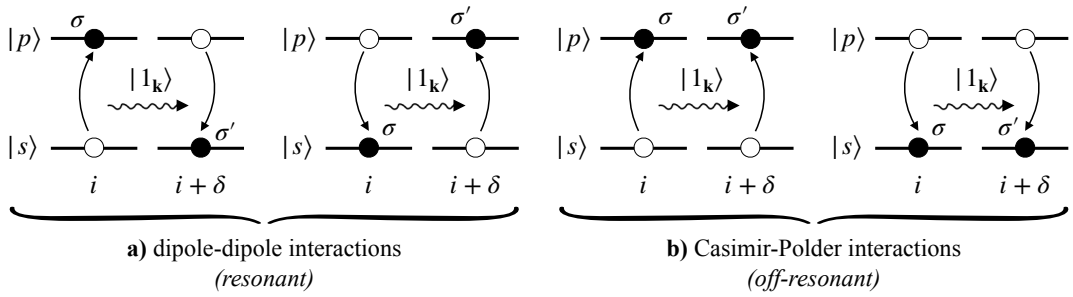

Figure 5.6 – **Second order photon-mediated interactions.** Diagrammatic representation of the higher-order processes composed from the type (i) and (ii) processes associated with on-site interaction of a single atoms with single photons. Black [white] circles denote electrons [the absence of electrons], $\sigma, \sigma' \in \{\uparrow, \downarrow\}$ denote the associated spin value, and the arrow represents the photon.

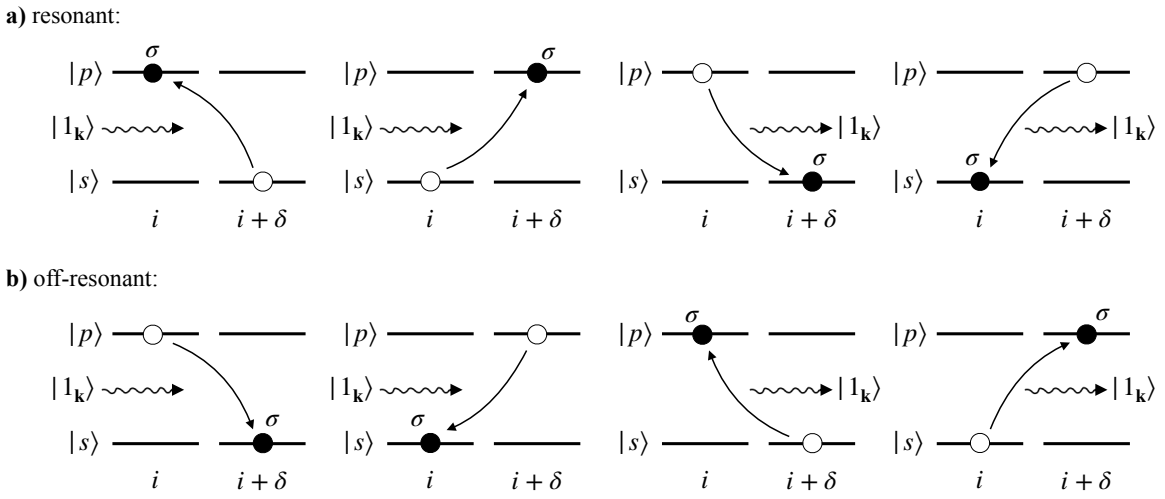

Figure 5.7 – **Dominant photon-assisted nearest-neighbour hopping.** Diagrammatic representation of the dominant type (iii) photon-assisted inter-band hopping. Black [white] circles denote electrons [the absence of electrons] and $\sigma \in \{\uparrow, \downarrow\}$ denotes the associated spin value, and the arrow represents the photon.

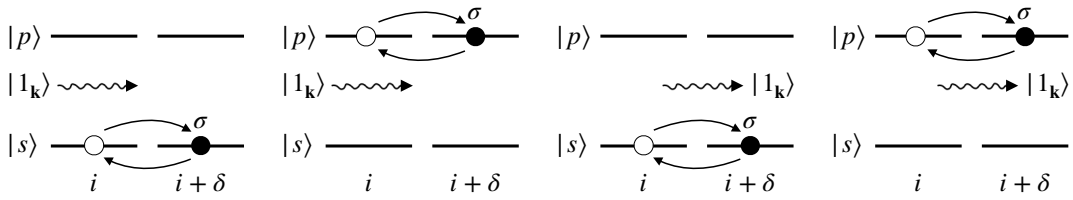

Figure 5.8 – **Sub-dominant photon-assisted nearest-neighbour hopping.** Diagrammatic representation of the sub-dominant type (iii) photon-assisted intra-band hopping. Black [white] circles denote electrons [the absence of electrons] and $\sigma \in \{\uparrow, \downarrow\}$ denotes the associated spin value, and the arrow represents the photon.

3 Quantum optics limit

The discussion above is summarised in Table 2. The bottom line is that the key dominant effects of quantum chemistry are dipole-dipole interactions (both due to direct atom-atom interactions and mediated by atom-field interactions), as well as on-site electron-electron repulsion and nearest-neighbour hopping. The other, less straightforward effects of quantum chemistry are negligible compared to these dominant processes or can be neatly integrated into the multiple scattering description, as also indicated. Having already discussed the interplay of hopping and on-site repulsion extensively in the last chapter, we will now derive in the section below a formal description of the dynamics associated with the (resonant) dipole-dipole interactions.

Physical process	**Effective description**	**Sec.**
On-site electron binding energy and electron-electron repulsion	***Hubbard model***	**1.1**
(Spin-correlated) nearest-neighbour hopping		**1.4.1,2**
Non-retarted dipole-dipole interactions	***Spin model***	**1.3.3**
Retarded dipole-dipole interactions		**2.2**
Higher-order hopping processes	***Magnetic polaron***	**1.4.4**
Photon-assisted nearest-neighbour hopping	*Inelastic decay rate*	**2.3**
Local Stark shift around holon-doublon pairs	*Local inhomogeneities*	**1.3.4**
Spin-correlated local energy fluctuations		**1.4.3**
Holon / doublon internal processes	*Negligible / not relevant*	**1.2**
Non-retarded van der Waals interactions		**1.3.3**
Retarded Casimir-Polder interactions		**2.2**

Table 2 – Categorisation of dominant physical processes. The table lists the dominant effects associated with the onset quantum chemistry, grouped in terms of their role in the optical response of the array.

3.1 Effective Hamiltonian

For the case of singly occupied sites, we can express the effective action of the Wannier operators in terms of atomic operators for the atoms, defined in this case as $\hat{\sigma}^+ = |p\rangle\langle s|$ and $\hat{\sigma}^- = |s\rangle\langle p|$. In particular, we can make the effective substitutions $\hat{c}^\dagger_{ip\sigma}\hat{c}_{is\sigma} \sim \hat{\sigma}^+_i$ and $\hat{c}^\dagger_{is\sigma}\hat{c}_{ip\sigma} \sim \hat{\sigma}^-_i$, as well as $\hat{n}_{ip\sigma} \sim \hat{\sigma}^+_i\hat{\sigma}^-_i$ and $\hat{n}_{is\sigma} \sim \hat{\sigma}^-_i\hat{\sigma}^+_i$. We will assume $\mathbf{d}_{sp} = d_{sp}\hat{\mathbf{x}}$ and express $\mathbf{R}_{ij}$ in spherical polar coordinates $(R_{ij}, \theta_{ij}, \phi_{ij})$. The Hamiltonian which captures the processes described in Sections 1.3.3 and 2.2 then takes the form

$$H = \underbrace{\sum_i \hbar\omega_0 \hat{\sigma}^+_i\hat{\sigma}^-_i}_{H_A} + \underbrace{\sum_{\mathbf{k}} \hbar\omega_{\mathbf{k}}\hat{a}^\dagger_{\mathbf{k}}\hat{a}_{\mathbf{k}}}_{H_F} \underbrace{-\mathrm{i}\omega_0 \sum_i (\mathbf{d}_{sp}\hat{\sigma}^+_i - \mathrm{h.c.}) \cdot \hat{\mathbf{A}}(\mathbf{R}_i)}_{H_{AF}} + \underbrace{\frac{|d_{sp}|^2}{4\pi\varepsilon_0} \sum_{i,j\neq i} \frac{1 - 3\sin^2\phi_{ij}}{R^3_{ij}} \hat{\sigma}^+_i\hat{\sigma}^-_j}_{H_{AA}} \tag{3.1}$$

where we have in H_{AF} re-substituted the mode decomposition of the vector potential and used the relation between the momentum and position matrix elements. Here and throughout the next sections, the subscripts A and F refer to the atomic (matter) and field (radiation) degrees of freedom, respectively. With reference to eq. (1.16) of Chapter 2, we recognise that

$$H_{AA} = -\mu_0\omega_0^2|d_{sp}|^2 \sum_{i,j\neq i} G^{\parallel}_{xx}(\omega_0, \mathbf{R}_{ij})\ \hat{\sigma}_i^{eg}\hat{\sigma}_j^{ge}\,. \tag{3.2}$$

Obtaining a similarly concise expression for the photon-mediated interactions encoded in H_{AF} is slightly less trivial; Since the spin model provides an 'all matter' description of the atomic array, to obtain a more suitable form of the interactions encoded in H_{AF} we should integrate our the radiative degrees of freedom. Below, we follow the formalism of Ref. [162] to do this, employing concepts from the theory of open quantum systems and from non-equilibrium statistical physics.

3.2 Master equation dynamics

3.2.1 Effective Hamiltonian I

We will describe the state of the compound atom-field system in terms of its density matrix ρ_{AF}. In what follows, we will use tildes to denote the interaction picture. The evolution of the density matrix $\tilde{\rho}_{AF}(t)$ is governed by the *Born-Markov master equation* [60]

$$\partial_t\tilde{\rho}_{AF}(t) = -\frac{1}{\hbar^2}\int_0^\infty d\tau[\tilde{H}_{AF}(t), [\tilde{H}_{AF}(t-\tau), \tilde{\rho}_{AF}(t)]]\,. \tag{3.3}$$

In deriving this equation, we make the approximations that the reservoir provided by the radiation field is large (*Born approx.*) so that $\tilde{\rho}_{AF}(t) \approx \tilde{\rho}_A(t)|0\rangle\langle 0|$, and that the field and atoms remain uncorrelated on the time-scales of the evolution of the atomic density matrix (*Markov approx.*) so that $\tilde{\rho}_A(t-\tau) \approx \tilde{\rho}_A(t)$ and we can extend the integration limit $\tau \to \infty$ [16]. Tracing out the field subsystem,

$$\partial_t\rho_A(t) = \underbrace{-\frac{\mathrm{i}}{\hbar}[H_A, \rho_A(t)] - \frac{1}{\hbar^2}\int_0^\infty d\tau U_A^\dagger(t)\left(\langle 0|\tilde{H}_{AF}(t)\tilde{H}_{AF}(t-\tau)|0\rangle\tilde{\rho}_A(t) + \text{h.c.}\right)U_A(t)}_{-\frac{\mathrm{i}}{\hbar}(\mathcal{H}'_{\text{eff}}\rho_A(t) - \rho_A(t)\mathcal{H}'^{\dagger}_{\text{eff}})} + \ldots \tag{3.4}$$

Here we have isolated terms corresponding with Hamiltonian dynamics under an effective (non-Hermitian) Hamiltonian $\mathcal{H}'_{\text{eff}}$, which we can infer as

$$\mathcal{H}'_{\text{eff}} = H_A - \frac{\mathrm{i}}{\hbar}\int_0^\infty d\tau\langle 0|U_A^\dagger(t)\tilde{H}_{AF}(t)\tilde{H}_{AF}(t-\tau)U_A(t)|0\rangle\,. \tag{3.5}$$

3.2.2 Linear response approach

From the explicit expression for the interaction-picture atom-field coupling Hamiltonian $\tilde{H}_{AF}(t)$, we see

$$\begin{aligned} &U_0^\dagger(t)\tilde{H}_{AF}(t)\tilde{H}_{AF}(t-\tau)U_0(t) \\ &\quad= \omega_0^2\sum_{i,j}\sum_{\alpha,\beta}\left[\left(d_{sp}^\alpha(d_{sp}^*)^\beta\hat{\sigma}_i^+\hat{\sigma}_j^-\mathrm{e}^{\mathrm{i}\omega_0\tau} + \text{h.c.}\right) - \left(d_{sp}^\alpha d_{sp}^\beta\hat{\sigma}_i^+\hat{\sigma}_j^+\mathrm{e}^{-\mathrm{i}\omega_0\tau} + \text{h.c.}\right)\right]C^{\alpha\beta}(\mathbf{R}_i, \mathbf{R}_j, \tau)\,, \end{aligned} \tag{3.6}$$

where we have defined the real-space 2-point correlation function for the vector potential,

$$C^{\alpha\beta}(\mathbf{R}_i, \mathbf{R}_j, \tau) = \langle A^\alpha(\mathbf{R}_i, \tau) A^\beta(\mathbf{R}_i, 0) \rangle \,. \tag{3.7}$$

In fact, we can drop the second term in the square brackets in eq. (3.6), since for $i = j$ it vanishes exactly ($\hat{\sigma}_i^\pm \hat{\sigma}_i^\pm = 0$) and for $i \neq j$ it encodes the off-resonant van der Waals interactions (cf. Table 2). We express the correlator as $C_{\alpha\beta}(\mathbf{r}, \mathbf{r}', \tau) = 1/2(S_{\alpha\beta}(\mathbf{r}, \mathbf{r}', \tau) + \chi''_{\alpha\beta}(\mathbf{r}, \mathbf{r}', \tau))$ where

$$\begin{aligned} S_{\alpha\beta}(\mathbf{r}, \mathbf{r}', \tau) &= \langle \{ \tilde{A}^\alpha(\mathbf{r}, \tau), \tilde{A}^\beta(\mathbf{r}', 0) \} \rangle \\ \chi''_{\alpha\beta}(\mathbf{r}, \mathbf{r}', \tau) &= \langle [\tilde{A}^\alpha(\mathbf{r}, \tau), \tilde{A}^\beta(\mathbf{r}', 0)] \rangle \end{aligned} \tag{3.8}$$

are the (anti)symmetrised correlators. By the Fluctuation-Dissipation Theorem (FDT) [163], the symmetrised and antisymmetrised correlators are related at temperature $T = 1/(\beta k_B)$ according to

$$S_{\alpha\beta}(\mathbf{r}, \mathbf{r}', \tau) = \coth\left(\frac{\hbar\beta\omega}{2}\right) \chi''_{\alpha\beta}(\mathbf{r}, \mathbf{r}', \tau) \,,$$

which implies that at zero temperature ($\beta \to \infty$) we have $C_{\alpha\beta}(\mathbf{r}, \mathbf{r}', \tau) = \chi''_{\alpha\beta}(\mathbf{r}, \mathbf{r}', \tau)$. Then,

$$\mathcal{H}'_{\text{eff}} = H_A - \frac{\mathrm{i}\omega_0^2}{\hbar} \sum_{i,j} \sum_{\alpha,\beta} \int_0^\infty d\tau \left(d^\alpha_{sp} (d^*_{sp})^\beta \hat{\sigma}_i^+ \hat{\sigma}_j^- \mathrm{e}^{\mathrm{i}\omega_0 \tau} + \text{h.c.} \right) \chi''_{\alpha\beta}(\mathbf{R}_i, \mathbf{R}_j, \tau) \,. \tag{3.9}$$

The challenge now becomes the evaluation of the antisymmetric correlator $\chi''_{\alpha\beta}(\mathbf{R}_i, \mathbf{R}_j, \tau)$. One way to do this is to calculate it from the linear response function $\chi_{\alpha\beta}(\mathbf{R}_i, \mathbf{R}_j, \omega) = (2\mathrm{i}/\hbar)\chi''_{\alpha\beta}(\mathbf{R}_i, \mathbf{R}_j, \tau)$ of the vector potential in analogy to the calculation in Ref. [164] for the physical electric field. As pointed out in Ref. [164], the virtue of this approach is that, while $\chi''_{\alpha\beta}(\mathbf{R}_i, \mathbf{R}_j, \omega)$ is a quantum mechanical quantity, $\chi_{\alpha\beta}(\mathbf{R}_i, \mathbf{R}_j, \omega)$ can be computed directly and classically. Specifically, we start from Maxwell's equations with an external source term $\mathbf{J}_{\text{ext}}(\mathbf{r}', \omega)$, which we know are solved in the Coulomb gauge by [59]

$$\mathbf{A}(\mathbf{r}, \omega) = \mu_0 \int d^3\mathbf{r}' \mathbf{G}^\perp(\mathbf{r} - \mathbf{r}', \omega) \cdot \mathbf{J}_{\text{ext}}(\mathbf{r}', \omega) \,.$$

In the language of linear response theory, $\mathbf{A}(\mathbf{r}, \omega)$ and $\mathbf{J}_{\text{ext}}(\mathbf{r}', \omega)$ are a conjugate generalised displacement and force. The linear response function of the vector potential can therefore be computed as

$$\chi_{\alpha\beta}(\mathbf{r}, \mathbf{r}', \omega) = \frac{\delta \langle A^\alpha(\mathbf{r}, \omega) \rangle}{\delta J^\beta_{\text{ext}}(\mathbf{r}', \omega)} = \mu_0 G^\perp_{\alpha\beta}(\mathbf{r} - \mathbf{r}', \omega) \,, \tag{3.10}$$

whereby the Fourier transform of the antisymmetrised correlator is $\chi''_{\alpha\beta}(\mathbf{r}, \mathbf{r}', \omega) = (-\mathrm{i}\hbar\mu_0/2) G^\perp_{\alpha\beta}(\mathbf{r} - \mathbf{r}', \omega)$. Substituting the result for $\chi''_{\alpha\beta}(\mathbf{R}_i, \mathbf{R}_j, \omega)$ into the expression for the effective Hamiltonian,

$$\mathcal{H}'_{\text{eff}} = H_A - \mu_0 \omega_0^2 \sum_{i,j} \underbrace{\sum_{\alpha,\beta} \int_{-\infty}^\infty \frac{d\omega}{2\pi} \int_0^\infty d\tau \, \mathrm{e}^{-\mathrm{i}\omega\tau} \left(d^\alpha_{sp} (d^*_{sp})^\beta \hat{\sigma}_i^+ \hat{\sigma}_j^- \mathrm{e}^{\mathrm{i}\omega_0\tau} + \text{h.c.} \right) G^\perp_{\alpha\beta}(\mathbf{R}_{ij}, \omega)}_{J_{ij}} \,. \tag{3.11}$$

3.2.3 Effective Hamiltonian II

We look at the terms with $i = j$ and $i \neq j$ separately, starting with the on-site terms ($i = j$),

$$J_{ii} = \int_{-\infty}^\infty \frac{d\omega}{2\pi} \int_0^\infty d\tau \left(\hat{\sigma}_i^+ \hat{\sigma}_i^- \mathrm{e}^{\mathrm{i}(\omega_0 - \omega)\tau} + \hat{\sigma}_i^- \hat{\sigma}_i^+ \mathrm{e}^{-\mathrm{i}(\omega_0 + \omega)\tau} \right) \mathbf{d}_{sp} \cdot \mathbf{G}^\perp(\mathbf{0}, \omega) \cdot \mathbf{d}^*_{sp} \,.$$

Physically, the second term in this expression reflects a renormalization of the ground state energy due to coupling with a vacuum field, which we do not compute explicitly here. We also note that the exponential $\mathrm{e}^{\mathrm{i}(\omega_0-\omega)\tau}$ is fast-oscillating away from $\omega=\omega_0$, so that the integrand is attenuated for $\omega\neq\omega_0$. Hence,

$$J_{ii}\approx\hat{\sigma}_i^+\hat{\sigma}_i^-\mathbf{d}_{sp}\cdot\mathbf{G}^\perp(\mathbf{0},\omega_0)\cdot\mathbf{d}_{sp}^*\int_0^\infty\frac{d\omega}{2\pi}\int_{-\infty}^\infty d\tau\ \mathrm{e}^{\mathrm{i}(\omega_0-\omega)\tau} \tag{3.12}$$

To evaluate the remaining integrals, Ref. [67] notes that in the Markov approximation we may write

$$\int_0^\infty d\tau\int_{-\infty}^\infty d\omega\ \mathrm{e}^{-\mathrm{i}(\omega_0-\omega)\tau}\approx 2\pi\int_0^\infty d\tau\delta(\tau)=\pi\,, \tag{3.13}$$

where in the last step we have split the delta function because the peak of the delta function lies at the limit of integration. Here we have ignored a (divergent) principal value term associated with a renormalisation of the excited atomic energy, which again we do not compute explicitly. Absorbing implicitly both the ground- and excited-state renormalisation into our description of the atomic spectrum, $J_{ii}=\hat{\sigma}_i^+\hat{\sigma}_i^-|d_{sp}|^2G_{xx}^\perp(\mathbf{0},\omega_0)$ using also the fact that $\mathbf{G}(\mathbf{r},\omega)=\mathbf{G}^{\mathrm{T}}(\mathbf{r},\omega)$ and $\mathbf{d}_{sp}=d_{sp}\hat{\mathbf{x}}$.

This expression is actually not trivial, since it is clear from eq. (1.9) in Chapter 2 that $G_{xx}^\perp(\mathbf{r},\omega)$ diverges as $\mathbf{r}\to 0$. In fact, significant efforts have been devoted to finding suitable regularisation techniques for this divergence (see e.g. Ref. [69]). In our case, we observe that physically, the real part of $G_{xx}^\perp(\mathbf{0},\omega)$ will be associated with an on-site energy (which we again ignore), while the imaginary part can be identified with a spontaneous decay rate (e.g. by comparison with Wigner-Weisskopf theory for single atoms [67]). Indeed, from eq. (1.16) in Chapter 2 we infer that

$$G_{xx}^\perp(\mathbf{r},\omega)=\underbrace{\frac{1+\cos^2\theta\cos^2\varphi}{8\pi r}}_{\text{divergent Re }G_{xx}^\perp(\mathbf{r},\omega)}+\frac{\mathrm{i}k}{6\pi}+\mathrm{O}(r) \tag{3.14}$$

where we have temporarily switched to polar coordinates (r,θ,φ) for $\mathbf{r}$. Hence we see that

$$J_{ii}=\frac{\mathrm{i}|d_{sp}|^2\omega_0}{6\pi c}\hat{\sigma}_i^+\hat{\sigma}_i^-\,. \tag{3.15}$$

For the off-site terms ($i\neq j$), exactly the same approximations as above then lead to

$$J_{ij}\approx|d_{sp}|^2G_{xx}^\perp(\mathbf{R}_{ij},\omega_0)\hat{\sigma}_i^+\hat{\sigma}_j^-\,. \tag{3.16}$$

This allows us to write the final effective atomic Hamiltonian $\mathcal{H}_{\text{eff}}=\mathcal{H}'_{\text{eff}}+H_{AA}$ as

$$\mathcal{H}_{\text{eff}}=\hbar\left(\omega_0-\mathrm{i}\frac{\Gamma_0}{2}\right)\sum_i\hat{\sigma}_i^+\hat{\sigma}_i^--\mu_0\omega_0^2|d_{sp}|^2\sum_{i,j\neq i}G_{xx}(\mathbf{R}_{ij},\omega_0)\ \hat{\sigma}_i^+\hat{\sigma}_j^-\,, \tag{3.17}$$

where we have re-inserted the expression for H_{AA} and identified the single-atom spontaneous decay rate $\Gamma_0=\omega_0^3|d_{sp}|^2/(3\pi\varepsilon_0\hbar c^3)$. Clearly this has the form of the non-hermitian spin model Hamiltonian introduced in Chapter 2: *by ignoring the ground state density-density fluctuations and retaining only the leading order terms in the expansion in a_0/a, we formally recover the quantum optics limit.*

Chapter 6

Conclusion

1 Summary of results

In this thesis, we have presented for the first time a strategy to incorporate the dominant effects of quantum chemistry into the description of an atomic array in a perturbative fashion: starting from the full quantum chemistry Hamiltonian for a lattice of hydrogenic atoms (i.e. the formal Hamiltonian without any simplifying assumptions beyond the Born-Oppenheimer approximation), we have systematically derived the corrections to the quantum optics limit of discrete scatterers due to the onset of quantum chemistry in the lattice by performing a controlled expansion of the full Hamiltonian in $a_0/a \ll 1$. In particular, this has allowed us to estimate the modifications to the well-studied collective optical response of the atomic array as the inter-atomic spacing is decreased.

The picture which we arrive at is that among all the quantum chemistry corrections, there are two distinct processes which become the dominant optical effects that emerge with the onset of quantum chemistry: 1. inelastic scattering of incident light by the buildups of density-density correlations in the ground state and 2. the creation and diffusion of a magnetic polaron in response to an incident photon. Although the latter is even more dominant than the former at larger atomic separations, in this thesis we have focused on the former and, using asymptotic analytical results for the ground state model of the array, we were able to infer the scaling of the associated inelastic linewidth.

While our analysis showed that at the onset of quantum chemistry, the optical response of the atomic array is well-captured by the conventional spin model of multiple scattering applied to a punctured lattice to reflect the electron imbalance on individual sites, we were also able to methodically deal with the other processes which arise at the lowest orders of the expansion in a_0/a: rather than an untameable collection of complicated effects, we saw that to lowest order, the essence of quantum chemistry lies in a manageable number of processes which can be conveniently categorised in terms of their influence on the optical response of the array. Specifically, we found processes which contribute an inelastic linewidth to the collective response but which are sub-leading compared to the two effects mentioned above (e.g. photon-assisted short-range inter-band tunneling) and effects which are essentially irrelevant to our problem (e.g. negligible local Stark shifts due to holon-doublon pairs in the ground state or spin-correlated renormalisation of system parameters which does not effect our results qualitatively).

Most importantly, our analysis of quantum chemistry effects in a 2D array enabled us, via the

construction of a simple minimal model for the refractive index in 3D crystals, to for the first time combine non-perturbative multiple scattering and quantum chemistry to make realistic statements about the saturation of the refractive index. Based on our results, the two dominant optical effects are, at least for moderate atomic densities, solely responsible for the attenuation of the index. Leaving aside for a moment the magnetic polaron effect, the question which remains is whether the holon-doublon inelastic linewidth Γ alone is in fact large enough relative to the ideal cooperative linewidth Γ_{coop} to attenuate the refractive index to the experimentally observed orders of magnitude (i.e. whether the optical response of a lattice with individual atoms removed is sufficiently different from a fully filled lattice to deflect the curve in Fig. 1.1b significantly). If we are able to show that this is indeed the case, we will have identified a single mechanism (or rather one of two mechanism) practically single-handedly responsible for the low maximum refractive index of real atomic materials.

2 Density-density correlations

The missing piece of information is the doublon scattering cross-section σ_{eff}, or rather the ratio $\sigma_{\text{eff}}/\sigma_{\text{sc}}$ which enters our definition of the holon-doublon inelastic linewidth. However, since the problem of the lattice with missing atoms can be treating under the assumption of discrete scatterers at the onset of quantum chemistry, we can estimate σ_{eff} simply by refining the multiple scattering analysis of Chapter 2 to account for a single empty site.

2.1 Response in 2D revisited

We consider again a square lattice with sites $\mathbf{R}_i$ $(i = 1, \ldots, N)$ in the xy-plane, onto which we place $N-1$ two-level atoms modelled as classical dipoles $\mathbf{d}_i$ $(i = 1, \ldots, N,\ i \neq h)$. We consider a uniform incident plane wave polarised along the x-axis (implying $\mathbf{d}_i = d_i\hat{\mathbf{x}}$), with amplitude E_0 and wavevector $\mathbf{k}$ with $\mathbf{k}_\parallel = 0$. Formally, removing the single dipole at the lattice position $\mathbf{R}_h$ from a fully filled lattice leads to new coupled-dipole equations

$$d_i = \alpha E_0 + \alpha\mu_0\omega^2 \sum_{j\neq i,h} G_{xx}(\mathbf{R}_{ij},\omega)d_j\,. \tag{2.1}$$

We write the self-consistent solutions to these equations as $d_i = d_0 + c_i$ where d_0 denotes the (uniform) solution to the problem with no hole (see Chapter 2),

$$d_0 = -\underbrace{\frac{3\pi\varepsilon_0}{k_0^3}\Gamma_0}_{\alpha_0}\frac{1}{\omega-\omega_{\text{coop}}+\mathrm{i}\Gamma_{\text{coop}}/2}E_0\,. \tag{2.2}$$

The coefficients c_i denote the corrections to the solution with no holes and they obey

$$c_i = \alpha\mu_0\omega^2\left(\sum_{j\neq i,h} G_{xx}(\mathbf{R}_{ij},\omega)c_j - G_{xx}(\mathbf{R}_{ih},\omega)d_0\right)\,. \tag{2.3}$$

This implies that the problem of a lattice with a single dipole removed at site $\mathbf{R}_h$ is equivalent to a superposition of two problems: the ideal problem (i.e. a lattice with no holes) and the problem of a single dipole oscillating perfectly out of phase with the solution to the ideal problem.

The expression (2.3) does not treat the site of the hole on equal footing with the others, since the c_i are defined only for $i \neq h$. To extend this formula to all sites, we can equivalently introduce a local driving field Ω_i, leading to the new equations

$$c_i = \alpha\Omega_i + \alpha\mu_0\omega^2 \sum_{j\neq i} G_{xx}(\mathbf{R}_{ij},\omega)c_j \,, \tag{2.4}$$

with $i = 1,\ldots,N$. From these equations, we recover $c_i = -d_0$ for $i = h$ and eq. (2.3) for $i \neq h$ when we define the driving field self-consistently as

$$\Omega_i = \begin{cases} -\dfrac{d_0}{\alpha} - \mu_0\omega^2 \sum_{j\neq h} G_{xx}(\mathbf{R}_{hj},\omega)c_j \,, & i = h \\ 0 \,, & i \neq h \end{cases} \tag{2.5}$$

In Appendix A, we derive a reciprocal-space solution to eqs. (2.4) and (2.5), as well as the associated self-consistent definition of the driving field,

$$\Omega_h = \frac{d_0}{\alpha_0}\left(\frac{2\pi}{a}\right)^2 \underbrace{\left(\int d^2\mathbf{k}_\parallel \frac{1}{\Delta + \Delta_{e,xx}(\mathbf{k}_\parallel) + \mathrm{i}\Gamma_{e,xx}(\mathbf{k}_\parallel)/2}\right)^{-1}}_{I^{-1}} \tag{2.6}$$

Evaluating this explicitly and computing the associated real-space solution requires an understanding of the band structure $\Delta_{e,xx}(\mathbf{k}_\parallel)$ and decay rate $\Gamma_{e,xx}(\mathbf{k}_\parallel)$ and is non-trivial [75]. However, using general arguments, we can already estimate from eq. (2.6) the magnitude of the optical effect of the hole.

2.2 Holon/doublon cross-section

2.2.1 Lossless propagation in guided modes

The cross-section σ_{eff} manifests itself in the fraction of light that enters the lattice and does not re-emerge. Since we consider non-absorbing atoms, the only mechanism under which this is possible is if the incident light scatters into guided modes in the array, allowing it to propagate losslessly. For the square lattice, these modes lie outside the circular reciprocal-space volume defined by $|\mathbf{k}_\parallel| < k_0$ [17].

To estimate σ_{eff}, the main qualitative approximation we make is therefore to assume that the integral I is dominated by those trajectories in reciprocal-space along which $\Gamma_{x,ee}(\mathbf{k}_\parallel) = 0$. Under a lowest-order approximation to the band structure $\Delta_{e,xx}(\mathbf{k}_\parallel)$ around $\mathbf{k}_0$, we then have

$$I \approx \int d^2\mathbf{k}_\parallel \frac{1}{\Delta + \Delta_{e,xx}(\mathbf{k}_\parallel)} \approx \int d^2\mathbf{k}_\parallel \frac{1}{(\mathbf{k}_\parallel - \mathbf{k}_{0,\parallel})\cdot\nabla\Delta_{e,xx}(\mathbf{k}_\parallel)|_{\mathbf{k}_0}} \,. \tag{2.7}$$

In fact, for the case of a 2D array, the guided modes are associated with isoenergetic curves which are approximately straight in reciprocal space. Now if, for instance, we define such a curve as lying along a

constant value of k_x, then

$$I \approx \int dk_x \int dk_y \frac{1}{(k_y - k_{0,y}) \left.\frac{\partial \Delta_{e,xx}(\mathbf{k}_\parallel)}{\partial k_y}\right|_{\mathbf{k}_0}} \sim \frac{\mathrm{i}}{a} \int dk_y \frac{1}{\left.\frac{d\Delta_{e,xx}(\mathbf{k}_\parallel)}{dk_y}\right|_{\mathbf{k}_0}} \delta(k_y - k_{0,y}) \,, \tag{2.8}$$

where we have evaluated the integral along the k_x-axis of the 1BZ and used the *Sokhotski–Plemelj theorem* $\frac{1}{x-\mathrm{i}0^+} = \mathrm{i}\pi\delta(x) + P\frac{1}{x}$, neglecting the principal value term since we are interested in the resonant contributions only.

2.2.2 Effective hole size

If we want to examine purely a rough scaling of this expression, we can note that the band structure is characterised by the near-field interactions, and therefore $d\Delta_{e,xx}(\mathbf{k}_\parallel) \sim \Gamma_0/(ka)^3$. The characteristic scale of k_y is set by the first Brillouin zone, hence $dk_y \sim 1/a$, which implies that

$$\Omega_h \sim -\frac{d_0}{\alpha_0} \frac{\mathrm{i}\Gamma_0}{(k_0 a)^3} \tag{2.9}$$

To estimate the ratio $\sigma_{\mathrm{eff}}/\sigma_{\mathrm{sc}}$, we first calculate the time-averaged energy transferred to the hole dipole due to the driving by the local field Ω_h as $\mathrm{Im}(\Omega_h c_h) \sim d_0^2\Gamma_0/(\alpha_0 k_0^3 a^3)$. We can compare this to the work done by the external field on a dipole in the perfectly cooperative lattice, $\mathrm{Im}(E_0 d_0)$. The ratio of the two effectively corresponds with the fraction of energy lost by the hole, compared to the energy radiated per atom in the perfect case, which is essentially equivalent to the desired figure of merit $\sigma_{\mathrm{eff}}/\sigma_{\mathrm{sc}}$. Using the fact that on-resonance, $d_0 \sim \mathrm{i}\alpha_0 E_0/\Gamma_{\mathrm{coop}} \sim \mathrm{i}(k_0 a)^2 \alpha_0 E_0/\Gamma_0$, we find that

$$\frac{\mathrm{Im}(\Omega_h c_h)}{\mathrm{Im}(E_0 d_0)} = \frac{\sigma_{\mathrm{eff}}}{\sigma_{\mathrm{sc}}} \sim \frac{1}{k_0 a} \,. \tag{2.10}$$

Physically, this is the very meaningful result which we already anticipated: the hole removes an amount of energy from the incident field equivalent to the energy absorbed by $1/(k_0 a) \gg 1$ sites. *In other words, the holon-doublon pairs do not only effectively remove single atoms from the array but lead to the breakdown of the cooperative response of a large number of surrounding atoms. We may therefore safely assume that the inelastic scattering of incident light by the density-density correlation buildups in the ground state significantly affects the optical response of the 2D arrays. According to our reasoning above, the ground state fluctuations then represent the dominant effect leading to the saturation of the refractive index with the onset of quantum chemistry.*

3 Discussion & outlook

With this last calculation, we have arrived at a remarkable result with possibly wide-reaching implications: at least for the simplest case of hydrogenic atoms, it is not an intractable amalgamation of quantum chemistry effects which leads to a saturation of the refractive index. Instead, we can identify concrete process whose (disproportionately large) optical effect can be straightforwardly estimated using standard methods from condensed matter theory and quantum optics. While we have focused here only

on one of these processes, and while our calculations are to some extent exemplary in nature, the relevance of our analysis seems undeniable: *on the one hand, our result uproots the traditional understanding of the optical properties of dense atomic media and, on the other hand, it could inspire the purposeful design of optical materials with ultrahigh refractive index.*

This work represents only the first step towards a comprehensive theory of the optical properties of atomic media at the interface between quantum optics and quantum chemistry. There are some technical details which we have neglected in this work, most importantly a rigorous calculation of the effective hole size and a thorough analysis of the magnonic polaron effect, but also a more quantitative assessment of those sub-leading process which also contribute an inelastic linewidth. Additionally, the connection to the formal quantum chemistry regime could be firmed up by confirming some of our assumptions (e.g. the equivalence of the ground state manifold and the Hubbard model) using state-of-the-art quantum chemistry simulations on 2D lattices. Similarly, our result could be validated from the perspective of condensed matter theory, by applying the slave-fermion formalism to the full 3D lattice to calculate the impurity scattering associated with individual holons and doublons. Most of these avenues will be explored in future work.

Beyond this, a generalisation of the ideas we have presented also requires an extension to more complicated atomic species. A feasible point of entry are common approaches in atomic physics and quantum chemistry which model the core electrons of larger atoms as simply affecting the pseupotential in which the valence electrons move [165, 166], and generalisations of the spin model to more complicated atomic structures [167]. Heuristically speaking, the variation in the dipole moment for different atoms may affect the dominance of certain effects and therefore the exact mechanisms which saturate the refractive index. However, it seems reasonable to assume that in these cases we will still be able to make qualitatively similar statements about the source of the maximal refractive index – that there are few individual corrections to the quantum optics limit with dominant effects on the optical response.

Our results are also impactful beyond the immediate question of the maximum refractive index: the notion that individual far-detuned atoms in an array break the collective optical response of the array across a much larger effective number of emitters is a highly interesting observation in its own right. It could lead to a much better understanding of the stability of collective optical properties of ordered geometries of quantum emitters, and could on the other hand perhaps be exploited to engineer exotic new cooperative behaviour.

Bibliography

[1] D. Jackson, *Classical electrodynamics*, 1st ed. (John Wiley and Sons, Chichester, 1999).

[2] V. Veselago, L. Braginsky, V. Shklover, and C. Hafner, Journal of Computational and Theoretical Nanoscience **3** (2006).

[3] V. M. Shalaev, Nature Photonics **1** (2007).

[4] R. Kitamura, L. Pilon, and M. Jonasz, Applied Optics **46** (2007).

[5] P. L. Lamy, Applied Optics **16** (1977).

[6] H. R. Philipp and H. Ehrenreich, Physical Review **129** (1963).

[7] D. E. Aspnes and A. A. Studna, Physical Review B **27** (1983).

[8] O. P. Rustgi, J. S. Nodvik, and G. L. Weissler, Physical Review **122** (1961).

[9] A. D. Papadopoulos and E. Anastassakis, Physical Review B **43** (1991).

[10] W. C. Walker and J. Osantowski, Physical Review **134** (1964).

[11] S. G. Warren, Applied Optics **23** (1984).

[12] P. de Vries, D. V. van Coevorden, and A. Lagendijk, Reviews of Modern Physics **70** (1998).

[13] D. J. Griffiths, *Introduction to electrodynamics* (Prentice Hall, New Jersey, 1999).

[14] G. Grynberg, A. Aspect, and C. Fabre, *Introduction to quantum optics: From the semi-classical approach to quantised light* (Cambridge University Press, Cambridge, 2010).

[15] R. H. Dicke, Physical Review **93** (1954).

[16] M. Gross and S. Haroche, Physics Reports **93** (1982).

[17] A. Asenjo-Garcia, M. Moreno-Cardoner, A. Albrecht, H. J. Kimble, and D. E. Chang, Physical Review X **7** (2017).

[18] J. Keaveney, A. Sargsyan, U. Krohn, I. G. Hughes, D. Sarkisyan, and C. S. Adams, Physical Review Letters **108** (2012).

[19] J. Javanainen, J. Ruostekoski, Y. Li, and S.-M. Yoo, Physical Review Letters **112** (2014).

[20] J. T. Manassah, Advances in Optics and Photonics **4** (2012).

[21] R. J. Bettles, S. A. Gardiner, and C. S. Adams, Physical Review A **92** (2015).

[22] R. J. Bettles, S. A. Gardiner, and C. S. Adams, Physical Review Letters **116** (2016).

[23] M. K. Tey, G. Maslennikov, T. C. H. Liew, S. A. Aljunid, F. Huber, B. Chng, Z. Chen, V. Scarani, and C. Kurtsiefer, New Journal of Physics **11** (2009).

[24] E. Shahmoon, D. S. Wild, M. D. Lukin, and S. F. Yelin, Physical Review Letters **118** (2017).

[25] J. Rui, D. Wei, A. Rubio-Abadal, S. Hollerith, J. Zeiher, D. M. Stamper-Kurn, C. Gross, and I. Bloch, Nature **583** (2020).

[26] N. M. Lawandy, R. M. Balachandran, A. S. L. Gomes, and E. Sauvain, Nature **368** (1994).

[27] F. Andreoli, M. J. Gullans, A. A. High, A. Browaeys, and D. E. Chang, en, Physical Review X **11** (2021).

[28] F. Iglói and C. Monthus, Physics Reports **412** (2005).

[29] G. Refael and E. Altman, Comptes Rendus Physique, Disordered systems / Systèmes désordonnés **14** (2013).

[30] L. Pauling, *The nature of the chemical bond and the structure of molecules and crystals: An introduction to modern structural chemistry*, 3rd ed. (New York, 1960).

[31] C. E. Housecroft and A. G. Sharpe, *Inorganic chemistry*, 2nd ed. (Pearson, Harlow, 2005).

[32] L. Piela, *Ideas of quantum chemistry* (Elsevier, Amsterdam, 2007).

[33] M. Fox, *Optical properties of solids*, 2nd ed. (Oxford University Press, Oxford, 2010).

[34] S. Saha, T. P. Sinha, and A. Mookerjee, Phys. Rev. B **62** (2000).

[35] A. P. Thorne, *Spectrophysics* (Springer Netherlands, Dordrecht, 1988).

[36] R. Parr, International Journal of Quantum Chemistry **37**, 327 (1990).

[37] T. Helgaker, P. Jørgensen, and J. Olsen, *Molecular electronic-structure theory* (John Wiley & Sons, Ltd, 2000).

[38] F. Jensen, *Introduction to computational chemistry*, 3rd ed. (John Wiley & Sons, Ltd, 2017).

[39] A. Szabo and N. S. Ostlund, *Modern quantum chemistry*, 1st ed., rev. (Dover, New York, 1996).

[40] R. G. Parr and W. Yang, *Density-Functional Theory of Atoms and Molecules.* (Oxford University Press, New York, 1995).

[41] W. Thiel, WIREs Computational Molecular Science **4** (2014).

[42] G. Seifert and J.-O. Joswig, WIREs Computational Molecular Science **2** (2012).

[43] M. Elstner and G. Seifert, Philosophical Transactions. Series A, Mathematical, Physical, and Engineering Sciences **372** (2014).

[44] C. Møller and M. S. Plesset, Physical Review **46** (1934).

[45] J. Cizek, Journal of Chemical Physics **45** (1966).

[46] T. Crawford and H. F. Schaefer III, Reviews of Computational Chemistry **14** (2007).

[47] S. Suehara, T. Konishi, and S. Inoue, Physical Review B **73** (2006).

[48] M.-Q. Cai, Z. Yin, and M.-S. Zhang, Chemical Physics Letters **388** (2004).

[49] H. Sano and G. Mizutani, AIP Advances **5** (2015).

[50] J. P. F. LeBlanc, A. E. Antipov, F. Becca, I. W. Bulik, G. K.-L. Chan, C.-M. Chung, Y. Deng, M. Ferrero, T. M. Henderson, C. A. Jiménez-Hoyos, E. Kozik, X.-W. Liu, A. J. Millis, N. V. Prokof'ev, M. Qin, G. E. Scuseria, H. Shi, B. V. Svistunov, L. F. Tocchio, I. S. Tupitsyn, S. R. White, S. Zhang, B.-X. Zheng, Z. Zhu, and E. Gull, Physical Review X **5** (2015).

[51] M. Moreno-Cardoner, D. Goncalves, and D. E. Chang, arXiv:2101.01936 [quant-ph] (2021).

[52] A. Asenjo-Garcia, J. D. Hood, D. E. Chang, and H. J. Kimble, Physical Review A **95** (2017).

[53] M. T. Manzoni, M. Moreno-Cardoner, A. Asenjo-Garcia, J. V. Porto, A. V. Gorshkov, and D. E. Chang, New Journal of Physics **20** (2018).

[54] B. Huttner and S. M. Barnett, Physical Review A **46** (1992).

[55] T. Gruner and D.-G. Welsch, Physical Review A **53** (1996).

[56] H. T. Dung, L. Knöll, and D.-G. Welsch, Physical Review A **65** (2002).

[57] H. T. Dung, L. Knöll, and D.-G. Welsch, Physical Review A **66** (2002).

[58] D. E. Chang, L. Jiang, A. V. Gorshkov, and H. J. Kimble, New Journal of Physics **14** (2012).

[59] L. Novotny and B. Hecht, *Principles of nano-optics*, 2nd ed. (Cambridge University Press, Cambridge, 2012).

[60] H.-P. Breuer and F. Petruccione, *The theory of open quantum systems* (Oxford University Press, Oxford, 2002).

[61] D. E. Chang, K. Sinha, J. M. Taylor, and H. J. Kimble, Nature Communications **5** (2014).

[62] T. Shi, D. E. Chang, and J. I. Cirac, Physical Review A **92** (2015).

[63] V. A. Markel and A. K. Sarychev, Physical Review B **75** (2007).

[64] T. Caneva, M. T. Manzoni, T. Shi, J. S. Douglas, J. I. Cirac, and D. E. Chang, New Journal of Physics **17** (2015).

[65] S. Xu and S. Fan, Physical Review A **91** (2015).

[66] A. Lagendijk and B. A. van Tiggelen, Physics Reports **270** (1996).

[67] D. A. Steck, *Quantum and Atom Optics* (2007).

[68] N. W. Ashcroft and N. D. Mermin, *Solid state physics*, 1st ed. (Hartcourt College Publishers, Fort Worth, 1976).

[69] F. J. García de Abajo, Reviews of Modern Physics **79** (2007).

[70] R. Loudon, *The quantum theory of light* (Oxford University Press, Oxford, 2000).

[71] R. Loudon and S. M. Barnett, Journal of Physics B: Atomic, Molecular and Optical Physics **39** (2006).

[72] C. J. Foot, *Atomic physics*, 1st ed., Oxford master series in physics (Oxford University Press, Oxford, 2005).

[73] M. Antezza and Y. Castin, Physical Review A **80** (2009).

[74] M. Antezza and Y. Castin, Physical Review Letters **103** (2009).

[75] J. Perczel, J. Borregaard, D. E. Chang, H. Pichler, S. F. Yelin, P. Zoller, and M. D. Lukin, Physical Review A **96** (2017).

[76] S. P. Rath, T. Yefsah, K. J. Günter, M. Cheneau, R. Desbuquois, M. Holzmann, W. Krauth, and J. Dalibard, Physical Review A **82** (2010).

[77] J. Keaveney, A. Sargsyan, U. Krohn, J. Gontcharov, I. G. Hughes, D. Sarkisyan, and C. S. Adams, arXiv:1109.3669 [atom-ph] (2011).

[78] K. Kemp, S. J. Roof, M. D. Havey, I. M. Sokolov, and D. V. Kupriyanov, arXiv:1410.2497 [atom-ph] (2014).

[79] J. Pellegrino, R. Bourgain, S. Jennewein, Y. R. P. Sortais, A. Browaeys, S. D. Jenkins, and J. Ruostekoski, Phys. Rev. Lett. **113** (2014).

[80] I. H. Deutsch, R. J. C. Spreeuw, S. L. Rolston, and W. D. Phillips, Physical Review A **52** (1995).

[81] B. Olmos, D. Yu, Y. Singh, F. Schreck, K. Bongs, and I. Lesanovsky, Phys. Rev. Lett. **110** (2013).

[82] T. Fukuhara, S. Sugawa, M. Sugimoto, S. Taie, and Y. Takahashi, Phys. Rev. A **79** (2009).

[83] D. F. Walls and G. J. Milburn, *Quantum optics*, 2nd ed. (Springer, Berlin, 2008).

[84] S. H. Simon, *The Oxford solid state basics* (Oxford University Press, Oxford, 2013).

[85] G. H. Wannier, Physical Review **52** (1937).

[86] N. Marzari, A. A. Mostofi, J. R. Yates, I. Souza, and D. Vanderbilt, Reviews of Modern Physics **84** (2012).

[87] E. Blount, in *Solid State Physics*, Vol. 13 (Elsevier, 1962), pp. 305–373.

[88] N. Marzari and D. Vanderbilt, Physical Review B **56** (1997).

[89] G. Panati and A. Pisante, Communications in Mathematical Physics **322** (2013).

[90] W. Nolting, "Second quantisation", in *Theoretical physics 9: fundamentals of many-body physics*, 2nd ed. (Springer International, 2018).

[91] R. T. Scalettar, *An Introduction to the Hubbard Hamiltonian*, 2016.

[92] R. Blankenbecler, D. J. Scalapino, and R. L. Sugar, Physical Review D **24** (1981).

[93] J. E. Hirsch and S. Tang, Physical Review Letters **62** (1989).

[94] M. Rasetti, *The hubbard model* (World Scientific, 1991).

[95] A. Montorsi, *The hubbard model* (World Scientific, 1992).

[96] M. Motta, C. Genovese, F. Ma, Z.-H. Cui, R. Sawaya, G. K.-L. Chan, N. Chepiga, P. Helms, C. Jiménez-Hoyos, A. J. Millis, U. Ray, E. Ronca, H. Shi, S. Sorella, E. M. Stoudenmire, S. R. White, S. Zhang, and Simons Collaboration on the Many-Electron Problem, Physical Review X **10** (2020).

[97] L. Stella, C. Attaccalite, S. Sorella, and A. Rubio, Physical Review B **84** (2011).

[98] M. C. Gutzwiller, Physical Review Letters **10** (1963).

[99] J. Hubbard and B. H. Flowers, Proceedings of the Royal Society of London. Series A. Mathematical and Physical Sciences **276** (1963).

[100] M. Imada, A. Fujimori, and Y. Tokura, Reviews of Modern Physics **70** (1998).

[101] J. H. d. Boer and E. J. W. Verwey, Proceedings of the Physical Society **49** (1937).

[102] N. F. Mott and R. Peierls, Proceedings of the Physical Society **49** (1937).

[103] N. F. Mott, Contemporary Physics **14** (1973).

[104] J. C. Slater, Physical Review **82** (1951).

[105] E. H. Lieb and F. Y. Wu, Physical Review Letters **20** (1968).

[106] W. Metzner and D. Vollhardt, Physical Review Letters **62** (1989).

[107] S. Raghu, S. A. Kivelson, and D. J. Scalapino, Physical Review B **81** (2010).

[108] X.-J. Han, Y. Liu, Z.-Y. Liu, X. Li, J. Chen, H.-J. Liao, Z.-Y. Xie, B. Normand, and T. Xiang, New Journal of Physics **18** (2016).

[109] T. A. Kaplan, P. Horsch, and P. Fulde, Physical Review Letters **49** (1982).

[110] N. Nagaosa, *Quantum field theory in strongly correlated electronic systems* (Springer, Berlin, 1999).

[111] A. S. T. Pires, in *Theoretical tools for spin models in magnetic systems* (IOP Publishing, 2021), 5-1 to 5-27.

[112] P. W. Anderson, Physical Review **115** (1959).

[113] A. Auerbach, *Interacting electrons and quantum magnetism* (Springer, New York, 1994).

[114] D. C. Mattis, *The Theory of Magnetism I*, edited by M. Cardona, P. Fulde, K. von Klitzing, and H.-J. Queisser, Vol. 17, Springer Series in Solid-State Sciences (Springer, Berlin, 1981).

[115] T. Hartke, B. Oreg, N. Jia, and M. Zwierlein, Phys. Rev. Lett. **125** (2020).

[116] E. Manousakis, Reviews of Modern Physics **63** (1991).

[117] H. Bethe, Zeitschrift für Physik **71** (1931).

[118] T. Kennedy, E. H. Lieb, and B. S. Shastry, Journal of Statistical Physics **53** (1988).

[119] E. J. Neves and J. F. Perez, Physics Letters A **114** (1986).

[120] I. Affleck, T. Kennedy, E. H. Lieb, and H. Tasaki, Communications in Mathematical Physics **115** (1988).

[121] S. Schmitt-Rink, C. M. Varma, and A. E. Ruckenstein, Physical Review Letters **60** (1988).

[122] N. D. Mermin and H. Wagner, Physical Review Letters **17** (1966).

[123] P. W. Anderson, Physical Review **86** (1952).

[124] R. Kubo, Phys. Rev. **87** (1952).

[125] T. Holstein and H. Primakoff, Phys. Rev. **58** (1940).

[126] A. L. Fetter and J. D. Walecka, *Quantum theory of many-particle systems* (McGraw-Hill, San Francisco, 1971).

[127] C. L. Kane, P. A. Lee, and N. Read, Phys. Rev. B **39** (1989).

[128] F. Marsiglio, A. E. Ruckenstein, S. Schmitt-Rink, and C. M. Varma, Physical Review B **43** (1991).

[129] G. Martinez and P. Horsch, Physical Review B **44** (1991).

[130] J. Bal/a, A. M. Ole ś, and J. Zaanen, Physical Review B **52** (1995).

[131] T. Xiang and J. M. Wheatley, Physical Review B **54** (1996).

[132] S. Engelsberg and J. R. Schrieffer, Phys. Rev. **131** (1963).

[133] D. Dunn, Physical Review **174** (1968).

[134] V. Mishra, Physical Review B **91** (2015).

[135] A. Altland and B. D. Simons, *Condensed matter field theory* (Cambridge, 2010).

[136] S. R. White, D. J. Scalapino, R. L. Sugar, E. Y. Loh, J. E. Gubernatis, and R. T. Scalettar, Physical Review B **40** (1989).

[137] T. Miyagawa and H. Yokoyama, Physica C: Superconductivity and its Applications **471** (2011).

[138] W.-H. Leong, S.-L. Yu, T. Xiang, and J.-X. Li, Physical Review B **90** (2014).

[139] G. W. King and J. H. van Vleck, Phys. Rev. **55** (1939).

[140] S. Y. Buhmann and D.-G. Welsch, Progress in Quantum Electronics **31** (2007).

[141] H. Margenau and N. R. Kestner, *Theory of intermolecular forces*, 2nd ed. (Pergamon Press, Oxford, 1969).

[142] B. R. Holstein, American Journal of Physics **69** (2001).

[143] A. C. Ipsen and K. Splittorff, American Journal of Physics **83** (2015).

[144] R. Eisenschitz and F. London, Zeitschrift für Physik **60** (1929).

[145] F. London, Zeitschrift für Physik **63** (1930).

[146] R. de Melo e Souza, W. J. M. Kort-Kamp, C. Sigaud, and C. Farina, American Journal of Physics **81** (2013).

[147] S. Y. Buhmann, *Dispersion Forces I: Macroscopic Quantum Electrodynamics and Ground-State Casimir, Casimir–Polder and van der Waals Forces*, Vol. 247, Springer Tracts in Modern Physics (Springer Berlin Heidelberg, Berlin, 2012).

[148] M. M. Taddei, T. N. C. Mendes, and C. Farina, European Journal of Physics **31** (2010).

[149] H. Nakashima and H. Nakatsuji, The Journal of Chemical Physics **149** (2018).

[150] W. F. Brinkman and T. M. Rice, Physical Review B **2** (1970).

[151] S. Sachdev, Physical Review B **39** (1989).

[152] Z. Liu and E. Manousakis, Physical Review B **45** (1992).

[153] A. S. Mishchenko and N. Nagaosa, Physical Review Letters **93** (2004).

[154] A. Damascelli, Z. Hussain, and Z.-X. Shen, Reviews of Modern Physics **75** (2003).

[155] G. Ji, M. Xu, L. H. Kendrick, C. S. Chiu, J. C. Brüggenjürgen, D. Greif, A. Bohrdt, F. Grusdt, E. Demler, M. Lebrat, and M. Greiner, Physical Review X **11** (2021).

[156] J. Carlström, N. Prokof'ev, and B. Svistunov, Physical Review Letters **116** (2016).

[157] M. J. Stephen, The Journal of Chemical Physics **40** (1964).

[158] R. R. McLone and E. A. Power, Mathematika **11** (1964).

[159] W. J. Meath, The Journal of Chemical Physics **48** (1968).

[160] H. B. G. Casimir and D. Polder, Physical Review **73** (1948).

[161] E. A. Power and T. Thirunamachandran, Physical Review A **47** (1993).

[162] G. S. Agarwal, Physical Review A **12** (1975).

[163] N. Pottier, *Nonequilibrium statistical physics: Linear irreversible processes* (Oxford University Press, Oxford, 2010).

[164] G. S. Agarwal, Physical Review A **11** (1975).

[165] C. F. Melius and W. A. Goddard, Physical Review A **10** (1974).

[166] G. B. Bachelet, D. R. Hamann, and M. Schlüter, Physical Review B **26** (1982).

[167] A. Piñeiro Orioli and A. M. Rey, Phys. Rev. A **101** (2020).

[168] P. Coleman, *Introduction to many-body physics* (Cambridge University Press, Cambridge, 2015).

Appendices

Appendix A

Multiple scattering in 2D

In this appendix we provide the details of the two multiple scattering calculations presented in Chapter 2.2 (Section 1) and Chapter 6.2 (Section 2), which were omitted from the main text for the sake of readability. We define the Fourier transforms on an infinite 2D lattice as

$$F(\mathbf{k}_\parallel) = \frac{1}{N}\sum_i F(\mathbf{R}_i)\mathrm{e}^{-\mathrm{i}\mathbf{k}_\parallel\cdot\mathbf{R}_i}$$
$$F(\mathbf{R}_i) = Na^2\int_{1\mathrm{BZ}}\frac{d^2\mathbf{k}_\parallel}{(2\pi)^2}F(\mathbf{k}_\parallel)\mathrm{e}^{\mathrm{i}\mathbf{k}_\parallel\cdot\mathbf{R}_i}$$

1 Square array without holes

1.1 Mode-wise optical response

We note that at a lattice site the incident field in eq. (2.3) of Chapter 2 is simply $\mathbf{E}_0(\mathbf{R}_i) = \sum_{\mathbf{k}_\parallel}\mathbf{E}_{0,\mathbf{k}_\parallel}\mathrm{e}^{\mathrm{i}\mathbf{k}_\parallel\cdot\mathbf{R}_i}$ and the discrete Fourier spectrum implied by this expression can be formally written as

$$\mathbf{E}_0(\mathbf{k}_\parallel) = \frac{1}{Na^2}\sum_{\mathbf{q}_\parallel}\mathbf{E}_{0,\mathbf{q}_\parallel}(2\pi)^2\delta^{(2)}(\mathbf{q}_\parallel-\mathbf{k}_\parallel) \tag{1.1}$$

Accordingly, we are able to Fourier transform the dipole equation in eq. (2.1) of Chapter 2 to obtain

$$\begin{aligned}
\mathbf{d}(\mathbf{k}_\parallel) &= \alpha\mathbf{E}_0(\mathbf{k}_\parallel) + \frac{4\pi^2\alpha}{\lambda^2\varepsilon_0 N}\sum_{i,j\neq i}\mathbf{G}^{i-j}\cdot\mathbf{d}_j\mathrm{e}^{-\mathrm{i}\mathbf{k}_\parallel\cdot\mathbf{R}_i}\\
&= \frac{\alpha}{Na^2}\sum_{\mathbf{q}_\parallel}\mathbf{E}_{0,\mathbf{q}_\parallel}(2\pi)^2\delta^{(2)}(\mathbf{q}_\parallel-\mathbf{k}_\parallel) + \frac{4\pi^2\alpha a^2}{\lambda^2\varepsilon_0}\int_{1\mathrm{BZ}}\frac{d^2\mathbf{q}_\parallel}{(2\pi)^2}\sum_{i,j\neq i}\mathbf{G}^{i-j}\cdot\mathbf{d}(\mathbf{q}_\parallel)\mathrm{e}^{\mathrm{i}\mathbf{q}_\parallel\cdot\mathbf{R}_j-\mathrm{i}\mathbf{k}_\parallel\cdot\mathbf{R}_i}\\
&= \frac{\alpha}{Na^2}\sum_{\mathbf{q}_\parallel}\mathbf{E}_{0,\mathbf{q}_\parallel}(2\pi)^2\delta^{(2)}(\mathbf{q}_\parallel-\mathbf{k}_\parallel) + \frac{4\pi^2\alpha}{\lambda^2\varepsilon_0 N}Na^2\int_{1\mathrm{BZ}}\frac{d^2\mathbf{q}_\parallel}{(2\pi)^2}\sum_{i,k\neq 0}\mathbf{G}^{k}\cdot\mathbf{d}(\mathbf{q}_\parallel)\mathrm{e}^{-\mathrm{i}\mathbf{q}_\parallel\cdot\mathbf{R}_k+\mathrm{i}(\mathbf{q}_\parallel-\mathrm{i}\mathbf{k}_\parallel)\cdot\mathbf{R}_i}\\
&= \sum_{\mathbf{q}_\parallel}\frac{\alpha\mathbf{E}_{0,\mathbf{q}_\parallel}}{Na^2}(2\pi)^2\delta^{(2)}(\mathbf{q}_\parallel-\mathbf{k}_\parallel) + \frac{4\pi^2\alpha a^2}{\lambda^2\varepsilon_0}\int_{1\mathrm{BZ}}\frac{d^2\mathbf{q}_\parallel}{(2\pi)^2}\underbrace{\left(\sum_{k\neq 0}\mathbf{G}^k\mathrm{e}^{-\mathrm{i}\mathbf{q}_\parallel\cdot\mathbf{R}_k}\right)}_{\equiv\,\mathbf{g}(\mathbf{q}_\parallel)}\cdot\mathbf{d}(\mathbf{q}_\parallel)\underbrace{\left(\sum_i\mathrm{e}^{-\mathrm{i}(\mathbf{k}_\parallel-\mathrm{i}\mathbf{q}_\parallel)\cdot\mathbf{R}_i}\right)}_{=\left(\frac{2\pi}{a}\right)^2\delta^{(2)}(\mathbf{q}_\parallel-\mathbf{k}_\parallel)}\\
&= \sum_{\mathbf{q}_\parallel}\frac{\alpha\mathbf{E}_{0,\mathbf{q}_\parallel}}{Na^2}(2\pi)^2\delta^{(2)}(\mathbf{q}_\parallel-\mathbf{k}_\parallel) + \frac{4\pi^2\alpha}{\lambda^2\varepsilon_0}\mathbf{g}(\mathbf{k}_\parallel)\cdot\mathbf{d}(\mathbf{k}_\parallel)\,.
\end{aligned}$$

where we have used the shorthand notation $\mathbf{G}^{i-j}\equiv\mathbf{G}(\mathbf{R}_{ij},\omega)$. This leads to the Fourier-space solution stated in eq. (2.4) of Chapter 2.

1.2 Cooperative radiative response

To obtain the more intuitive expression $\mathbf{d}_i = \sum_{\mathbf{k}_\parallel} \mathbf{d}_{0,\mathbf{k}_\parallel} \mathrm{e}^{\mathrm{i}\mathbf{k}_\parallel\cdot\mathbf{R}_i}$ with $\mathbf{d}_{0,\mathbf{k}_\parallel} = \boldsymbol{\alpha}_e(\mathbf{k}_\parallel)\cdot\mathbf{E}_{0,\mathbf{k}_\parallel}$, we perform the inverse Fourier transform,

$$\begin{aligned}
\mathbf{d}_i &= Na^2 \int_{1\mathrm{BZ}} \frac{d^2\mathbf{k}_\parallel}{(2\pi)^2} \mathbf{d}(\mathbf{k}_\parallel)\mathrm{e}^{\mathrm{i}\mathbf{k}_\parallel\cdot\mathbf{R}_i} \\
&= Na^2 \int_{1\mathrm{BZ}} \frac{d^2\mathbf{k}_\parallel}{(2\pi)^2} \mathrm{e}^{\mathrm{i}\mathbf{k}_\parallel\cdot\mathbf{R}_i} \left(\frac{\alpha}{Na^2} \left(\mathbb{1} - \frac{4\pi^2\alpha}{\lambda^2\varepsilon_0}\mathbf{g}(\mathbf{k}_\parallel) \right)^{-1} \cdot \sum_{\mathbf{q}_\parallel} \mathbf{E}_{0,\mathbf{q}_\parallel} (2\pi)^2 \delta^{(2)}(\mathbf{q}_\parallel - \mathbf{k}_\parallel) \right) \\
&= \left(\int_{1\mathrm{BZ}} d^2\mathbf{k}_\parallel \mathrm{e}^{\mathrm{i}\mathbf{k}_\parallel\cdot\mathbf{R}_i} \left(\mathbb{1} - \frac{4\pi^2\alpha}{\lambda^2\varepsilon_0}\mathbf{g}(\mathbf{k}_\parallel) \right)^{-1} \delta^{(2)}(\mathbf{q}_\parallel - \mathbf{k}_\parallel) \right) \cdot \sum_{\mathbf{q}_\parallel} \alpha \mathbf{E}_{0,\mathbf{q}_\parallel} \\
&= \sum_{\mathbf{q}_\parallel} \underbrace{\alpha \left(\mathbb{1} - \frac{4\pi^2\alpha}{\lambda^2\varepsilon_0}\mathbf{g}(\mathbf{q}_\parallel) \right)^{-1}}_{\equiv \boldsymbol{\alpha}_e(\mathbf{q}_\parallel)} \cdot \mathbf{E}_{0,\mathbf{q}_\parallel} \mathrm{e}^{\mathrm{i}\mathbf{q}_\parallel\cdot\mathbf{R}_i} \,.
\end{aligned}$$

The formal definition of $\boldsymbol{\alpha}_e(\mathbf{q}_\parallel)$ can easily be re-arranged into the form in eq. (2.5) of Chapter 2.

1.3 Cooperative linewidth

The starting point for deriving eq. (2.8) of Chapter 2 is the plane wave decomposition [1, 24]

$$G_0(\mathbf{r}, ck) = \frac{\mathrm{i}}{8\pi^2} \int d^2\mathbf{k}'_\parallel \mathrm{e}^{-\mathrm{i}\mathbf{k}'_\parallel\cdot\mathbf{r}} \frac{\mathrm{e}^{\mathrm{i}k'_z|z|}}{k'_z} \tag{1.2}$$

with $k'_z = \sqrt{k^2 - |\mathbf{k}'_\parallel|^2}$. From this, we are able to find a more tractable form of $g_{xx}(\mathbf{k}_\parallel)$,

$$\begin{aligned}
g_{xx}(\mathbf{k}_\parallel) &= \sum_i G_{xx}(\mathbf{R}_i, ck)\mathrm{e}^{-\mathrm{i}\mathbf{k}_\parallel\cdot\mathbf{R}_i} - G_{xx}(0, ck) \\
&= \int d^2\mathbf{r}_\parallel G_{xx}(\mathbf{r}_\parallel, ck)\mathrm{e}^{-\mathrm{i}\mathbf{k}_\parallel\cdot\mathbf{r}_\parallel} \sum_i \delta^{(2)}(\mathbf{r}_\parallel - \mathbf{R}_i) - G_{xx}(0, ck) \\
&= \frac{\mathrm{i}}{8\pi^2} \int d^2\mathbf{k}'_\parallel \frac{1}{k'_z} \left(1 - \frac{k'^2_x}{k^2} \right) \int d^2\mathbf{r}_\parallel \mathrm{e}^{-\mathrm{i}(\mathbf{k}_\parallel + \mathbf{k}'_\parallel)\cdot\mathbf{r}_\parallel} \underbrace{\sum_i \delta^{(2)}(\mathbf{r}_\parallel - \mathbf{R}_i)}_{=\rho(\mathbf{r}_\parallel)} - G_{xx}(0, ck) \,,
\end{aligned}$$

where we have identified the formal density of lattice points in real space, $\rho(\mathbf{r}_\parallel) = \sum_i \delta^{(2)}(\mathbf{r}_\parallel - \mathbf{R}_i)$. We can define the Fourier transform $\rho(\mathbf{k}_\parallel)$ using the *Poisson resummation formula* [84], which allows us to convert sums over infinite real-space lattices to sums over reciprocal-space lattices, as

$$\rho(\mathbf{k}_\parallel) = \int d^2\mathbf{r}_\parallel \mathrm{e}^{-\mathrm{i}\mathbf{k}_\parallel\cdot\mathbf{r}_\parallel} \rho(\mathbf{r}_\parallel) = \frac{(2\pi)^2}{a^2} \sum_{\mathbf{G}} \delta^{(2)}(\mathbf{k} - \mathbf{G}) \,,$$

where the second sum is over all reciprocal vectors $\mathbf{G}$. Then $g_{xx}(\mathbf{k}_\parallel)$ easily simplifies to

$$\begin{aligned}
g_{xx}(\mathbf{k}_\parallel) &= \frac{\mathrm{i}}{2(ka)^2} \sum_{\mathbf{G}} \int d^2\mathbf{k}'_\parallel \left(\frac{k^2 - k'^2_x}{\sqrt{k^2 - k'^2_x - k'^2_y}} \right) \delta^{(2)}(\mathbf{k}_\parallel + \mathbf{k}'_\parallel - \mathbf{G}) - G_{xx}(k, 0a) \\
&= \frac{\mathrm{i}}{2(ka)^2} \sum_{\mathbf{G}} \frac{k^2 - |\mathbf{k}_\parallel - \mathbf{G}|^2_x}{\sqrt{k^2 - |\mathbf{k}_\parallel - \mathbf{G}|^2}} - G_{xx}(k, 0) \,.
\end{aligned} \tag{1.3}$$

A final simplification can be made if we note that, neglecting the Lamb shift contribution that we have already taken care of implicitly, $G_{xx}(k, 0) = \mathrm{i}/(3\lambda)$ [24]. This leads to eq. (2.8) of Chapter 2.

2 Square array with a single hole

2.1 Fourier-space solution

Starting from the equations for the corrections c_i to the ideal solution d_0, we Fourier transform to obtain

$$\begin{aligned} c(\mathbf{k}_\parallel) &= \frac{\alpha}{N}\underbrace{\left(\sum_i \Omega_i \mathrm{e}^{-\mathrm{i}\mathbf{k}_\parallel\cdot\mathbf{R}_i}\right)}_{N\Omega(\mathbf{k}_\parallel)} + \alpha\mu_0\omega^2 a^2 \int \frac{d^2\mathbf{q}_\parallel}{(2\pi)^2} \sum_{i,j\neq i} G_{xx}(\mathbf{R}_{ij},\omega)\; c(\mathbf{q}_\parallel)\; \mathrm{e}^{\mathrm{i}\mathbf{q}_\parallel\cdot\mathbf{R}_j - \mathrm{i}\mathbf{k}_\parallel\cdot\mathbf{R}_i} \\ &= \alpha\Omega(\mathbf{k}_\parallel) + \alpha\mu_0\omega^2 a^2 \int \frac{d^2\mathbf{q}_\parallel}{(2\pi)^2}\; c(\mathbf{q}_\parallel) \underbrace{\left(\sum_{k\neq 0} G_{xx}(\mathbf{R}_k,\omega)\; \mathrm{e}^{-\mathrm{i}\mathbf{q}_\parallel\cdot\mathbf{R}_k}\right)}_{g_{xx}(\mathbf{q}_\parallel)} \underbrace{\left(\sum_i \mathrm{e}^{-\mathrm{i}(\mathbf{k}_\parallel-\mathrm{i}\mathbf{q}_\parallel)\cdot\mathbf{R}_i}\right)}_{=\left(\frac{2\pi}{a}\right)^2\delta^{(2)}(\mathbf{q}_\parallel-\mathbf{k}_\parallel)} \\ &= \alpha\Omega(\mathbf{k}_\parallel) + \alpha\mu_0\omega^2\; g_{xx}(\mathbf{k}_\parallel)\; c(\mathbf{k}_\parallel) \end{aligned}$$

This can be algebraically solved to obtain $c(\mathbf{k}_\parallel) = \alpha\Omega(\mathbf{k}_\parallel)(1-\alpha\mu_0\omega^2\; g_{xx}(\mathbf{k}_\parallel))^{-1}$. From the derivation in the previous section, we recall that $\alpha(1-\alpha\mu_0\omega^2\; g_{xx}(\mathbf{k}_\parallel))^{-1} = \alpha_{e,xx}(\mathbf{k}_\parallel)$ so that

$$c(\mathbf{k}_\parallel) \approx -\frac{3\pi\varepsilon_0}{k_0^3}\Gamma_0 \frac{\Omega(\mathbf{k}_\parallel)}{\Delta + \Delta_{e,xx}(\mathbf{k}_\parallel) + \mathrm{i}\Gamma_{e,xx}(\mathbf{k}_\parallel)/2} \tag{2.1}$$

2.2 Self-consistent driving field

From the self-consistent real-space definition of the driving field, we have

$$\Omega(\mathbf{k}_\parallel) = \frac{1}{N}\sum_i \Omega_i \mathrm{e}^{-\mathrm{i}\mathbf{k}_\parallel\cdot\mathbf{R}_i} = \frac{1}{N}\Omega_h \mathrm{e}^{-\mathrm{i}\mathbf{k}_\parallel\cdot\mathbf{R}_h}\,.$$

We can write the non-zero field Ω_h in terms of the solution above as

$$\begin{aligned} \alpha\Omega_h &= -d_0 - \alpha\mu_0\omega^2 N a^2 \sum_{j\neq h} G_{xx}(\mathbf{R}_{hj},\omega) \int \frac{d^2\mathbf{q}_\parallel}{(2\pi)^2}\; \Omega(\mathbf{q}_\parallel)\; c(\mathbf{q}_\parallel)\; \mathrm{e}^{\mathrm{i}\mathbf{q}_\parallel\cdot\mathbf{R}_j} \\ &= -d_0 - \alpha\mu_0\omega^2 a^2 \Omega_h \int \frac{d^2\mathbf{q}_\parallel}{(2\pi)^2} \underbrace{\left(\sum_{j\neq h} G_{xx}(\mathbf{R}_{hj},\omega)\; \mathrm{e}^{-\mathrm{i}\mathbf{q}_\parallel\cdot\mathbf{R}_{hj}}\right)}_{g_{xx}(\mathbf{q}_\parallel)} c(\mathbf{q}_\parallel) \\ &\approx -d_0 + \alpha a^2 \Omega_h \int \frac{d^2\mathbf{q}_\parallel}{(2\pi)^2} \frac{3\lambda\Gamma_0 g_{xx}(\mathbf{q}_\parallel)/2}{\Delta + \Delta_{e,xx}(\mathbf{k}_\parallel) + \mathrm{i}\Gamma_{e,xx}(\mathbf{k}_\parallel)/2} \end{aligned}$$

where we have used $(\lambda_0/\lambda)^3 \approx 1$ as in the previous section. Using $\Delta + \Delta_{e,xx}(\mathbf{q}_\parallel) + \mathrm{i}\Gamma_{e,xx}(\mathbf{q}_\parallel)/2 = \Delta + \mathrm{i}\Gamma_0/2 + 3\lambda\Gamma_0 g_{xx}(\mathbf{q}_\parallel)/2$ and the fact that the 1BZ volume is $(2\pi/a)^2$, we can solve for Ω_h to obtain

$$\begin{aligned} \Omega_h &= -\frac{d_0}{\alpha}\left(\frac{2\pi}{a}\right)^2 \left[\int d^2\mathbf{q}_\parallel \left(1 - \frac{3\lambda\Gamma_0 g_{xx}(\mathbf{q}_\parallel)/2}{\Delta + \mathrm{i}\Gamma_0/2 + 3\lambda\Gamma_0 g_{xx}(\mathbf{q}_\parallel)/2}\right)\right]^{-1} \\ &= -\frac{d_0}{\alpha}\left(\frac{2\pi}{a}\right)^2 \left[\left(\Delta + \frac{\mathrm{i}\Gamma_0}{2}\right)\int d^2\mathbf{q}_\parallel \frac{1}{\Delta + \Delta_{e,xx}(\mathbf{q}_\parallel) + \mathrm{i}\Gamma_{e,xx}(\mathbf{q}_\parallel)/2}\right]^{-1} \end{aligned}$$

Appendix B

Hubbard many-body field theory

In this appendix, we review briefly some relevant basic concepts of many-body QFT (Section 1), in particular the basic conventions of one-particle Green's functions (Section 2), and we also provide some technical detail on the field calculations from Chapter 4 of the main text (Sections 3 and 4). For an expansion on the ideas outlined in this section, see Ref. [168], whose conventions we mostly follow.

1 QFT for many-body problems

In the context of many-body systems, we are typically interested in two distinct types of quantum fields: *collective bosonic fields*, describing collective quasiparticle excitations, and the more conventional fermionic and bosonic fields with fixed particle number. In both cases, the field operator and its conjugate play the role of the destruction and creation operators for the particle, with the particle statistics encoded in the field (anti)commutation relations.

The Schrödinger field operator $\hat{\psi}(\mathbf{r})$ can be written as $\hat{\psi}(\mathbf{r}) = \sum_{\mathbf{k}} \hat{\psi}_{\mathbf{k}} \mathrm{e}^{-\mathrm{i}\mathbf{k}\cdot\mathbf{x}}$ for both collective and fixed particle number fields. The difference between the two manifests itself in the structure of the Fourier amplitudes $\hat{\psi}_{\mathbf{k}}$. We can denote by $\hat{a}_{\mathbf{k}}$ mode operators which create a single particle at momentum $\mathbf{k}$. For a field with fixed particle number, $\hat{\psi}_{\mathbf{k}} \sim \hat{a}_{\mathbf{k}}$ so that $\hat{\psi}(\mathbf{r})^\dagger$ creates a particle well-localised in $\mathbf{r}$. The classical field describing a collective excitation is real, therefore $\hat{\psi}(\mathbf{r})$ must be hermitian in this case, and hence $\hat{\psi}_{\mathbf{k}} \sim \hat{a}_{\mathbf{k}} + \hat{a}^\dagger_{-\mathbf{k}}$. Physically, this is the statement that the wavepacket of a collective excitation localised around $\mathbf{r}$ involves both the creation and annihilation of quanta.

2 One-particle Green's functions

For a general quantum field $\hat{\psi}(\mathbf{x}, t)$, we define the *Green's function* $G(\mathbf{x}, t)$ according to

$$G(\mathbf{x} - \mathbf{x}', t - t') = -\mathrm{i}\langle G|T\hat{\psi}(\mathbf{x}, t)\hat{\psi}^\dagger(\mathbf{x}', t')|G\rangle\,, \tag{2.1}$$

where $|G\rangle$ is the many-body ground state and T is the time-ordering operator. Using the Fourier decomposition of the real-space fields as $\hat{\psi}(\mathbf{x}, t) = \sum_{\mathbf{k}} \mathrm{e}^{\mathrm{i}\mathbf{k}\cdot\mathbf{x}}\ \hat{\psi}_{\mathbf{k}}(t)$, we define

$$G(\mathbf{x} - \mathbf{x}', t - t') = -\mathrm{i}\sum_{\mathbf{k},\mathbf{k}'} \mathrm{e}^{\mathrm{i}\mathbf{k}\cdot\mathbf{x} - \mathrm{i}\mathbf{k}'\cdot\mathbf{x}'} \underbrace{\langle G|T\hat{\psi}_{\mathbf{k}}(t)\hat{\psi}^\dagger_{\mathbf{k}'}(t')|G\rangle}_{\delta_{\mathbf{k}\mathbf{k}'}G(\mathbf{k}, t - t')} = -\mathrm{i}\sum_{\mathbf{k}} \mathrm{e}^{\mathrm{i}\mathbf{k}\cdot(\mathbf{x}-\mathbf{x}')} G(\mathbf{k}, t - t')\,,$$

where we have not specified the particle statistics and defined $G(\mathbf{k}, t-t') = -\mathrm{i}\langle G|T\hat{\psi}_{\mathbf{k}}(t)\hat{\psi}^{\dagger}_{\mathbf{k}'}(t')|G\rangle$ with the field modes in the Heisenberg / interaction picture. Transforming to the frequency-domain and using the spacetime translation invariance of the 2-point correlator, we arrive at the *propagator*

$$G(\mathbf{k},\omega) = -\mathrm{i}\int dt\ \mathrm{e}^{\mathrm{i}\omega t}\langle G|T\hat{\psi}_{\mathbf{k}}(t)\hat{\psi}^{\dagger}_{\mathbf{k}}(0)|G\rangle\,. \tag{2.2}$$

2.1 Free fermionic propagator

We denote the free theory propagator as $G^{(0)}(\mathbf{k},\omega)$. We consider first a free (spinless) fermionic field ($\hat{\psi}_{\mathbf{k}} = \hat{c}_{\mathbf{k}}$) with generic Hamiltonian $H = \sum_{\mathbf{k}} E_{\mathbf{k}}\hat{c}^{\dagger}_{\mathbf{k}}\hat{c}_{\mathbf{k}}$ (interaction picture operators $\hat{c}_{\mathbf{k}}(t) = \hat{c}_{\mathbf{k}}\mathrm{e}^{-\mathrm{i}E_{\mathbf{k}}t}$). Then,

$$G^{(0)}(\mathbf{k},t) = -\mathrm{i}\langle G|T\hat{c}_{\mathbf{k}}(t)\hat{c}^{\dagger}_{\mathbf{k}}(0)|G\rangle = -\mathrm{i}\mathrm{e}^{-\mathrm{i}E_{\mathbf{k}}t}\Theta(t)\,. \tag{2.3}$$

The propagator can be calculated by evaluating the integral (2.2) (inserting a convergence factor δ), as

$$G^{(0)}(\mathbf{k},\omega) = -\mathrm{i}\int_0^{\infty} dt\ \mathrm{e}^{\mathrm{i}(\omega - E_{\mathbf{k}} + \mathrm{i}\delta)t} = \frac{1}{\omega - E_{\mathbf{k}} + \mathrm{i}\delta}\,. \tag{2.4}$$

2.2 Free bosonic propagator

We consider now a bosonic field ($\hat{\psi}_{\mathbf{k}} \sim \hat{b}_{\mathbf{k}} + \hat{b}^{\dagger}_{-\mathbf{k}}$) with generic free Hamiltonian $H = \sum_{\mathbf{k}} \Omega_{\mathbf{k}}\hat{b}^{\dagger}_{\mathbf{k}}\hat{b}_{\mathbf{k}}$ (interaction picture operators $\hat{b}_{\mathbf{k}}(t) = \hat{b}_{\mathbf{k}}\mathrm{e}^{-\mathrm{i}\Omega_{\mathbf{k}}t}$). Since $|G\rangle$ is the bosonic vacuum, the bosonic propagator decomposes as $G^{(0)}(\mathbf{k},\omega) = D^{(0)}_1(\mathbf{k},\omega) + D^{(0)}_2(\mathbf{k},\omega)$ with two non-vanishing components,

$$\begin{aligned} D^{(0)}_1(\mathbf{k},\omega) &= -\mathrm{i}\langle G|T\hat{b}_{\mathbf{k}}(t)\hat{b}^{\dagger}_{\mathbf{k}}(0)|G\rangle = -\mathrm{i}\mathrm{e}^{-\mathrm{i}\Omega_{\mathbf{k}}t}\Theta(t) \\ D^{(0)}_2(\mathbf{k},\omega) &= -\mathrm{i}\langle G|T\hat{b}^{\dagger}_{\mathbf{k}}(t)\hat{b}_{\mathbf{k}}(0)|G\rangle = -\mathrm{i}\mathrm{e}^{\mathrm{i}\Omega_{\mathbf{k}}t}\Theta(-t)\,, \end{aligned} \tag{2.5}$$

where we can see that $D^{(0)}_1(\mathbf{k},\omega)$ and $D^{(0)}_2(\mathbf{k},\omega)$ correspond with forwards- and backwards-propagation in time, respectively. Evaluating the integral (2.2) (inserting a convergence factor δ),

$$\begin{aligned} D^{(0)}_1(\mathbf{k},\omega) &= -\mathrm{i}\int_0^{\infty} dt\ \mathrm{e}^{\mathrm{i}(\omega - E_{\mathbf{k}} + \mathrm{i}\delta)t} = \frac{1}{\omega - E_{\mathbf{k}} + \mathrm{i}\delta} \\ D^{(0)}_2(\mathbf{k},\omega) &= -\mathrm{i}\int_{-\infty}^{0} dt\ \mathrm{e}^{\mathrm{i}(\omega + E_{\mathbf{k}} + \mathrm{i}\delta)t} = \frac{1}{\omega + E_{\mathbf{k}} + \mathrm{i}\delta}\,. \end{aligned} \tag{2.6}$$

2.3 Spectral function

The free propagators above contain a single pole, associated with the energy needed to create a single particle from the vacuum. For interacting field theories, the divergence structure of the propagator is more complicated, and we can write

$$G(\mathbf{k},\omega) = \int d\omega'\ A(\mathbf{k},\omega')\ G^{(0)}(\mathbf{k},\omega') = \int d\omega' \frac{A(\mathbf{k},\omega')}{\omega - \omega' + \mathrm{i}\delta}\,. \tag{2.7}$$

We call $A(\mathbf{k},\omega)$ the *spectral function*, and according to the above relation,

$$A(\mathbf{k},\omega) = -\frac{1}{\pi}\mathrm{Im}\ G(\mathbf{k},\omega - \mathrm{i}\delta') \tag{2.8}$$

where the limit $\delta' \to 0^{+}$ is implied.

3 Bogoliubov-transformed Hamiltonians

In this section, we fill in the omitted steps of the calculations leading to the reciprocal-space Hamiltonian (2.5), as well as the Bogoliubov transformed Hamiltonians (2.7), (3.3), and (3.6) in Chapter 4. Throughout, we will assume periodic boundary conditions, which implies the operator Fourier transforms

$$\begin{aligned}\hat{a}_{\mathbf{k}} &= \frac{1}{\sqrt{N}}\sum_i \mathrm{e}^{-\mathrm{i}\mathbf{k}\cdot\mathbf{r}_i}\hat{a}_i \\ \hat{a}_i &= \frac{1}{\sqrt{N}}\sum_{\mathbf{k}\in 1\mathrm{BZ}} \mathrm{e}^{\mathrm{i}\mathbf{k}\cdot\mathbf{r}_i}\hat{a}_{\mathbf{k}}\end{aligned} \tag{3.1}$$

for generic annihilation operators $\hat{a}_i$, as well as the equivalent transforms for the creation operators $\hat{a}_i^\dagger$.

3.1 Heisenberg model

3.1.1 Reciprocal-space Hamiltonian

Here we derive the reciprocal-space version of the Heisenberg Hamiltonian in the linear spin-wave formalism. We start from the Holstein-Primakoff transformed Hamiltonian

$$H_{\text{eff}} \approx -\frac{Jb_0^2NS^2z}{2} + Jb_0^2S\sum_i\sum_{\boldsymbol{\delta}}\left(\hat{b}_i^\dagger\hat{b}_i + \hat{b}_{i+\boldsymbol{\delta}}^\dagger\hat{b}_{i+\boldsymbol{\delta}} + \hat{b}_i\hat{b}_{i+\boldsymbol{\delta}} + \hat{b}_i^\dagger\hat{b}_{i+\boldsymbol{\delta}}^\dagger\right).$$

Substituting the inverse Fourier transform, we obtain the momentum-space form

$$\begin{aligned}H_{\text{eff}} &= -\frac{Jb_0^2NS^2z}{2} + \frac{Jb_0^2S}{N}\sum_{\mathbf{k},\mathbf{q}\in 1\mathrm{BZ}}\sum_{i,\boldsymbol{\delta}}\Big(\mathrm{e}^{\mathrm{i}\mathbf{r}_i\cdot(\mathbf{q}-\mathbf{k})}\left(1+\mathrm{e}^{\mathrm{i}\boldsymbol{\delta}\cdot(\mathbf{q}-\mathbf{k})}\right)\hat{b}_{\mathbf{k}}^\dagger\hat{b}_{\mathbf{q}} \\ &\qquad + \left(\mathrm{e}^{\mathrm{i}\mathbf{r}_i\cdot(\mathbf{q}+\mathbf{k})}\mathrm{e}^{\mathrm{i}\boldsymbol{\delta}\cdot\mathbf{q}}\hat{b}_{\mathbf{k}}\hat{b}_{\mathbf{q}} + \mathrm{e}^{-\mathrm{i}\mathbf{r}_i\cdot(\mathbf{q}+\mathbf{k})}\mathrm{e}^{-\mathrm{i}\boldsymbol{\delta}\cdot\mathbf{q}}\hat{b}_{\mathbf{k}}^\dagger\hat{b}_{\mathbf{q}}^\dagger\right)\Big) \\ &= -\frac{Jb_0^2NS^2z}{2} + Jb_0^2S\sum_{\mathbf{k},\mathbf{q}\in 1\mathrm{BZ}}\sum_{\boldsymbol{\delta}}\Big(\delta_{\mathbf{qk}}\left(1+\mathrm{e}^{\mathrm{i}\boldsymbol{\delta}\cdot(\mathbf{q}-\mathbf{k})}\right)\hat{b}_{\mathbf{k}}^\dagger\hat{b}_{\mathbf{q}} \\ &\qquad + +\delta_{-\mathbf{qk}}\left(\mathrm{e}^{\mathrm{i}\boldsymbol{\delta}\cdot\mathbf{q}}\hat{b}_{\mathbf{k}}\hat{b}_{\mathbf{q}} + \mathrm{e}^{-\mathrm{i}\boldsymbol{\delta}\cdot\mathbf{q}}\hat{b}_{\mathbf{k}}^\dagger\hat{b}_{\mathbf{q}}^\dagger\right)\Big) \\ &= -\frac{Jb_0^2NS^2z}{2} + Jb_0^2S\sum_{\mathbf{k}\in 1\mathrm{BZ}}\sum_{\boldsymbol{\delta}}\left(2\hat{b}_{\mathbf{k}}^\dagger\hat{b}_{\mathbf{k}} + \left(\mathrm{e}^{-\mathrm{i}\boldsymbol{\delta}\cdot\mathbf{k}}\hat{b}_{\mathbf{k}}\hat{b}_{-\mathbf{k}} + \mathrm{e}^{\mathrm{i}\boldsymbol{\delta}\cdot\mathbf{k}}\hat{b}_{\mathbf{k}}^\dagger\hat{b}_{-\mathbf{k}}^\dagger\right)\right),\end{aligned}$$

where we have used the definition $\delta_{\mathbf{kq}} = 1/N\sum_i \mathrm{e}^{\pm\mathrm{i}\mathbf{r}_i\cdot(\mathbf{k}-\mathbf{q})}$. Flipping the sign on the dummy momentum to set $\mathbf{k}\to-\mathbf{k}$ in the first and second terms, and then using the commutators for the $\hat{b}_{\mathbf{k}}$, we obtain

$$\begin{aligned}H_{\text{eff}} &= -\frac{Jb_0^2NS^2z}{2} + Jb_0^2S\sum_{\mathbf{k}\in 1\mathrm{BZ}}\sum_{\boldsymbol{\delta}}\left(\hat{b}_{\mathbf{k}}^\dagger\hat{b}_{\mathbf{k}} + \hat{b}_{-\mathbf{k}}^\dagger\hat{b}_{-\mathbf{k}} + \mathrm{e}^{\mathrm{i}\boldsymbol{\delta}\cdot\mathbf{k}}\left(\hat{b}_{-\mathbf{k}}\hat{b}_{\mathbf{k}} + \hat{b}_{\mathbf{k}}^\dagger\hat{b}_{-\mathbf{k}}^\dagger\right)\right) \\ &= -\frac{Jb_0^2NS^2z}{2} + \frac{Jb_0^2Sz}{2}\sum_{\mathbf{k}\in 1\mathrm{BZ}}\left(\hat{b}_{\mathbf{k}}^\dagger\hat{b}_{\mathbf{k}} + \hat{b}_{-\mathbf{k}}^\dagger\hat{b}_{-\mathbf{k}} + \gamma_{\mathbf{k}}\left(\hat{b}_{-\mathbf{k}}\hat{b}_{\mathbf{k}} + \hat{b}_{\mathbf{k}}^\dagger\hat{b}_{-\mathbf{k}}^\dagger\right)\right) \\ &= -\frac{Jb_0^2NS^2z}{2} + \frac{Jb_0^2Sz}{2}\sum_{\mathbf{k}\in 1\mathrm{BZ}}\left(\hat{b}_{\mathbf{k}}^\dagger\hat{b}_{\mathbf{k}} + \hat{b}_{-\mathbf{k}}\hat{b}_{-\mathbf{k}}^\dagger - 1 + \gamma_{\mathbf{k}}\left(\hat{b}_{-\mathbf{k}}\hat{b}_{\mathbf{k}} + \hat{b}_{\mathbf{k}}^\dagger\hat{b}_{-\mathbf{k}}^\dagger\right)\right) \\ &= \underbrace{-\frac{Jb_0^2NS(S+1)z}{2}}_{\mathcal{E}_0} + \frac{Jb_0^2Sz}{2}\sum_{\mathbf{k}\in 1\mathrm{BZ}}\left(\hat{b}_{\mathbf{k}}^\dagger\hat{b}_{\mathbf{k}} + \hat{b}_{-\mathbf{k}}\hat{b}_{-\mathbf{k}}^\dagger + \gamma_{\mathbf{k}}\left(\hat{b}_{-\mathbf{k}}\hat{b}_{\mathbf{k}} + \hat{b}_{\mathbf{k}}^\dagger\hat{b}_{-\mathbf{k}}^\dagger\right)\right), ,\end{aligned}$$

where we have defined the *tight-binding parameter* $\gamma_{\mathbf{k}} = 2z^{-1}\sum_{\boldsymbol{\delta}}\mathrm{e}^{\mathrm{i}\mathbf{k}\cdot\boldsymbol{\delta}}$ as in the main text. We re-cast this Hamiltonian trivially in terms of a matrix multiplication to obtain eq. (2.5) from Chapter 4.

3.1.2 Diagonalisation by Bogoliubov transformation

We now diagonalise H_{eff}. Under the Bogoliubov transformation defined in eq. (2.6) of Chapter 4,

$$\begin{aligned} H_{\text{eff}} &= \mathcal{E}_0 + \frac{Jb_0^2Sz}{2}\sum_{\mathbf{k}\in 1\text{BZ}} \begin{pmatrix} \hat{\beta}_{\mathbf{k}}^\dagger & \hat{\beta}_{-\mathbf{k}} \end{pmatrix} \begin{pmatrix} u_{\mathbf{k}} & v_{\mathbf{k}} \\ v_{\mathbf{k}} & u_{\mathbf{k}} \end{pmatrix} \begin{pmatrix} 1 & \gamma_{\mathbf{k}} \\ \gamma_{\mathbf{k}} & 1 \end{pmatrix} \begin{pmatrix} u_{\mathbf{k}} & v_{\mathbf{k}} \\ v_{\mathbf{k}} & u_{\mathbf{k}} \end{pmatrix} \begin{pmatrix} \hat{\beta}_{\mathbf{k}} \\ \hat{\beta}_{-\mathbf{k}}^\dagger \end{pmatrix} \\ &= \mathcal{E}_0 + \frac{Jb_0^2Sz}{2}\sum_{\mathbf{k}\in 1\text{BZ}} \begin{pmatrix} \hat{\beta}_{\mathbf{k}}^\dagger & \hat{\beta}_{-\mathbf{k}} \end{pmatrix} \begin{pmatrix} u_{\mathbf{k}}^2+v_{\mathbf{k}}^2+2u_{\mathbf{k}}v_{\mathbf{k}}\gamma_{\mathbf{k}} & (u_{\mathbf{k}}^2+v_{\mathbf{k}}^2)\gamma_{\mathbf{k}}+2u_{\mathbf{k}}v_{\mathbf{k}} \\ (u_{\mathbf{k}}^2+v_{\mathbf{k}}^2)\gamma_{\mathbf{k}}+2u_{\mathbf{k}}v_{\mathbf{k}} & u_{\mathbf{k}}^2+v_{\mathbf{k}}^2+2u_{\mathbf{k}}v_{\mathbf{k}}\gamma_{\mathbf{k}} \end{pmatrix} \begin{pmatrix} \hat{\beta}_{\mathbf{k}} \\ \hat{\beta}_{-\mathbf{k}}^\dagger \end{pmatrix}, \end{aligned}$$

which is diagonal when $u_{\mathbf{k}}^2+v_{\mathbf{k}}^2+2u_{\mathbf{k}}v_{\mathbf{k}}\gamma_{\mathbf{k}}=0$. Substituting this,

$$\begin{aligned} H &= \mathcal{E}_0 + \frac{Jb_0^2Sz}{2}\sum_{\mathbf{k}\in 1\text{BZ}} \left(u_{\mathbf{k}}^2+v_{\mathbf{k}}^2\right)\left(1-\gamma_{\mathbf{k}}^2\right)\left(\hat{\beta}_{\mathbf{k}}^\dagger\hat{\beta}_{\mathbf{k}}+\hat{\beta}_{-\mathbf{k}}\hat{\beta}_{-\mathbf{k}}^\dagger\right) \\ &= \mathcal{E}_0 + Jb_0^2Sz\sum_{\mathbf{k}\in 1\text{BZ}} \left(u_{\mathbf{k}}^2+v_{\mathbf{k}}^2\right)\left(1-\gamma_{\mathbf{k}}^2\right)\left(\hat{\beta}_{\mathbf{k}}^\dagger\hat{\beta}_{\mathbf{k}}+\frac{1}{2}\right). \end{aligned}$$

For $\sqrt{1-\gamma_{\mathbf{k}}^2}\equiv\omega_{\mathbf{k}}$, we can see that choosing $u_{\mathbf{k}}^2=1/2+1/2\omega_{\mathbf{k}}$ and $v_{\mathbf{k}}^2=-1/2+1/2\omega_{\mathbf{k}}$ is consistent with the condition $u_{\mathbf{k}}^2-v_{\mathbf{k}}^2=1$ and leads to the final expression in the main text.

3.2 Hubbard model

3.2.1 Spin sector Bogoliubov transformation for $H^{(1)}$

Here we re-write the Hubbard Hamiltonian in terms of Bogoliubov transformed operators, starting from eq. (3.2). Explicitly inserting the inverse Bogoliubov transformation $\hat{b}_{-\mathbf{q}}=u_{-\mathbf{q}}\hat{\beta}_{-\mathbf{q}}+v_{-\mathbf{q}}\hat{\beta}_{\mathbf{q}}^\dagger$ in $H^{(1)}$,

$$\begin{aligned} H^{(1)} &= \sum_{\mathbf{k},\mathbf{q}\in 1\text{BZ}} \frac{tb_0z}{\sqrt{N}}\left(g_1(\mathbf{k},\mathbf{q})\hat{\beta}_{-\mathbf{q}}+g_2(\mathbf{k},\mathbf{q})\hat{\beta}_{\mathbf{q}}^\dagger\right)\hat{d}_{\mathbf{Q}-\mathbf{k}}^\dagger\hat{d}_{\mathbf{Q}-\mathbf{k}+\mathbf{q}} \\ &\quad - \sum_{\mathbf{k},\mathbf{q}\in 1\text{BZ}} \frac{tb_0z}{\sqrt{N}}\left(g_2(\mathbf{k},\mathbf{q})\hat{\beta}_{-\mathbf{q}}+g_1(\mathbf{k},\mathbf{q})\hat{\beta}_{\mathbf{q}}^\dagger\right)\hat{e}_{\mathbf{k}}\hat{e}_{\mathbf{k}-\mathbf{q}}^\dagger \\ &= \sum_{\mathbf{k},\mathbf{q}\in 1\text{BZ}} \frac{tb_0z}{\sqrt{N}}\left(g_2(\mathbf{Q}-\mathbf{k},\mathbf{q})\hat{d}_{\mathbf{k}}^\dagger\hat{d}_{\mathbf{k}+\mathbf{q}}\hat{\beta}_{\mathbf{q}}^\dagger+g_1(\mathbf{Q}-\mathbf{k}-\mathbf{q},-\mathbf{q})\hat{d}_{\mathbf{k}+\mathbf{q}}^\dagger\hat{d}_{\mathbf{k}}\hat{\beta}_{\mathbf{q}}\right) \\ &\quad - \sum_{\mathbf{k},\mathbf{q}\in 1\text{BZ}} \frac{tb_0z}{\sqrt{N}}\left(g_2(\mathbf{k},-\mathbf{q})\hat{e}_{\mathbf{k}}\hat{e}_{\mathbf{k}+\mathbf{q}}^\dagger\hat{\beta}_{\mathbf{q}}+g_1(\mathbf{k}-\mathbf{q},-\mathbf{q})\hat{e}_{\mathbf{k}+\mathbf{q}}\hat{e}_{\mathbf{k}}^\dagger\hat{\beta}_{\mathbf{q}}^\dagger\right) \end{aligned}$$

where we have used the fact that we are summing over the entire 1BZ and defined the coefficients

$$\begin{aligned} g_1(\mathbf{k},\mathbf{q}) &= \gamma_{\mathbf{k}-\mathbf{q}}v_{-\mathbf{q}}+\gamma_{\mathbf{k}}u_{-\mathbf{q}} \\ g_2(\mathbf{k},\mathbf{q}) &= \gamma_{\mathbf{k}-\mathbf{q}}u_{-\mathbf{q}}+\gamma_{\mathbf{k}}v_{-\mathbf{q}}\,. \end{aligned} \tag{3.2}$$

Using the spherical symmetry of the Bogoliubov coefficients in momentum-space (i.e. $u_{\mathbf{k}}=u_{-\mathbf{k}}$ and $v_{\mathbf{k}}=v_{-\mathbf{k}}$), as well as the fact that $\gamma_{\mathbf{k}}=\gamma_{-\mathbf{k}}$ and $\gamma_{\mathbf{Q}+\mathbf{k}}=-\gamma_{\mathbf{k}}$, we can see that

$$\begin{aligned} g_2(\mathbf{Q}-\mathbf{k},\mathbf{q}) &= \gamma_{\mathbf{Q}-\mathbf{k}-\mathbf{q}}u_{-\mathbf{q}}+\gamma_{\mathbf{Q}-\mathbf{k}}v_{-\mathbf{q}} = -(\gamma_{\mathbf{k}+\mathbf{q}}u_{\mathbf{q}}+\gamma_{\mathbf{k}}v_{\mathbf{q}}) \\ g_1(\mathbf{Q}-\mathbf{k}-\mathbf{q},-\mathbf{q}) &= \gamma_{\mathbf{Q}-\mathbf{k}-\cancel{\mathbf{q}+\mathbf{q}}}v_{\mathbf{q}}+\gamma_{\mathbf{Q}-\mathbf{k}-\mathbf{q}}u_{\mathbf{q}} = -(\gamma_{\mathbf{k}}v_{\mathbf{q}}+\gamma_{\mathbf{k}+\mathbf{q}}u_{\mathbf{q}}) \\ g_2(\mathbf{k},-\mathbf{q}) &= \gamma_{\mathbf{k}+\mathbf{q}}u_{\mathbf{q}}+\gamma_{\mathbf{k}}v_{\mathbf{q}} \\ g_1(\mathbf{k}+\mathbf{q},\mathbf{q}) &= \gamma_{\mathbf{k}+\cancel{\mathbf{q}-\mathbf{q}}}v_{-\mathbf{q}}+\gamma_{\mathbf{k}+\mathbf{q}}u_{-\mathbf{q}} = \gamma_{\mathbf{k}}v_{\mathbf{q}}+\gamma_{\mathbf{k}+\mathbf{q}}u_{\mathbf{q}} \end{aligned}$$

which leads to eq. (3.3) in Chapter 4 with $m(\mathbf{k},\mathbf{q})=-tb_0z(\gamma_{\mathbf{k}+\mathbf{q}}u_{\mathbf{q}}+\gamma_{\mathbf{k}}v_{\mathbf{q}})/\sqrt{N}$.

3.2.2 Charge sector Bogoliubov transformation for $H^{(0)}$

We now derive the Bogoliubov transformation that diagonalises $H^{(0)}$. According to eq. (3.4) in Chapter 4,

$$H^{(0)} = \frac{NU}{4} + \sum_{\mathbf{k}\in 1\mathrm{BZ}} \begin{pmatrix} \hat{f}^\dagger_{\mathbf{k}} & \hat{g}_{\mathbf{k}} \end{pmatrix} \begin{pmatrix} \frac{U}{2}(u^2_{\mathbf{k}} - v^2_{\mathbf{k}}) - 2u_{\mathbf{k}}v_{\mathbf{k}}tb_0^2 z\gamma_{\mathbf{k}} & Uu_{\mathbf{k}}v_{\mathbf{k}} + tb_0^2 z\gamma_{\mathbf{k}}(u^2_{\mathbf{k}} - v^2_{\mathbf{k}}) \\ Uu_{\mathbf{k}}v_{\mathbf{k}} + tb_0^2 z\gamma_{\mathbf{k}}(u^2_{\mathbf{k}} - v^2_{\mathbf{k}}) & -\frac{U}{2}(u^2_{\mathbf{k}} - v^2_{\mathbf{k}}) + 2u_{\mathbf{k}}v_{\mathbf{k}}tb_0^2 z\gamma_{\mathbf{k}} \end{pmatrix} \begin{pmatrix} \hat{f}_{\mathbf{k}} \\ \hat{g}^\dagger_{\mathbf{k}} \end{pmatrix},$$

which is diagonal when $u_{\mathbf{k}}v_{\mathbf{k}} = -\frac{tb_0^2 z\gamma_{\mathbf{k}}}{U}(u^2_{\mathbf{k}} - v^2_{\mathbf{k}})$. Imposing this,

$$\begin{aligned} H^{(0)} &= \frac{NU}{4} + \sum_{\mathbf{k}\in 1\mathrm{BZ}} \frac{2E^2_{\mathbf{k}}\left(u^2_{\mathbf{k}} - v^2_{\mathbf{k}}\right)}{U}\left(\hat{f}^\dagger_{\mathbf{k}}\hat{f}_{\mathbf{k}} - \hat{g}_{\mathbf{k}}\hat{g}^\dagger_{\mathbf{k}}\right) \\ &= \underbrace{\frac{NU}{4} - \sum_{\mathbf{k}\in 1\mathrm{BZ}} E_{\mathbf{k}}}_{\mathcal{E}'_0} + \sum_{\mathbf{k}\in 1\mathrm{BZ}} \frac{2E^2_{\mathbf{k}}\left(u^2_{\mathbf{k}} - v^2_{\mathbf{k}}\right)}{U}\left(\hat{f}^\dagger_{\mathbf{k}}\hat{f}_{\mathbf{k}} + \hat{g}^\dagger_{\mathbf{k}}\hat{g}_{\mathbf{k}}\right), \end{aligned}$$

where we have defined $E_{\mathbf{k}} = \sqrt{U^2/4 + (tb_0^2 z\gamma_k)^2}$. If we choose $u_{\mathbf{k}}, v_{\mathbf{k}}$ to satisfy $u^2_{\mathbf{k}} = 1/2 + U/4E_{\mathbf{k}}$ and $v^2_{\mathbf{k}} = 1/2 - U/4E_{\mathbf{k}}$, then $u_{\mathbf{k}}v_{\mathbf{k}} = -tb_0^2 z\gamma_{\mathbf{k}}/4E_{\mathbf{k}}$ and we can see that this is indeed consistent with what we have done above. We therefore arrive at the final Hamiltonian stated in the main text.

3.2.3 Charge sector Bogoliubov transformation for $H^{(1)}$

In terms of the Bogoliubov transformed operators,

$$H^{(1)} = \sum_{\mathbf{k}\in 1\mathrm{BZ}} \begin{pmatrix} \hat{f}^\dagger_{-\mathbf{k}} & \hat{g}_{\mathbf{k}} \end{pmatrix} \begin{pmatrix} M_{21}(\mathbf{k},\mathbf{q})\hat{\beta}^\dagger_{\mathbf{q}} + M_{12}(\mathbf{k},\mathbf{q})\hat{\beta}_{-\mathbf{q}} & M_{34}(\mathbf{k},\mathbf{q})\hat{\beta}^\dagger_{\mathbf{q}} + M_{43}(\mathbf{k},\mathbf{q})\hat{\beta}_{-\mathbf{q}} \\ M_{43}(\mathbf{k},\mathbf{q})\hat{\beta}^\dagger_{\mathbf{q}} + M_{34}(\mathbf{k},\mathbf{q})\hat{\beta}_{-\mathbf{q}} & -M_{12}(\mathbf{k},\mathbf{q})\hat{\beta}^\dagger_{\mathbf{q}} - M_{21}(\mathbf{k},\mathbf{q})\hat{\beta}_{-\mathbf{q}} \end{pmatrix} \begin{pmatrix} \hat{f}_{-\mathbf{k}+\mathbf{q}} \\ \hat{g}^\dagger_{\mathbf{k}-\mathbf{q}} \end{pmatrix}$$

where the matrix elements are

$$\begin{aligned} M_{21}(\mathbf{k},\mathbf{q}) &= -\frac{tb_0 z}{\sqrt{N}}\left(g_2(\mathbf{k},\mathbf{q})\mu_{\mathbf{k}}\mu_{\mathbf{k}-\mathbf{q}} - g_1(\mathbf{k},\mathbf{q})\nu_{\mathbf{k}}\nu_{\mathbf{k}-\mathbf{q}}\right) \\ M_{12}(\mathbf{k},\mathbf{q}) &= -\frac{tb_0 z}{\sqrt{N}}\left(g_1(\mathbf{k},\mathbf{q})\mu_{\mathbf{k}}\mu_{\mathbf{k}-\mathbf{q}} - g_2(\mathbf{k},\mathbf{q})\nu_{\mathbf{k}}\nu_{\mathbf{k}-\mathbf{q}}\right) \\ M_{34}(\mathbf{k},\mathbf{q}) &= -\frac{tb_0 z}{\sqrt{N}}\left(g_1(\mathbf{k},\mathbf{q})\mu_{\mathbf{k}-\mathbf{q}}\nu_{\mathbf{k}} + g_2(\mathbf{k},\mathbf{q})\mu_{\mathbf{k}}\nu_{\mathbf{k}-\mathbf{q}}\right) \\ M_{43}(\mathbf{k},\mathbf{q}) &= -\frac{tb_0 z}{\sqrt{N}}\left(g_2(\mathbf{k},\mathbf{q})\mu_{\mathbf{k}-\mathbf{q}}\nu_{\mathbf{k}} + g_1(\mathbf{k},\mathbf{q})\mu_{\mathbf{k}}\nu_{\mathbf{k}-\mathbf{q}}\right). \end{aligned} \tag{3.3}$$

Again using the fact that we are summing over the entire 1BZ,

$$\begin{aligned} H^{(1)} = &\sum_{\mathbf{k}\in 1\mathrm{BZ}} \left(M_{21}(-\mathbf{k},\mathbf{q})\hat{f}^\dagger_{\mathbf{k}}\hat{f}_{\mathbf{k}+\mathbf{q}}\hat{\beta}^\dagger_{\mathbf{q}} + M_{12}(-\mathbf{k}-\mathbf{q},-\mathbf{q})\hat{f}^\dagger_{\mathbf{k}+\mathbf{q}}\hat{f}_{\mathbf{k}}\hat{\beta}_{\mathbf{q}}\right) \\ &- \sum_{\mathbf{k}\in 1\mathrm{BZ}} \left(M_{12}(\mathbf{k}+\mathbf{q},\mathbf{q})\hat{g}_{\mathbf{k}+\mathbf{q}}\hat{g}^\dagger_{\mathbf{k}}\hat{\beta}^\dagger_{\mathbf{q}} + M_{21}(\mathbf{k},-\mathbf{q})\hat{g}_{\mathbf{k}}\hat{g}^\dagger_{\mathbf{k}+\mathbf{q}}\hat{\beta}_{\mathbf{q}}\right) \\ &+ \sum_{\mathbf{k},\mathbf{q}\in 1\mathrm{BZ}} \left(M_{43}(\mathbf{k},-\mathbf{q})\hat{f}^\dagger_{-\mathbf{k}}\hat{g}^\dagger_{\mathbf{k}+\mathbf{q}}\hat{\beta}_{\mathbf{q}} + M_{43}(\mathbf{k}+\mathbf{q},\mathbf{q})\hat{g}_{\mathbf{k}+\mathbf{q}}\hat{f}_{-\mathbf{k}}\hat{\beta}^\dagger_{\mathbf{q}}\right) \\ &+ \sum_{\mathbf{k},\mathbf{q}\in 1\mathrm{BZ}} \left(M_{34}(\mathbf{k},-\mathbf{q})\hat{f}^\dagger_{-\mathbf{k}}\hat{g}^\dagger_{\mathbf{k}+\mathbf{q}}\hat{\beta}^\dagger_{-\mathbf{q}} + M_{34}(\mathbf{k}+\mathbf{q},\mathbf{q})\hat{f}_{-\mathbf{k}}\hat{g}_{\mathbf{k}+\mathbf{q}}\hat{\beta}_{-\mathbf{q}}\right) \end{aligned}$$

Using the property of the Bogoliubov coefficients $\mu_{\mathbf{k}} = \mu_{-\mathbf{k}}$ and $\nu_{\mathbf{k}} = \nu_{-\mathbf{k}}$, as well as

$$g_{1,2}(-\mathbf{k}, \mathbf{q}) = g_{2,1}(-\mathbf{k} - \mathbf{q}, -\mathbf{q})$$
$$g_{1,2}(\mathbf{k} + \mathbf{q}, \mathbf{q}) = g_{2,1}(\mathbf{k}, -\mathbf{q})$$

which follows directly from the properties of $g_{1,2}(\mathbf{k}, \mathbf{q})$, we obtain the form of $H^{(1)}$ stated in the main text with coefficients that read, written out explicitly,

$$\begin{aligned} M_1(\mathbf{k}, \mathbf{q}) &= -\frac{tb_0 z}{\sqrt{N}} \left[(\gamma_{\mathbf{k}+\mathbf{q}} u_{\mathbf{q}} + \gamma_{\mathbf{k}} v_{\mathbf{q}}) \, \mu_{\mathbf{k}} \mu_{\mathbf{k}+\mathbf{q}} - (\gamma_{\mathbf{k}+\mathbf{q}} v_{\mathbf{q}} + \gamma_{\mathbf{k}} u_{\mathbf{q}}) \, \nu_{\mathbf{k}} \nu_{\mathbf{k}+\mathbf{q}} \right] = -M_2(\mathbf{k}, \mathbf{q}) \\ M_3(\mathbf{k}, \mathbf{q}) &= -\frac{tb_0 z}{\sqrt{N}} \left[(\gamma_{\mathbf{k}+\mathbf{q}} u_{\mathbf{q}} + \gamma_{\mathbf{k}} v_{\mathbf{q}}) \, \nu_{\mathbf{k}} \mu_{\mathbf{k}+\mathbf{q}} + (\gamma_{\mathbf{k}+\mathbf{q}} v_{\mathbf{q}} + \gamma_{\mathbf{k}} u_{\mathbf{q}}) \, \mu_{\mathbf{k}} \nu_{\mathbf{k}+\mathbf{q}} \right] \\ M_4(\mathbf{k}, \mathbf{q}) &= -\frac{tb_0 z}{\sqrt{N}} \left[(\gamma_{\mathbf{k}+\mathbf{q}} u_{\mathbf{q}} + \gamma_{\mathbf{k}} v_{\mathbf{q}}) \, \mu_{\mathbf{k}} \nu_{\mathbf{k}+\mathbf{q}} + (\gamma_{\mathbf{k}+\mathbf{q}} v_{\mathbf{q}} + \gamma_{\mathbf{k}} u_{\mathbf{q}}) \, \nu_{\mathbf{k}} \mu_{\mathbf{k}+\mathbf{q}} \right] \end{aligned} \tag{3.4}$$

4 Born approximation

Here we derive the 1-loop correction to the self-energy for an interacting field theory comprised from a fermionic field $\hat{f}_{\mathbf{k}}$ and a collective bosonic field $\hat{\beta}_{\mathbf{k}}$, with generic Hamiltonian

$$H = \sum_{\mathbf{k}} E_{\mathbf{k}} \hat{f}^\dagger_{\mathbf{k}} \hat{f}_{\mathbf{k}} + \sum_{\mathbf{k}} \Omega_{\mathbf{k}} \hat{\beta}^\dagger_{\mathbf{k}} \hat{\beta}_{\mathbf{k}} + \underbrace{\sum_{\mathbf{k},\mathbf{q}} M(\mathbf{k}, \mathbf{q}) \left(\hat{f}^\dagger_{\mathbf{k}+\mathbf{q}} \hat{f}_{\mathbf{k}} \hat{\beta}_{\mathbf{q}} + \text{h.c.} \right)}_{H_I} \tag{4.1}$$

We define the free theory momentum-space Green's functions by the Wick contractions

$$\begin{aligned} \langle \dots \overbrace{\hat{f}_{\mathbf{k}}(t) \hat{f}^\dagger_{\mathbf{k}}(t')} \dots \rangle &= \mathrm{i} G^{(0)}(\mathbf{k}, t - t') \, \langle \dots \rangle \\ \langle \dots \overbrace{\hat{\beta}_{\mathbf{k}}(t) \hat{\beta}^\dagger_{\mathbf{k}}(t')} \dots \rangle &= \mathrm{i} D^{(0)}_1(\mathbf{k}, t - t') \, \langle \dots \rangle \\ \langle \dots \overbrace{\hat{\beta}^\dagger_{\mathbf{k}}(t) \hat{\beta}_{\mathbf{k}}(t')} \dots \rangle &= \mathrm{i} D^{(0)}_2(\mathbf{k}, t - t') \, \langle \dots \rangle \end{aligned} \tag{4.2}$$

4.1 Dyson expansion

The Dyson expansion to 1-loop order gives

$$G(\mathbf{k}, t) = G^{(0)}(\mathbf{k}, t) - \mathrm{i} \frac{(-\mathrm{i})^2}{2} \int dt_1 \int dt_2 \langle H_I(t_1) H_I(t_2) \hat{f}_{\mathbf{k}}(t) \hat{f}^\dagger_{\mathbf{k}}(0) \rangle \,, \tag{4.3}$$

where $H_I(t)$ is the interaction picture interaction Hamiltonian. Expanding this out explicitly,

$$\begin{aligned} G(\mathbf{k}, t) &= G^{(0)}(\mathbf{k}, t) + \frac{\mathrm{i}}{2} \sum_{\mathbf{k}_1, \mathbf{k}_2} \sum_{\mathbf{q}_1, \mathbf{q}_2} M(\mathbf{k}_1, \mathbf{q}_1) M(\mathbf{k}_2, \mathbf{q}_2) \\ &\quad \times \int dt_1 \int dt_2 \, \langle \left(\hat{f}^\dagger_{\mathbf{k}_1+\mathbf{q}_1}(t_1) \hat{f}_{\mathbf{k}_1}(t_1) \hat{\beta}_{\mathbf{q}_1}(t_1) + \text{h.c.} \right) \left(\hat{f}^\dagger_{\mathbf{k}_2+\mathbf{q}_2}(t_2) \hat{f}_{\mathbf{k}_2}(t_2) \hat{\beta}_{\mathbf{q}_2}(t_2) + \text{h.c.} \right) \hat{f}_{\mathbf{k}}(t) \hat{f}^\dagger_{\mathbf{k}}(0) \rangle \\ &= G^{(0)}(\mathbf{k}, t) - \frac{1}{2} \sum_{\mathbf{k}_1, \mathbf{k}_2} \sum_{\mathbf{q}} M(\mathbf{k}_1, \mathbf{q}_1) M(\mathbf{k}_2, \mathbf{q}_2) \\ &\quad \times \Bigg(\int dt_1 \int dt_2 \; D^{(0)}_1(\mathbf{q}, t_1 - t_2) \, \langle \hat{f}^\dagger_{\mathbf{k}_1+\mathbf{q}}(t_1) \hat{f}_{\mathbf{k}_1}(t_1) \hat{f}^\dagger_{\mathbf{k}_2}(t_2) \hat{f}_{\mathbf{k}_2+\mathbf{q}}(t_2) \hat{f}_{\mathbf{k}}(t) \hat{f}^\dagger_{\mathbf{k}}(0) \rangle \\ &\quad + \int dt_1 \int dt_2 \; D^{(0)}_2(\mathbf{q}, t_1 - t_2) \, \langle \hat{f}^\dagger_{\mathbf{k}_1}(t_1) \hat{f}_{\mathbf{k}_1+\mathbf{q}}(t_1) \hat{f}^\dagger_{\mathbf{k}_2+\mathbf{q}}(t_2) \hat{f}_{\mathbf{k}_2}(t_2) \hat{f}_{\mathbf{k}}(t) \hat{f}^\dagger_{\mathbf{k}}(0) \rangle \Bigg) \end{aligned}$$

4.1.1 Wick contractions

For connected diagrams, the different Wick contractions that we have to consider are now

$$\langle \hat{f}^\dagger_{\mathbf{k}_1+\mathbf{q}}(t_1)\hat{f}_{\mathbf{k}_1}(t_1)\hat{f}^\dagger_{\mathbf{k}_2}(t_2)\hat{f}_{\mathbf{k}_2+\mathbf{q}}(t_2)\hat{f}_{\mathbf{k}}(t)\hat{f}^\dagger_{\mathbf{k}}(0)\rangle = +\mathrm{i}^3\delta_{\mathbf{k}_1\mathbf{k}_2}\delta_{\mathbf{k}_1\mathbf{k}-\mathbf{q}}G^{(0)}(\mathbf{k},t-t_1)G^{(0)}(\mathbf{k}_1,t_1-t_2)G^{(0)}(\mathbf{k},t_2)$$

$$\langle \hat{f}^\dagger_{\mathbf{k}_1+\mathbf{q}}(t_1)\hat{f}_{\mathbf{k}_1}(t_1)\hat{f}^\dagger_{\mathbf{k}_2}(t_2)\hat{f}_{\mathbf{k}_2+\mathbf{q}}(t_2)\hat{f}_{\mathbf{k}}(t)\hat{f}^\dagger_{\mathbf{k}}(0)\rangle = -\mathrm{i}^3\delta_{\mathbf{k}_1\mathbf{k}_2}\delta_{\mathbf{k}_1\mathbf{k}}G^{(0)}(\mathbf{k}_1,t_2-t_1)G^{(0)}(\mathbf{k},t_1)G^{(0)}(\mathbf{k},t-t_2)$$

$$\langle \hat{f}^\dagger_{\mathbf{k}_1}(t_1)\hat{f}_{\mathbf{k}_1+\mathbf{q}}(t_1)\hat{f}^\dagger_{\mathbf{k}_2+\mathbf{q}}(t_2)\hat{f}_{\mathbf{k}_2}(t_2)\hat{f}_{\mathbf{k}}(t)\hat{f}^\dagger_{\mathbf{k}}(0)\rangle = +\mathrm{i}^3\delta_{\mathbf{k}_1\mathbf{k}}\delta_{\mathbf{k}_1\mathbf{k}_2}G^{(0)}(\mathbf{k},t-t_1)G^{(0)}(\mathbf{k}_1,t_1-t_2)G^{(0)}(\mathbf{k},t_2)$$

$$\langle \hat{f}^\dagger_{\mathbf{k}_1}(t_1)\hat{f}_{\mathbf{k}_1+\mathbf{q}}(t_1)\hat{f}^\dagger_{\mathbf{k}_2+\mathbf{q}}(t_2)\hat{f}_{\mathbf{k}_2}(t_2)\hat{f}_{\mathbf{k}}(t)\hat{f}^\dagger_{\mathbf{k}}(0)\rangle = -\mathrm{i}^3\delta_{\mathbf{k}_1\mathbf{k}_2}\delta_{\mathbf{k}_1\mathbf{k}-\mathbf{q}}G^{(0)}(\mathbf{k}_1,t_2-t_1)G^{(0)}(\mathbf{k},t_1)G^{(0)}(\mathbf{k},t-t_2)$$

where we have accounted for the sign changes associated with the permutation of fermionic operators. Using this together with the fact that $D^{(0)}_1(\mathbf{k},t) = D^{(0)}_2(\mathbf{k},-t)$,

$$\begin{aligned}
G(\mathbf{k},t) &= G^{(0)}(\mathbf{k},t) \\
&\quad + \mathrm{i}\sum_{\mathbf{q}}\int dt_1\int dt_2\ M^2(\mathbf{k}-\mathbf{q},\mathbf{q})D^{(0)}_1(\mathbf{q},t_1-t_2)G^{(0)}(\mathbf{k},t-t_1)G^{(0)}(\mathbf{k}-\mathbf{q},t_1-t_2)G^{(0)}(\mathbf{k},t_2) \\
&\quad + \mathrm{i}\sum_{\mathbf{q}}\int dt_1\int dt_2\ M^2(\mathbf{k},\mathbf{q})D^{(0)}_1(\mathbf{q},t_1-t_2)G^{(0)}(\mathbf{k},t_2-t_1)G^{(0)}(\mathbf{k},t_1)G^{(0)}(\mathbf{k},t-t_2)
\end{aligned}$$

4.1.2 1-loop propagator

We now express the Green's function in terms of inverse Fourier transforms of the propagators:

$$\begin{aligned}
&\int dt_1\int dt_2\ M^2(\mathbf{k}-\mathbf{q},\mathbf{q})D^{(0)}_1(\mathbf{q},t_1-t_2)G^{(0)}(\mathbf{k},t-t_1)G^{(0)}(\mathbf{k}-\mathbf{q},t_1-t_2)G^{(0)}(\mathbf{k},t_2) \\
&\qquad = M^2(\mathbf{k}-\mathbf{q},\mathbf{q})\int\frac{d\omega}{2\pi}\mathrm{e}^{-\mathrm{i}\omega t}\int\frac{d\omega'}{2\pi}D^{(0)}_1(\mathbf{q},\omega-\omega')G^{(0)}(\mathbf{k},\omega)G^{(0)}(\mathbf{k}-\mathbf{q},\omega')G^{(0)}(\mathbf{k},\omega) \\
&\int dt_1\int dt_2\ M^2(\mathbf{k},\mathbf{q})D^{(0)}_1(\mathbf{q},t_1-t_2)G^{(0)}(\mathbf{k},t_2-t_1)G^{(0)}(\mathbf{k},t_1)G^{(0)}(\mathbf{k},t-t_2) \\
&\qquad = M^2(\mathbf{k},\mathbf{q})\int\frac{d\omega}{2\pi}\mathrm{e}^{-\mathrm{i}\omega t}\int\frac{d\omega'}{2\pi}D^{(0)}_1(\mathbf{q},\omega'-\omega)G^{(0)}(\mathbf{k},\omega')G^{(0)}(\mathbf{k},\omega)G^{(0)}(\mathbf{k},\omega)
\end{aligned}$$

Recalling that the propagator $G(\mathbf{k},\omega)$ can be expressed in terms of the self-energy $\Sigma(\mathbf{k},\omega)$ as

$$G(\mathbf{k},\omega) = \frac{1}{\omega - E_{\mathbf{k}} + \mathrm{i}\delta - \Sigma(\mathbf{k},\omega)} = G^{(0)}(\mathbf{k},\omega) + G^{(0)}(\mathbf{k},\omega)\Sigma(\mathbf{k},\omega)G^{(0)}(\mathbf{k},\omega) + \ldots \tag{4.4}$$

we arrive at the final expression for the 1-loop self-energy

$$\begin{aligned}
\Sigma(\mathbf{k},\omega) &= \sum_{\mathbf{q}} M^2(\mathbf{k}-\mathbf{q},\mathbf{q})\int\frac{d\omega'}{2\pi}D^{(0)}_1(\mathbf{q},\omega-\omega')G^{(0)}(\mathbf{k}-\mathbf{q},\omega') \\
&\quad + \sum_{\mathbf{q}} M^2(\mathbf{k},\mathbf{q})\int\frac{d\omega'}{2\pi}D^{(0)}_1(\mathbf{q},\omega'-\omega)G^{(0)}(\mathbf{k},\omega')
\end{aligned}$$

4.2 Contour integration

To calculate the integral in ω' we note the divergence structure of the two integrals. Firstly,

$$D_1^{(0)}(\mathbf{q}, \omega - \omega') \times G^{(0)}(\mathbf{k} - \mathbf{q}, \omega') = \frac{-1}{\omega' - (\omega - \Omega_{\mathbf{q}} + \mathrm{i}\delta)} \times \frac{1}{\omega' - (E_{\mathbf{k}-\mathbf{q}} - \mathrm{i}\delta)}$$

has a pole both above and below the real axis in the complex plane of ω'. On the other hand,

$$D_1^{(0)}(\mathbf{q}, \omega' - \omega) \times G^{(0)}(\mathbf{k}, \omega') = \frac{1}{\omega' - (\omega + \Omega_{\mathbf{q}} - \mathrm{i}\delta)} \times \frac{1}{\omega' - (E_{\mathbf{k}} - \mathrm{i}\delta)}$$

only has poles below the real axis. Introducing a convergence factor $\mathrm{e}^{\mathrm{i}\omega'\delta'}$ which diverges in the lower half plane and closing the integral in the upper half plane, by Cauchy's residue theorem

$$\Sigma(\mathbf{k}, \omega) = \sum_{\mathbf{q}} M^2(\mathbf{k} - \mathbf{q}, \mathbf{q}) \times G^{(0)}(\mathbf{k} - \mathbf{q}, \omega - \Omega_{\mathbf{q}})$$

Appendix C

Hydrogen calculations

In this appendix, we recall the structure of the $1s$ and $2p$ hydrogen orbitals and derive the results quoted in the main text for Wannier overlap integrals approximated using the hydrogen wavefunctions.

1 Gross structure wavefunctions

The electronic energy eigenvalue equation for the H atom has separable solutions $\psi_{nlm}(\mathbf{r}) = R_{nl}(r)Y_{lm}(\theta,\varphi)$, where n is the principal quantum number, l ($l \leq n-1$) is the angular momentum quantum number, and m ($|m| \leq l$) is the magnetic quantum number. We are interested in the $1s$ ground state ($n=1$, $l=0$, $m=0$) and the $2p$ first excited state ($n=2$, $l=1$, $m=\pm1$), since transitions from the ground state to the $2s$ first excited state ($n=2$, $l=0$, $m=0$) are not dipole-allowed.

The radial dependence of the $1s$ and $2p$ wavefunctions is given by [72]

$$\begin{aligned} R_{1,0}(r) &= \frac{2}{a_0^{3/2}}\mathrm{e}^{-r/a_0} \\ R_{2,1}(r) &= \frac{r}{\sqrt{3}(2a_0)^{5/2}}\mathrm{e}^{-r/(2a_0)} \end{aligned} \tag{1.1}$$

The angular wavefunctions of the $1s$ and $2p$ states are the spherical harmonics [72]

$$\begin{aligned} Y_{0,0}(\theta,\varphi) &= \frac{1}{\sqrt{4\pi}} \\ Y_{1,0}(\theta,\varphi) &= \sqrt{\frac{3}{4\pi}}\,\cos\theta \\ Y_{1,\pm1}(\theta,\varphi) &= \mp\sqrt{\frac{3}{4\pi}}\,\sin\theta\,\mathrm{e}^{\pm\mathrm{i}\varphi} \end{aligned} \tag{1.2}$$

The angular dependence of these functions is shown in Fig. C.1. Ignoring the coupling between the electron spin and orbital angular momentum (i.e. in the *gross structure* regime), the $m=\pm1$ states are degenerate, therefore any linear combination of $\psi_{21-1}(\mathbf{r})$ and $\psi_{211}(\mathbf{r})$ is also a suitable $2p$ energy eigenstate. In particular, we can define states $\psi_{p_x}(\mathbf{r})$ and $\psi_{p_y}(\mathbf{r})$, which are rotationally symmetric about the x-axis and y-axis, respectively. Explicitly,

$$\begin{aligned} \psi_{p_x}(\mathbf{r}) &= \psi_{21-1}(\mathbf{r}) - \psi_{211}(\mathbf{r}) = \frac{x}{4\sqrt{2\pi}a_0^{5/2}}\mathrm{e}^{-r/(2a_0)} \\ \psi_{p_y}(\mathbf{r}) &= -\psi_{21-1}(\mathbf{r}) - \psi_{211}(\mathbf{r}) = \frac{y}{4\sqrt{2\pi}a_0^{5/2}}\mathrm{e}^{-r/(2a_0)} \end{aligned} \tag{1.3}$$

We can see that together with $\psi_{p_z}(\mathbf{r}) \equiv \psi_{210}(\mathbf{r})$, these form a complete set of orbitals with identical (double-lobe) shape, each rotationally symmetric about one spatial axis.

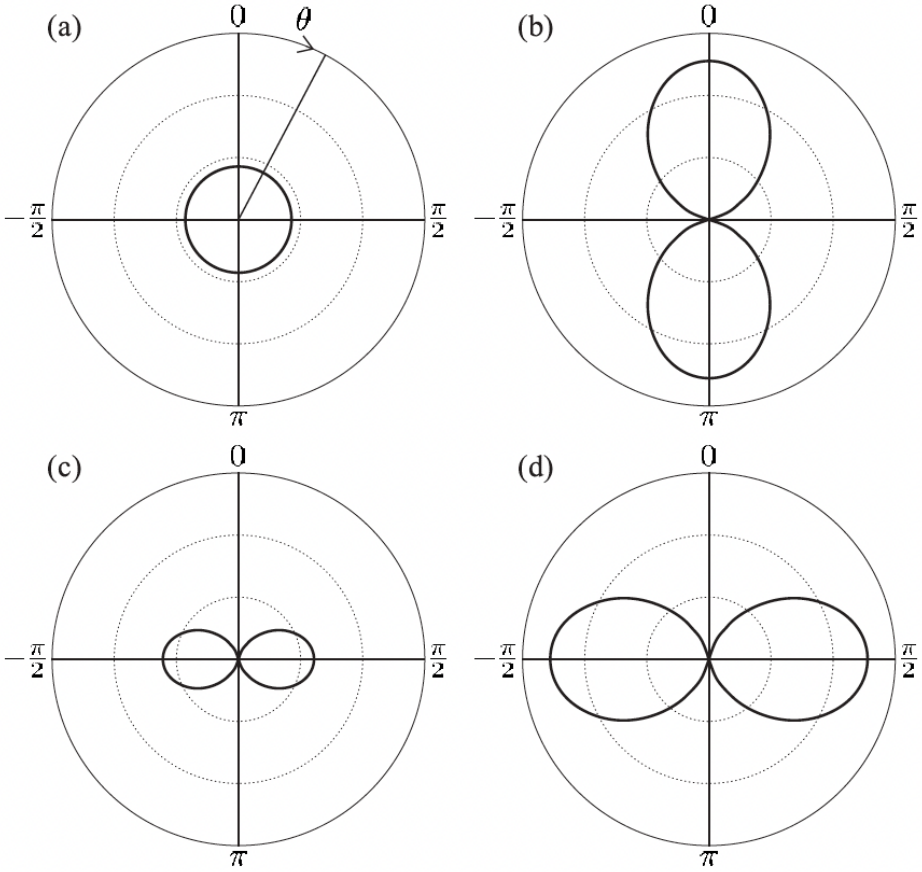

Figure C.1 – **Angular dependence of spherical harmonics.** Figure reproduced from Ref. [72]. The diagrams show angular plots as a function of θ. The plots **a)-c)** are symmetric under rotations in φ and so are plotted for arbitrary φ, and **d)** is plotted for $\varphi = 0$. The plotted functions are **a)** $|Y_{0,0}(\theta,\varphi)|^2$, **b)** $|Y_{1,0}(\theta,\varphi)|^2$, **c)** $|Y_{1,\pm1}(\theta,\varphi)|^2$, and **d)** $|Y_{1,-1}(\theta,\varphi) - Y_{1,1}(\theta,\varphi)|^2$.

2 Dipole matrix element $\mathbf{d}_{\mu\mu'}$

Consistently with the classical multiple scattering calculation, if we consider a field polarised along the x-axis the field will only couple to the orbital $\psi_{p_x}(\mathbf{r})$. The dipole moment between this $2p$ orbital and the ground state is

$$d^x_{sp} = \frac{q}{4\sqrt{2}\pi a_0^4} \underbrace{\int_0^{2\pi} d\varphi \cos^2\varphi}_{=\pi} \underbrace{\int_0^{\pi} d\theta \sin^3\theta}_{=4/3} \underbrace{\int_0^{\infty} dr\ r^4 \mathrm{e}^{-3r/2a_0}}_{=256a_0^5/81} = \frac{256}{243\sqrt{2}} a_0 q$$

$$d^y_{sp} = \frac{q}{4\sqrt{2}\pi a_0^4} \underbrace{\int_0^{2\pi} d\varphi \cos\varphi \sin\varphi}_{=0} \underbrace{\int_0^{\pi} d\theta \sin^3\theta}_{=4/3} \underbrace{\int_0^{\infty} dr\ r^4 \mathrm{e}^{-3r/2a_0}}_{=256a_0^5/81} = 0$$

$$d^z_{sp} = \frac{q}{4\sqrt{2}\pi a_0^4} \underbrace{\int_0^{2\pi} d\varphi \cos\varphi}_{=0} \underbrace{\int_0^{\pi} d\theta \sin^2\theta \cos\theta}_{=0} \underbrace{\int_0^{\infty} dr\ r^4 \mathrm{e}^{-3r/2a_0}}_{=256a_0^5/81} = 0$$

3 Hydrogen overlap integrals

3.1 On-site energies $T|_{ii\mu\mu}$ and $U_p|_{iii\mu\mu}$

We can see that the expressions for the cases where $\mu' = s$ and where $\mu' = p$ are practically equivalent, with only some different numerical factors. We therefore look at a general integral,

$$\begin{aligned}\int d^3\mathbf{x}\ \phi^*_\mu(\mathbf{x})\nabla^2_x\phi_{\mu'}(\mathbf{x}) &= \int d^3\mathbf{x}\frac{|\mathbf{x}|-\beta a_0}{\alpha a_0^2|\mathbf{x}|}\phi^*_\mu(\mathbf{x})\phi_{\mu'}(\mathbf{x}) \\ &= \int d^3\mathbf{x}\left(\frac{1}{\alpha a_0^2}-\frac{\beta}{\alpha a_0|\mathbf{x}|}\right)\phi^*_\mu(\mathbf{x})\phi_{\mu'}(\mathbf{x}) \\ &= \frac{1}{\alpha a_0^2}\underbrace{\int d^3\mathbf{x}\phi^*_\mu(\mathbf{x})\phi_{\mu'}(\mathbf{x})}_{\delta_{\mu\mu'}} - \frac{\beta}{\alpha a_0}\int d^3\mathbf{x}\frac{1}{|\mathbf{x}|}\phi^*_\mu(\mathbf{x})\phi_{\mu'}(\mathbf{x})\,,\end{aligned}$$

where $\alpha = 1, \beta = 2$ for $\mu' = s$ and $\alpha = 4, \beta = 8$ for $\mu' = p$ and we have used the orthonormality of the hydrogen wavefunctions. We just have to compute

$$\begin{aligned}\int d^3\mathbf{x}\frac{1}{|\mathbf{x}|}\phi^*_\mu(\mathbf{x})\phi_{\mu'}(\mathbf{x}) &= \int_0^{2\pi}d\varphi\int_0^{\pi}d\theta\sin\theta\int_0^{\infty}dr\ r\phi^*_\mu(r,\theta,\varphi)\phi_{\mu'}(r,\theta,\varphi) \\ &= \begin{cases}\dfrac{1}{\pi a_0^3}\underbrace{\displaystyle\int_0^{2\pi}d\varphi}_{=2\pi}\underbrace{\displaystyle\int_0^{\pi}d\theta\sin\theta}_{=2}\underbrace{\displaystyle\int_0^{\infty}dr r\mathrm{e}^{-2r/a_0}}_{=a_0^2/4}\,, & \mu=\mu'=s \\ \dfrac{1}{4\sqrt{2}\pi a_0^4}\underbrace{\displaystyle\int_0^{2\pi}d\varphi\cos\varphi}_{=0}\underbrace{\displaystyle\int_0^{\pi}d\theta\sin^2\theta}_{=\pi/2}\underbrace{\displaystyle\int_0^{\infty}dr r^2\mathrm{e}^{-3r/2a_0}}_{=16a_0^3/27}\,, & \mu\neq\mu' \\ \dfrac{1}{32\pi a_0^5}\underbrace{\displaystyle\int_0^{2\pi}d\varphi\cos^2\varphi}_{=\pi}\underbrace{\displaystyle\int_0^{\pi}d\theta\sin^3\theta}_{=4/3}\underbrace{\displaystyle\int_0^{\infty}dr r^3\mathrm{e}^{-r/a_0}}_{=6a_0^4}\,, & \mu=\mu'=p\end{cases} \\ &= \begin{cases}\dfrac{1}{a_0}\,, & \mu=\mu'=s \\ 0\,, & \mu\neq\mu' \\ \dfrac{1}{4a_0}\,, & \mu=\mu'=p\end{cases}.\end{aligned}$$

We recognise this to give us the result in eq. (1.2).

3.2 On-site repulsion U

To calculate U, we use the fact that we can express $1/|\mathbf{x}-\mathbf{y}|$ in terms of a sum of spherical harmonics: denoting $\mathbf{x} = (r,\theta,\phi)$ and $\mathbf{y} = (r',\theta',\phi')$, and defining $r_< = \min(r,r')$ and $r_> = \max(r,r')$,

$$\frac{1}{|\mathbf{x}-\mathbf{y}|} = \sum_{l=0}^{\infty}\sum_{m=-l}^{l}\frac{4\pi}{2l+1}\frac{r_<^l}{r_>^{l+1}}Y^*_{lm}(\theta,\phi)Y_{lm}(\theta',\phi')\,.$$

Inserting this expansion in the expression for u_μ,

$$\begin{aligned}
u_\mu &= \frac{q^2}{8\pi\varepsilon_0}\sum_{l=0}^{\infty}\sum_{m=-l}^{l}\frac{4\pi}{2l+1}\int d^3\mathbf{x}\int d^3\mathbf{y}\ |\phi_\mu(\mathbf{x})|^2|\phi_\mu(\mathbf{y})|^2\frac{r_<^l}{r_>^{l+1}}Y_{lm}^*(\theta,\phi)Y_{lm}(\theta',\phi') \\
&= \frac{q^2}{2\varepsilon_0}\sum_{l=0}^{\infty}\sum_{m=-l}^{l}\frac{1}{2l+1}\int_0^\infty dr r^2|\phi_\mu(r)|^2\int_0^\infty dr' r'^2|\phi_\mu(r')|^2\frac{r_<^l}{r_>^{l+1}}\int d\Omega\ Y_{lm}^*(\theta,\phi)\int d\Omega'\ Y_{lm}(\theta',\phi') \\
&= \frac{\sqrt{\pi}q^2}{4\varepsilon_0}\sum_{l=0}^{\infty}\sum_{m=-l}^{l}\frac{1}{2l+1}\int_0^\infty dr r^2|\phi_\mu(r)|^2\int_0^\infty dr' r'^2|\phi_\mu(r')|^2\frac{r_<^l}{r_>^{l+1}}\int d\Omega'\ \underbrace{Y_{00}(\theta,\phi)\ Y_{lm}^*(\theta,\phi)}_{=\delta_{l0}\delta_{m0}}\int d\Omega\ Y_{lm}(\theta',\phi') \\
&= \frac{\sqrt{\pi}q^2}{\varepsilon_0}\int_0^\infty dr r^2|\phi_\mu(r)|^2\int_0^\infty dr' r'^2|\phi_\mu(r')|^2\frac{1}{r_>}\underbrace{\int d\Omega\ Y_{00}(\theta',\phi')}_{=2\sqrt{\pi}} \\
&= \frac{2\pi q^2}{\varepsilon_0}\int_0^\infty dr r^2|\phi_\mu(r)|^2\int_0^\infty dr' r'^2|\phi_\mu(r')|^2\frac{1}{r_>}\,.
\end{aligned}$$

For $\mu = s$ we can calculate this explicitly:

$$\begin{aligned}
u_s &= \frac{2\pi q^2}{\varepsilon_0}\times\frac{1}{\pi^2 a_0^6}\int_0^\infty dr r^2 \mathrm{e}^{-2r/a_0}\int_0^\infty dr' r'^2\mathrm{e}^{-2r'/a_0}\frac{1}{r_>} \\
&= \frac{2q^2}{\pi\varepsilon_0 a_0^6}\Bigg(\underbrace{\int_0^\infty dr\int_0^r dr'\ r'^2 r\mathrm{e}^{-2(r+r')/a_0}}_{=5a_0^5/256} + \underbrace{\int_r^\infty dr'\int_0^\infty dr\ r^2 r'\mathrm{e}^{-2(r+r')/a_0}}_{=5a_0^5/256}\Bigg) = \frac{5\varepsilon_s}{4}
\end{aligned}$$